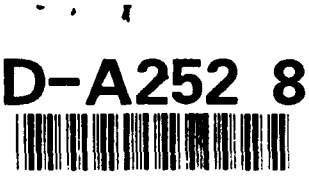

(2)

FINAL REPORT

THE MECHANICS OF PROGRESSIVE CRACKING IN CERAMIC MATRIX COMPOSITES AND LAMINATES

by

Norman Laws
Department of Mechanical Engineering
University of Pittsburgh
Pittsburgh, PA 15261

Submitted To:

Air Force Office of Scientific Research
Bolling Air Force Base, Washington, DC 20332-7448

Contract AFOSR-88-0104

September 1991

TABLE OF CONTENTS

ABSTRACT

This report provides a brief summary of the principal results obtained in a research program on the mechanics of progressive cracking in ceramic matrix composites and laminates. The report concentrates on (i) progressive transverse matrix cracking in cross-ply laminates, (ii) the effect of transverse matrix cracks on the axial response of unidirectional ceramic matrix composites, (iii) thermal conductivities of hot pressed SiC/BN composites, (iv) microcracking in polycrystalline ceramics, and (v) the effect of matrix cracking and fiber-matrix interfacial debonding on the response of unidirectional ceramic matrix composites.

1. INTRODUCTION

This research project addressed several basic problems in the damage mechanics of brittle composite materials. Many new results were obtained in the course of this work. The principal results may be summarized as follows:

1. The formulation of a complete model to predict both first ply failure and the subsequent progressive transverse cracking in cross-ply composite laminates. The accuracy of the predictions for AS-3501-06 and T300/934 systems is particularly gratifying. Both theoretically and experimentally it is clear that damage development in such brittle systems can be retarded by keeping the ply thickness to a minimum.
2. The formulation of a refined shear lag model for steady state matrix cracking in unidirectional ceramic matrix composites. Amongst other things, the analysis shows the sensitivity of the model to the mechanics of the interfacial debond regime.
3. The formulation of both the self consistent model and the differential scheme for the conductivity of three phase composites. In the case of some hot pressed SiC/BN composites containing voids, the theoretical predictions were compared with experimental data. For the conductivity parallel to the hot-pressing direction agreement was good. However for the conductivity perpendicular to the hot-pressing direction agreement was not good.
4. The investigation of the two-dimensional hexagonal array model for polycrystalline aggregates. It turns out that one can obtain an analytic solution of the problem for arbitrary grain orientation distributions. One significant conclusion to emerge is that accurate determination of interfacial stresses demands consideration of at least 200 contiguous grains. In addition a model was formulated to describe progressive grain boundary microcracking. The model has the advantages of simplicity, ease of calculation of process zone

microcrack shielding, allows for anisotropy of microcracking and compares favorably with models proposed by others.

5. The proper formulation and solution of stress analysis problems associated with interfacial debonding in unidirectional ceramic matrix composites. We take the opportunity to correct errors which are prevalent in the literature--even in the simplest case of an arc crack in a homogeneous material. The solution to the full problem is obtained from two coupled singular integral equations and thus provides a proper basis for all subsequent work on fiber-matrix interfacial debonding.

These principal findings, together with other related results, are described in the sequel.

2. SIGNIFICANT ACHIEVEMENTS

2.1 Progressive transverse cracking in cross-ply Gr/epoxy and E-glass epoxy laminates.

In a series of reports and papers which were produced under an earlier AFOSR grant (84-0366), Laws and Dvorak [1, 2, 3] gave extensive results on the incidence of the first transverse crack in cross-ply laminates and the subsequent damage development under increasing load. A feature of the Laws-Dvorak analysis was that the shear lag parameter was chosen to give the correct value of the stress for first ply failure. This was entirely due to the fact that the stress intensity reduction factors required by the Laws-Dvorak model [1, 2] were then unknown.

In the course of the present work this deficiency has been remedied by Laws and Wang [4]. By making use of the analysis contained in Wang's Ph.D. dissertation [5], Laws and Wang [4] have given a completely deductive model for the prediction of progressive transverse cracking in cross-ply composite laminates. It is of interest to observe the comparison between the Laws-Wang model, those of other authors and the experimental data. Some results for first ply failure are shown in Figs. 1, 2 and 3. Also included in Figs. 1, 2 and 3 are results obtained from the theoretical models of Bailey et al [6], Flaggs [7], Nuismer and Tan [8] and Hahn, Han and Croman [9]. Whilst the author has reservations on the status of the models of these various authors [6, 7, 8, 9] it is clear from Figs. 1, 2 and 3 that no model has a decisive advantage in the

prediction of first ply failure--at least as far as is shown by the data reported in these figures.

The situation is entirely different when we discuss progressive transverse cracking. When we wish to predict crack density as a function of applied load it is clear that the models given in [6, 7, 8, 9] are not successful. Indeed the only acceptable models known to the author, are the Laws-Wang improvement of the Laws-Dvorak model together with the model of Wang and Crossman [11]. It is noteworthy that predictions of both models are almost identical, as shown in Figs. 4 and 5, wherein the models are compared with data by Wang [11] for AS-3501-06 and T300/934 systems.

Finally we note that a significant implication of our results is that the amount of damage in laminates can be reduced by keeping the ply thickness to a minimum.

2.2 The effect of transverse matrix cracks on the axial response of unidirectional ceramic matrix composites

The work here has concentrated on an extension of the Laws-Dvorak shear lag [2] model to the steady state cracking regime discussed by Budiansky, Hutchinson and Evans [12]. We also note that the steady state cracking model has been extensively studies by others--most notably by Dharani, Chai and Pagano [13] and by McCartney [14]. In this context it is difficult to compare the various theoretical models and to compare with such data as is available. We are therefore content to describe some of the significant results which emerge from the model developed by the author [15] and to compare our results with those of Budiansky, Hutchinson and Evans [12].

First consider unbonded, frictionally constrained fibers. Then the non-dimensional critical cracking stress obtained from our model is compared with the BHE model in Figs. 6 and 7. Aside from the slight overshoot in Fig. 6, the two models are comparable. But differences emerge when we consider the critical matrix stress for initially bonded, debonding fibers. In this case our model is distinctly different from the BHE model. At the expense of over-simplification it is appropriate to say that our model [15] requires knowledge of the interfacial shear strength. Thus consider initially bonded, debonding fibers which are then constrained

by friction. The critical stress for various ratios of $G_d G_m$ (debonding toughness/matrix toughness) and τ_d/τ_s (interfacial shear strength/friction stress) are shown in Figs. 8, 9 and 10. In order to examine the effect of residual stress on the critical stress, Figs. 11, 12 and 13 show the different critical stresses when the fiber-matrix interface in the debonded zone remains in contact with friction or separates. We note that frictional contact produces a significant increase in the critical matrix cracking stress as is only to be expected.

2.3 Thermal conductivities of hot pressed SiC/BN composites containing voids.

The most significant results obtained in this part of our work has been our success in formulating the s.c.m. and d. s. models together with some success in predicting the experimental results of Ruh, Bentsen and Hasselman [16] parallel to the direction of hot pressing. However, as might be expected, the theoretical results differ rather widely from the experimental data for the direction perpendicular to the hot-pressing direction. The results shown in Figs. 14-17 provide confirmation of the above statements.

Of course, a major problem posed by any examination of the data of Ruh, Bentsen and Hasselman [16] is that they pertain to 3-phase composites. Indeed, as far as the author is aware, the work reported here is the first attempt to correlate 3-phase theoretical models with experiment.

It is abundantly clear that complete experimental data is essential for the successful application of any theoretical model.

2.4 Microcracking in polycrystalline ceramics.

In the first instance we mention the completion of some earlier work (partly funded by ALCOA) on the effect of residual stress in polycrystalline ceramics. The model proposed by Laws and Lee [17] is an extension of the Evans [18] two-dimensional hexagonal array model. It is assumed that each grain is elastically isotropic but thermally anisotropic. The orientation of the various grains in the array is arbitrary.

It is possible [17] to give an exact solution to this problem. Amongst other things, the

solution extends a result of Evans [18] to show that the stress singularity at triple points is always logarithmic. In addition, we were able to show that if accurate information on the residual stress at a given interface is required, it is essential to consider at least 2C.. surrounding grains. This result is in marked contrast to an earlier assertion by Evans and Fu [19, 10, 21].

A result of significant practical interest is the grain size for spontaneous microcracking during cooldown. As described by Laws and Lee [17] the model compares favorably with the model of Hutchinson and Tvergaard [12] and the experimental data of Rice and Pohanka [23].

A further area of concern is the progressive microcracking of the polycrystalline aggregate under continued mechanical loading. At this juncture it is perhaps important to emphasize that the development of models for progressive microcracking of polycrystalline ceramics play an important role in our work on ceramic matrix composites.

The data shows that such systems are essentially elastic in the sense that residual strains in simple tension tests are often negligible. Thus one is led to formulate models for microcracking solids but which have a macroscopic energy function. It is noteworthy that Hutchinson [24] and Charalambides and McMeeking [25] have emphasized that existence of a microscopic energy density does not imply existence of a macroscopic energy density in a microcracking solid. In fact, as is discussed by Laws [26] severe restrictions must be placed on the microcrack nucleation function in order that the microcracking polycrystalline aggregate can be regarded as macroscopically hyperelastic. These restrictions give rise to a nucleation function which closely approximates the nucleation function proposed by Charalambides and McMeeking [25]. In effect, the different nucleation functions are demanded by the assumed model for stiffness loss (e.g. self-consistent model, linear extrapolation, differential scheme etc). The technique has considerable advantages over earlier work in that it applies with comparative ease to anisotropic distributions of microcracks.

An issue of much current interest relates to the effect of shielding due to microcracking in the process zone of a stationary macroscopic crack. This problem has been discussed by

Hutchinson [24], Charalambides and McMeeking [25] Ortiz [27] and others. An assessment and comparison of the respective models is discussed by the present writer in [26]. For the present it suffices to say that, within the range of common applicability, the various models are in reasonable agreement. The advantage which is claimed for the writer's model [26], is that the extent of microcrack shielding is obtained with relatively little effort. In addition the model appears to have potential for application to more complicated systems.

2.5 The effect of matrix cracking and fiber-matrix interfacial debonding on the response of unidirectional ceramic matrix composites.

It is appropriate to repeat in this final report many stimulating conversations with Drs. Ted Nicholas and Nick Pagano and members of their groups at WRDC/MLLN. In addition it is important to record the excellent work by Zawada and Butkus [28].

As stated in earlier reports, an extensive round table discussion was held at WRDC/MLLN at which it was concluded that some exact solutions relevant to fiber-matrix debonding were highly desirable. Such solutions are extremely important for many reasons.

Thus a significant effort has been expended in solving, and applying, the solutions of a variety of fiber-matrix interfacial crack problems. For simplicity I concentrate on the two-dimensional problem associated with a single SiC fiber in an LAS matrix when there is an applied simple tension at infinity and there is a single debond crack at the interface. But before I describe the SiC fiber-LAS matrix, let me briefly discuss the associated problem wherein fiber and matrix are of the same material. The solution of this problem is given by Mushkelishvili [29]. This solution was used by Sih, Paris and Erdogan [30] to calculate the stress intensity factors at the crack tips. Unfortunately, as noted by Savin [31] the expression for the S.I.F. given in [30] is wrong. However, a significant feature of the Mushkelishvili solution, which appears to have escaped the attention of all previous workers , except Toya [32], is that it implies crack closure for certain orientations of the applied load, see Fig. 18. This unhappy situation has been remedied by Chao and Laws [33] who gave an exact solution of the problem for partially closed cracks. In Fig. 19 we present a graphic to show the extent of crack

closure under changing orientation of applied load. Obviously it is inappropriate to give comprehensive details of the techniques or results in this report. It is, however, instructive to show the comparison between the stress intensity factors given by Rooke and Cartwright [34] (who use the Savin [31] result) and the results obtained by Chao and Laws [33]. Despite the fact that the so-called handbook solution is not correct whenever crack closure occurs, it is obvious from Figs. 20-23 that the handbook result is remarkable close to the correct result. Further, in Fig. 24 we show the transverse stiffness of a solid containing a population of identical arc-cracks, with crack densities $\epsilon = 0.05$ and $\epsilon = 0.01$. It is again clear that the handbook solution is extremely accurate even when crack closure occurs. Thus we have the significant (but anticlimactic) result that the Muskhelishvili solution [29] is entirely sufficient for most practical purposes.

Turning now to the genuine interfacial crack problem, it is well known that this involves an enormous increase in complexity [32, 35, 36, 37, 38, 39]. In addition recent work by Rice [40] and Hutchinson [41] have thrown considerable light on the problem of a crack at the interface of two half spaces.

Of course, it is clear that in the case of an interfacial (arc) crack between an SiC fiber and an LAS matrix, we can get crack closure by two mechanisms: first by the so-called overlapping surfaces phenomenon and second because of load orientation. Nevertheless, it may be shown that the problem can be reduced to the solution of two coupled singular integral equations which must be solved numerically. It turns out that the shape of the interfacial crack with partial contact is similar to that shown in Fig. 19 for the arc crack--but detailed exposition is inappropriate here. It suffices to say that for arbitrary choice of fiber and matrix one can calculate contact lengths, stress intensity factors, energy release rates, loss of stiffness, etc., etc. The full details are available in the paper by Chao and Laws[42]. By way of illustration the actual contact lengths are shown in Figs. 24, 25--note the significant difference in magnitude of the contact length δ_1 (at the "open" end) compared with δ_2 (at the "closed" end) . Also, typical stress intensity factors are shown in Figs. 26 and 27. Perhaps the easiest graphs to interpret are those showing loss of transverse stiffness (E_T) as functions of material

parameters and crack and load geometry, shown in Figs. 28, 29 and 30. In this context, it is not possible to assert that one can use the "classical" overlapping solution with impunity.

These and other issues are discussed, at length, by Chao and Laws [42, 43]. It is also worth recording here that significant progress has been made by the author in analyzing the nature of the near-tip zones of the interfacial cracks. The analysis here shows that there is a definite "boundary layer" effect--similar to that obtained by Dundurs and Gautesen [44]. Further, the analysis gives additional weight to Hutchinson's [41] proposal to set $\beta = 0$ and thus avoid the terms which give rise to overlapping surfaces at the crack tips. The current, albeit tentative, conclusion from our exact analysis is that Hutchinson's [41] proposal should be entirely sufficient for practical purposes.

3. ACKNOWLEDGEMENTS

This work was monitored by Lieutenant-Colonel George Haritos who provided an important initiative and useful encouragement. It is also a pleasure to acknowledge stimulating discussions with Drs. Ted Nicholas and Nick Pagano and members of their groups at WRDC/MLLN.

4. REFERENCES

[1] Dvorak, G. J. and Laws, N., "Analysis of Progressive Matrix Cracking in Composite Laminates, II, First Ply Failure," *J. Composite Materials* 21, 1987, 309

[2] Laws, N. and Dvorak, G. J., "Progressive Transverse Cracking in Composite Laminates," *J. Composite Materials* 22 ,1988, 900.

[3] Dvorak, G. J. and Laws, N., "Analytical and Experimental Characterization of Damage Processes in Composite Laminates," Final Report AFOSR-84-0366.

[4] Laws, N. and Wang, J. B., "A Complete Model for Transverse Cracking of Composite Laminates," in preparation.

[5] Wang, J. B., "Stress Analysis of Cracked Cross-Ply Composite Laminates," Ph.D. dissertation, University of Pittsburgh, 1989.

[6] Bailey, J. E., Curtis, P. T. and Parvizi, A., "On the Transverse Cracking and Longitudinal Splitting Behavior of Glass and Carbon Fiber Reinforced Epoxy Cross Ply Laminates and the Effect of Poisson and Thermally Generated Strain," *Proc. R. Soc. Lond. A.*, Vol. 366, 1979, 599.

[7] Flaggs, D. L., "Prediction of Tensile Matrix Failure in Composite Laminates," *J. Composite Materials* 19, 1985, 29.

[8] Nuismer, R. J. and Tan, S. C., "Constitutive Equations ;of a Cracked Composite Lamina," *J. Composite Materials* 22, 1988, 306.

[9] Han, H. T., Hahn, T. W. and Croman, R. B., "A Simplified Analysis of Transverse Ply Cracking in Cross-Ply Laminates," *Composites Science and Technology 31*, 1988, 165.

[10] Wang, A. S. D. and Crossman, F. W., "Initiation and Growth of Transverse Cracks and Edge Delamination in Composite Laminates," *J. Composite Material Supplement 14*, 1980, 88.

[11] Wang, A. S. D., "Fracture Mechanics of Sublaminate Cracks in Composite Materials," *Composite Technology Review*, 1984, 45.

[12] Budiansky, B., Hutchinson, J. W. and Evans, A. G., "Matrix Fracture in Fiber-Reinforced Ceramics," *J. Mech. Phys. Solids* 34, 1986, 167.

[13] Dharani, L. R., Chai, L. and Pagano, N. J., "Steady-State Cracking in Ceramic Matrix Composites," *Comp. Sci. Tech.* 39, 1990, 29.

[14] McCartney, L. N., "Mechanics of Matrix Cracking in Brittle Matrix Fibre-Reinforced Composites," *Proc. R. Soc. Lond A* 409, 1987, 329.

[15] Laws, N., "A Refined Shear Lag Model for Steady State Matrix Cracking in Unidirectional Ceramic Matrix Composites," in preparation.

[16] Ruh, R., Bentsen, L.D. and Hasselman, D.P.H., "Thermal Diffusivity Anisotropy of SiC/BN Composites," *Communications American Ceramic Soc.* (1986) C-83.

[17] Laws, N. and Lee, J. C., "Microcracking in Polycrystalline Ceramics: Elastic

Isotropy and Thermal Anisotopy," *J. Mech. Phys. Solids* 37 , 1989, 603.

[18] Evans, A. G., "Microfracture from Thermal Expansion Anisotropy - I. Single Phase Systems," *Acta. Metall.* 26 , 1978, 1845.

[19] Fu, Y. and Evans A. G., "Microcrack Zone Formation in Single Phase Polycrystals," *Acta. Metall.* 30, 1982, 1619.

[20] Fu, Y. and Evans A. G., "Some Effects of Microcracks on the Mechanical Properties of Brittle Solids - I. Stress Strain Relations," *Acta. Metall.* 33 1985, 1515.

[21] Fu, Y. and Evans A. G., "Some Effects of Microcracks on the Mechanical Properties of Brittle Solids - II. Microcrack Toughening," *Acta. Metall.* 33 1988, 1525.

[22] Tvergaard, V. and Hutchinson, J. W., "Microcracking in Ceramics Induced by Thermal Expansion or Elastic Anisotropy," *J. Am. Ceram. Soc.* 71, 1988, 157.

[23] Rice, R. W. and Pohanka, R. C., "Grain-size Dependence of Spontaneous Cracking in Ceramics," *J. Am. Ceram. Soc.* 62, 1979, 559.

[24] Hutchinson, J.W., "Crack Tip Shielding by Microcracking in Brittle Solids," *Acta. Metall.* 35, 1987,1605.

[25] Charalambides, P. G. and McMeeking, R. M. "Finite Element Method Simulation of Crack Propagation in a Brittle Microcracking Solid," *Mech. of Materials* 6, 1987, 71.

[26] Laws, N., "The Effect of Microcracks on Energy Density," International Symposium on the Mechanics and Physics of Energy Density," (ed. E.E. Gdoutos, G.C. Sih), Xanthi, Elsevier Applied Science, 1990, pp. 189-195.

[27] Ortiz, M., "A Continuum Theory of Microcrack Shielding," *J. Appl. Mechanics* 54,.1987, 54.

[28] Zawada, L. and Butkus, L., "Room Temperature Tensile and Fatigue Properties of Silicon Carbide Fiber-Reinforced Aluminosilicate Glass," 14th Annual Conference on Composites and Advanced Ceramics, Cocoa Beach , Florida 1990.

[29] Muskhelishvili, N.I., "Some Basic Problems of the Mathematical Theory of Elasticity," Noordhoff, 1953.

[30] Sih, G.C., Paris, P.C. and Erdogan, F., "Crack Tip Stress Intensity Factors for Plane Extension and Plate Bending Problems," *J. Appl Mechanics* , 1962, 306.

[31] Savin, G.N. "Stress Distribution Around Holes," NASA TT F-607.

[32] Toya, M., "A Crack Along the Interface of a Circular Inclusion Embedded in an Infinite Solid," *J. Mech. Phys. Solids* 22, 1974, 325.

[33] Chao, R. and Laws, N., "Closure of an Arc Crack Due to Unidirectional Loading," in preparation.

[34] Rooke, D.P. and Cartwright, D.J. "A Compendium of Stress Intensity Factors," HMSO (London) 1976.

[35] Comninou, M., "The Interface Crack," *J. Appl. Mechanics* 44 , 1977, 631.

[36] Comninou, M., "The Interface Crack in a Shear Field," *J. Appl Mechanics* 45., 1977, 287.

[37] Comninou, M. and Schmueser, D., "The Interface Crack in a Combined Tension-Compression and Shear Field," *J. Appl. Mechanics* 46, 1979, 345.

[38] Dundurs, J. and Comninou, M., "Some Consequences of the Inequality Conditions in Contact and Crack Problems," *J. Elasticity* 9, 1979, 71.

[39] Gautesen, A.K. and Dundurs, J., "The Interface Crack in a Tension Field," *J. Appl. Mechanics* 54, 1987, 93.

[40] Rice, J.R., "Elastic Fracture Mechanics Concepts for Interfacial Cracks," *J. Appl Mechanics* 55, 1988, 98.

[41] Hutchinson, J.W. and Suo, Z., "Sandwich Test Specimens for Measuring Interface Crack Toughness," *Matls. Science and Engng. A107*, 1989, 135.

[42] Chao, R. and Laws, N., "Some Effects of Fiber-Matrix Interfacial Debonding on the Response of Unidirectional Ceramic Matrix Composite Materials," in preparation.

[43] Chao, R. and Laws, N., "Loss of Stiffness Due to Microcracking in Unidirectional Ceramic Matrix Composites," *ASME-AMD, Vol. 169*, 1990, pp. 57-62.

[44] Gautesen, A. K. and Dundurs, J., "The Interface Crack Under Combined Loading," *J. Appl. Mechanics* 55, 1988, 580.

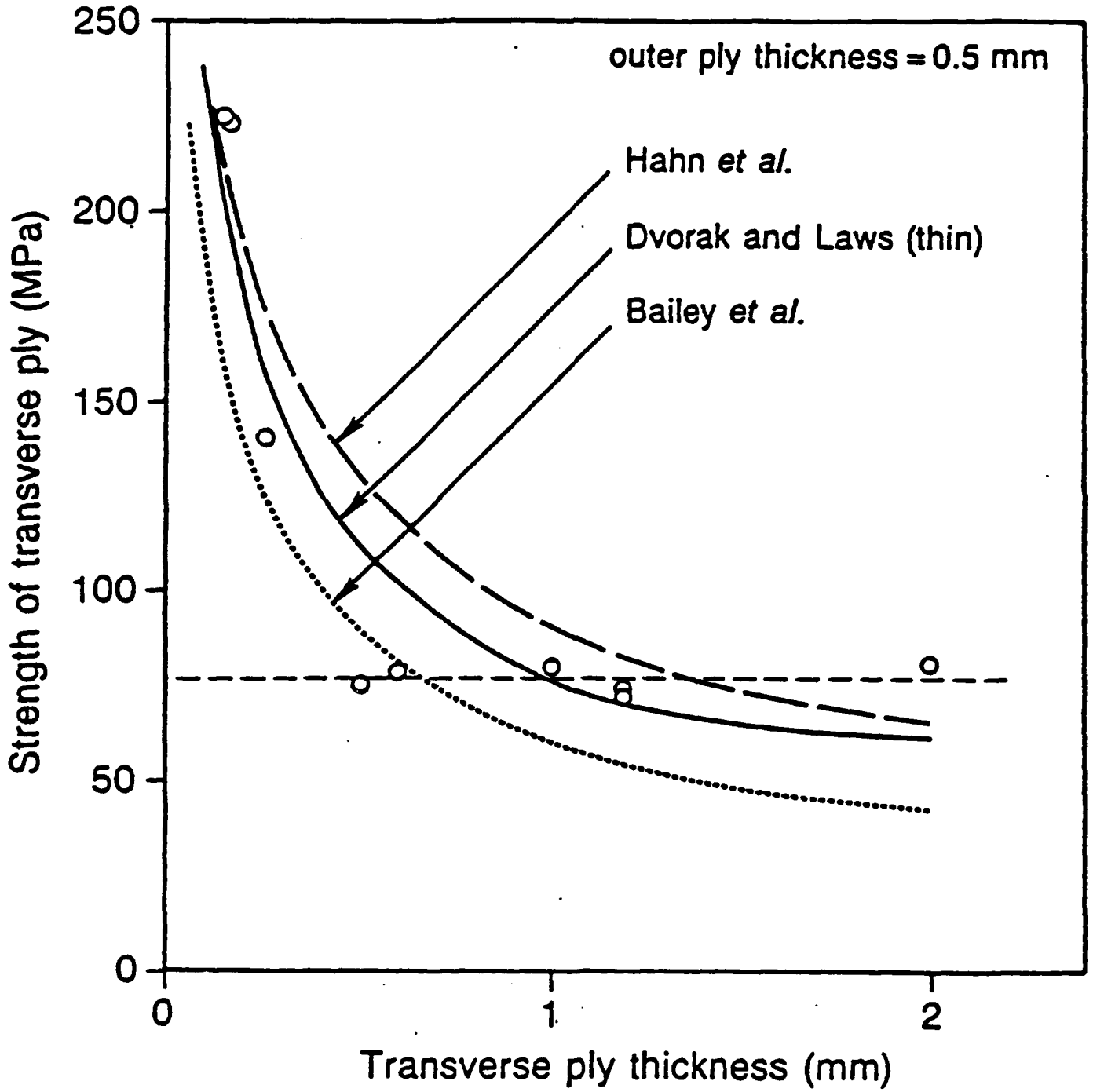

Fig. 1 Strength of transverse ply of various E-glass epoxy laminates, as predicted, and experimental data by Bailey et. al. [6].

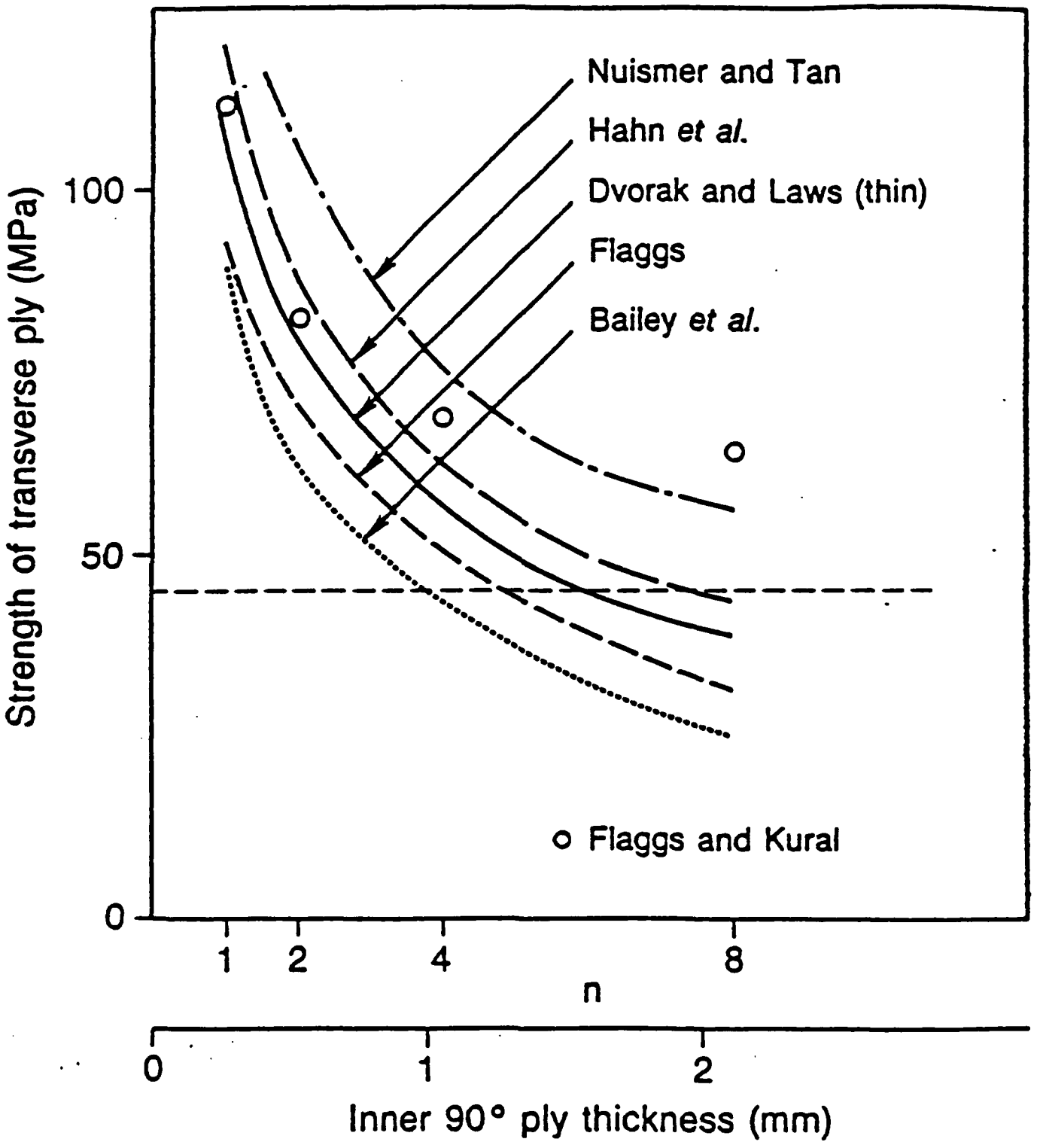

Fig. 2 Strength of transverse ply of various T300/934 laminates, as predicted, and experimental data by Flaggs and Dural [7]. Thick ply result of Dvorak and Laws [1] denoted by - - - - - - -.

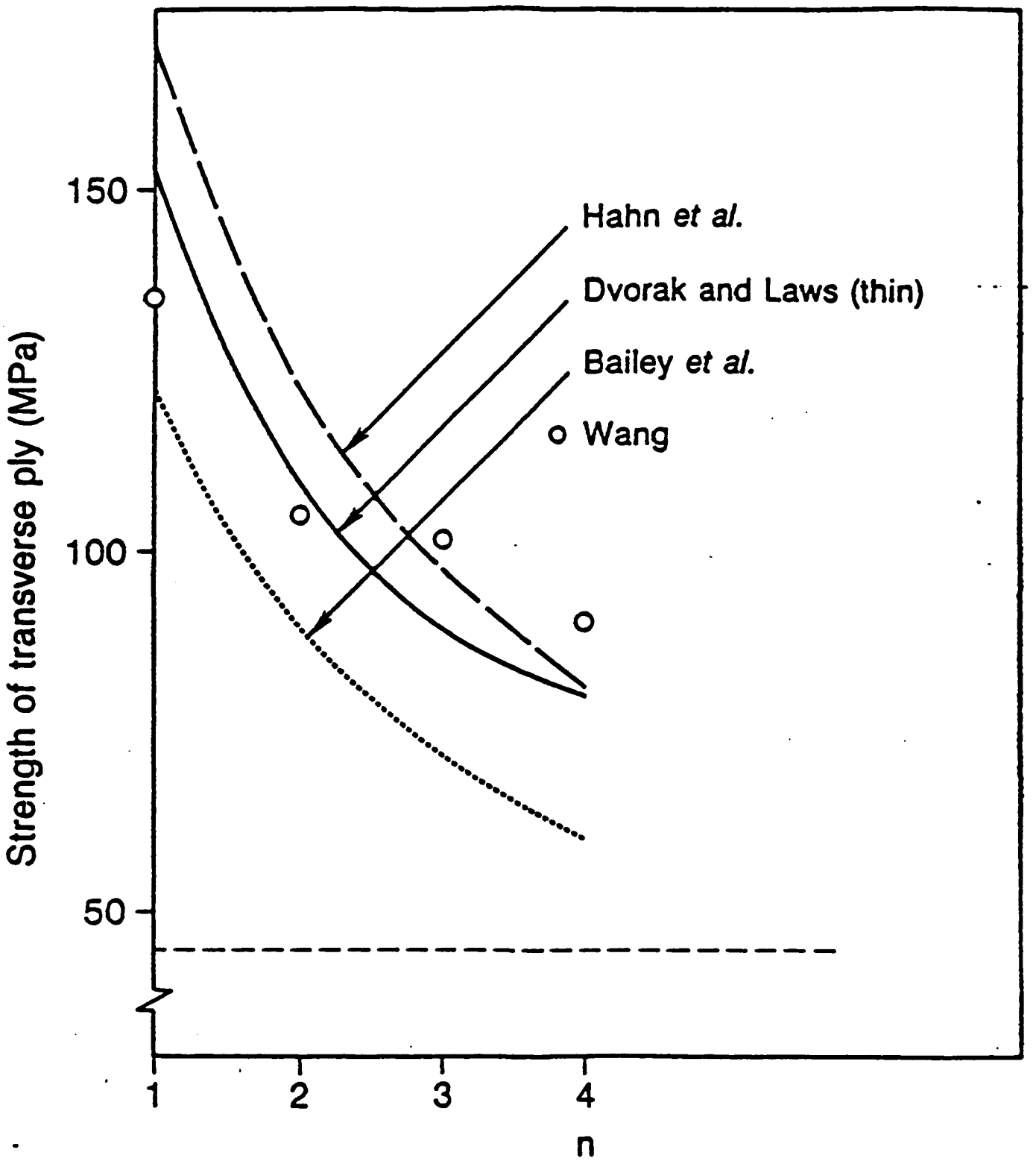

Fig. 3 Strength of transverse ply of various T300/934 laminates, as predicted, and experimental data by Wang [11].

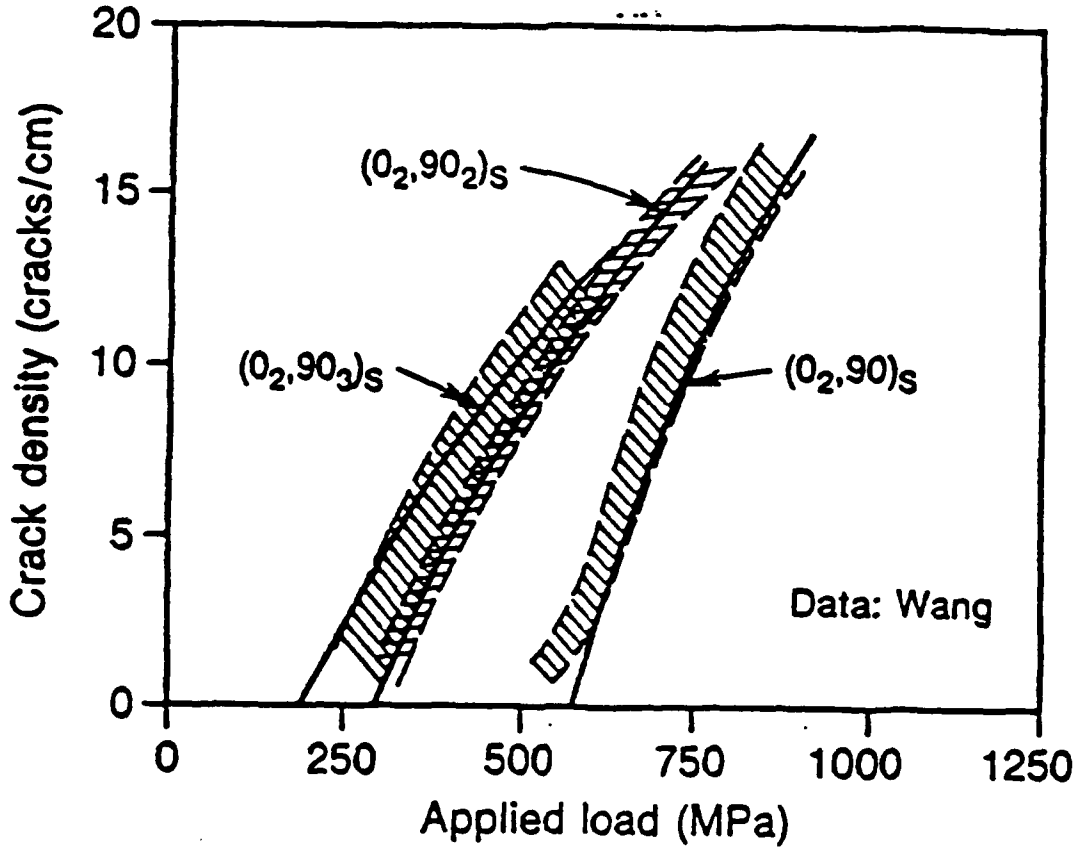

Fig. 4 Progressive cracking of AS-3501-06 cross-ply laminates, as predicted, compared with experimental data by Wang [11].

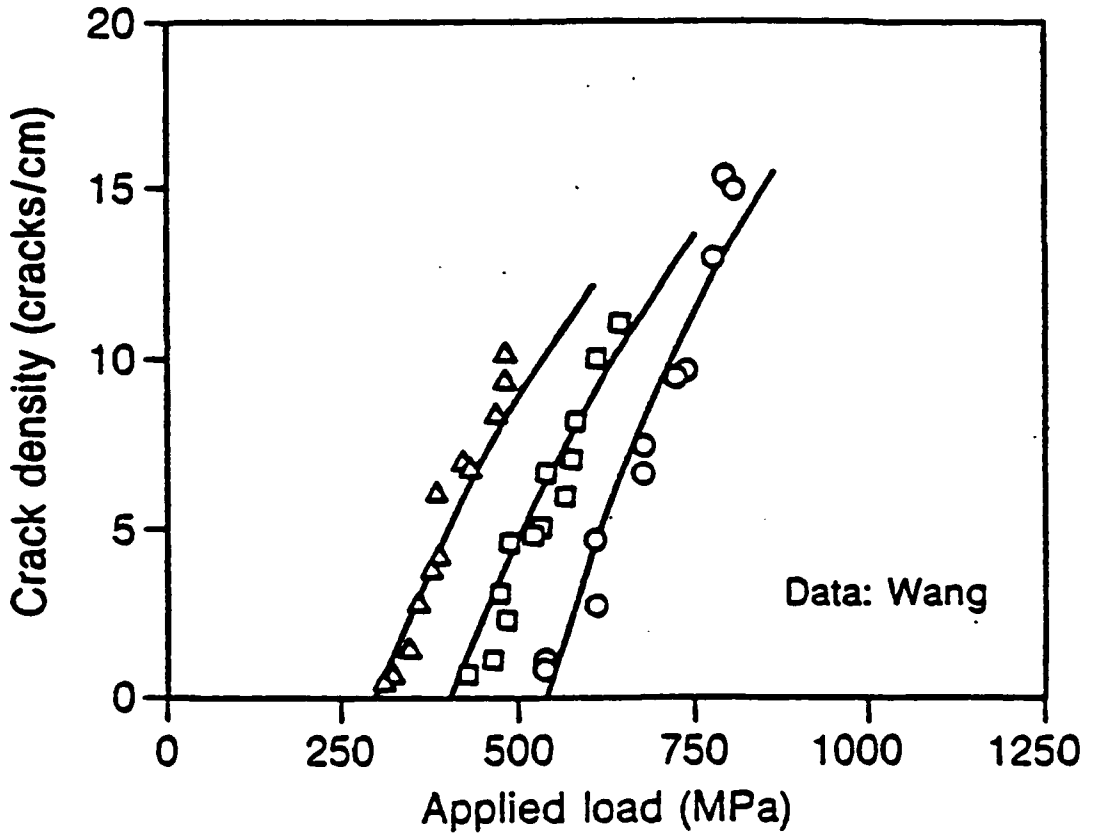

Fig. 5 Progressive cracking of T300/934 cross-ply laminates, as predicted, compared with experimental data by Wang [11].

$\Delta(0, 90_4, 0)$, $\square(0, 90_3, 0)$, $0(0, 90_2, 0)$

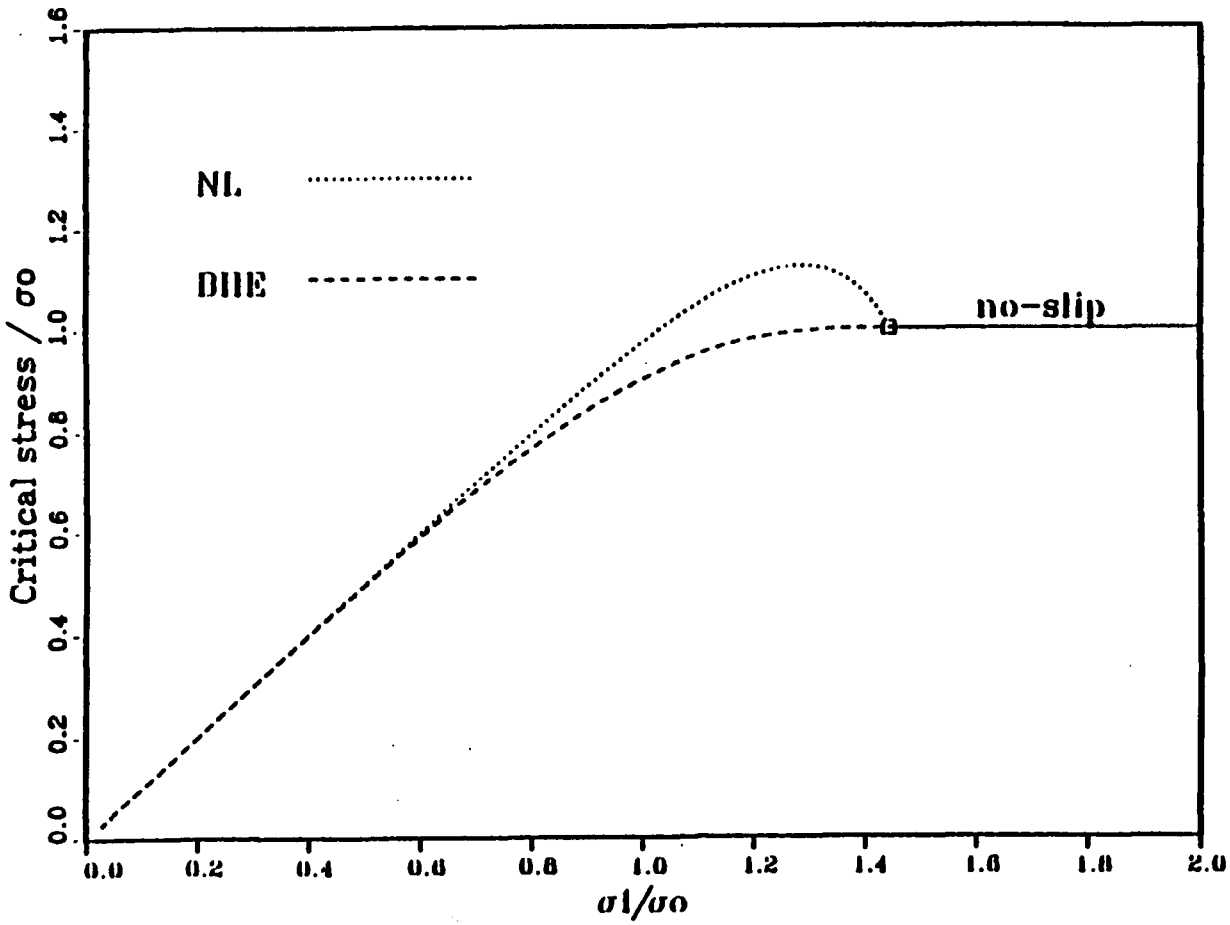

Fig. 6 Matrix cracking stress: unbonded, frictionally constrained fibers.

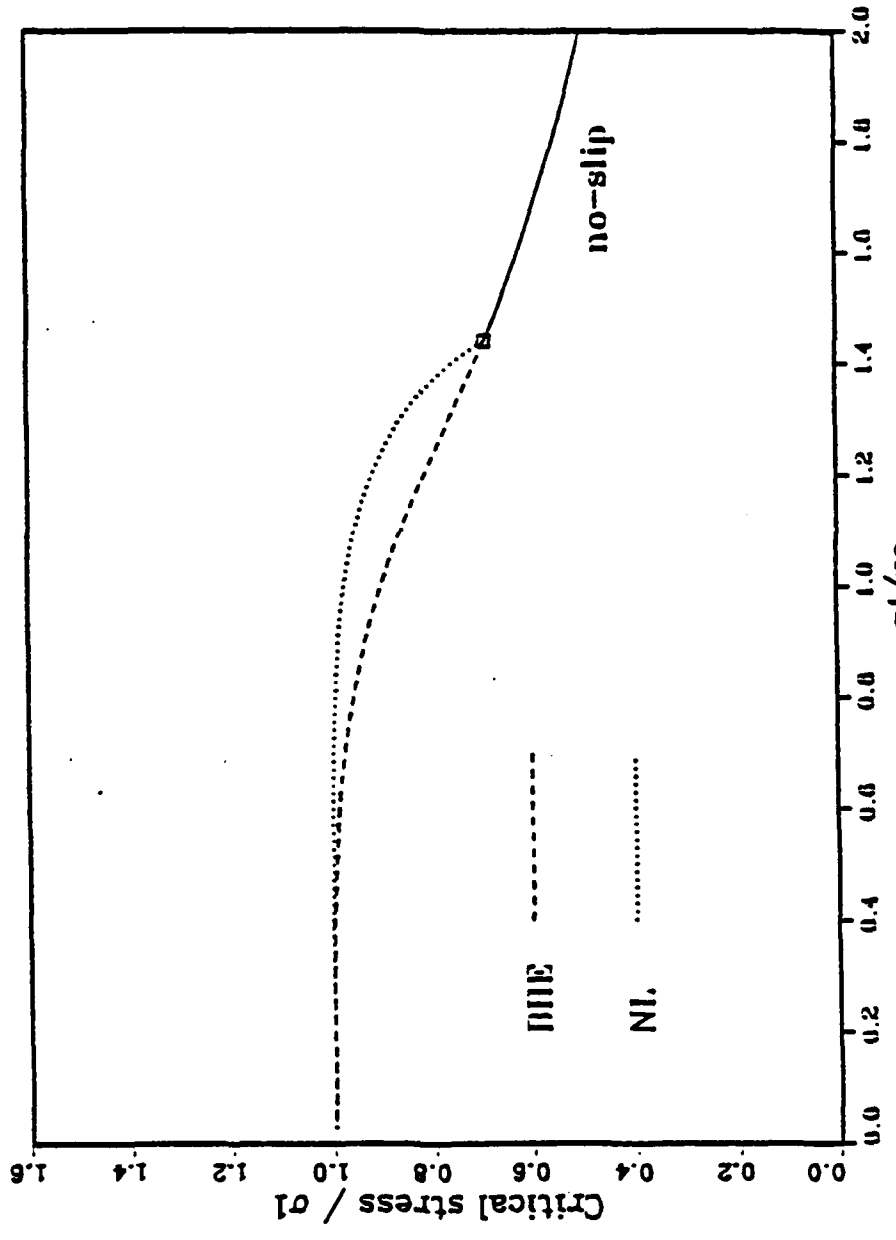

Fig. 7 Matrix cracking stress: unbonded, frictionally constrained fibers.

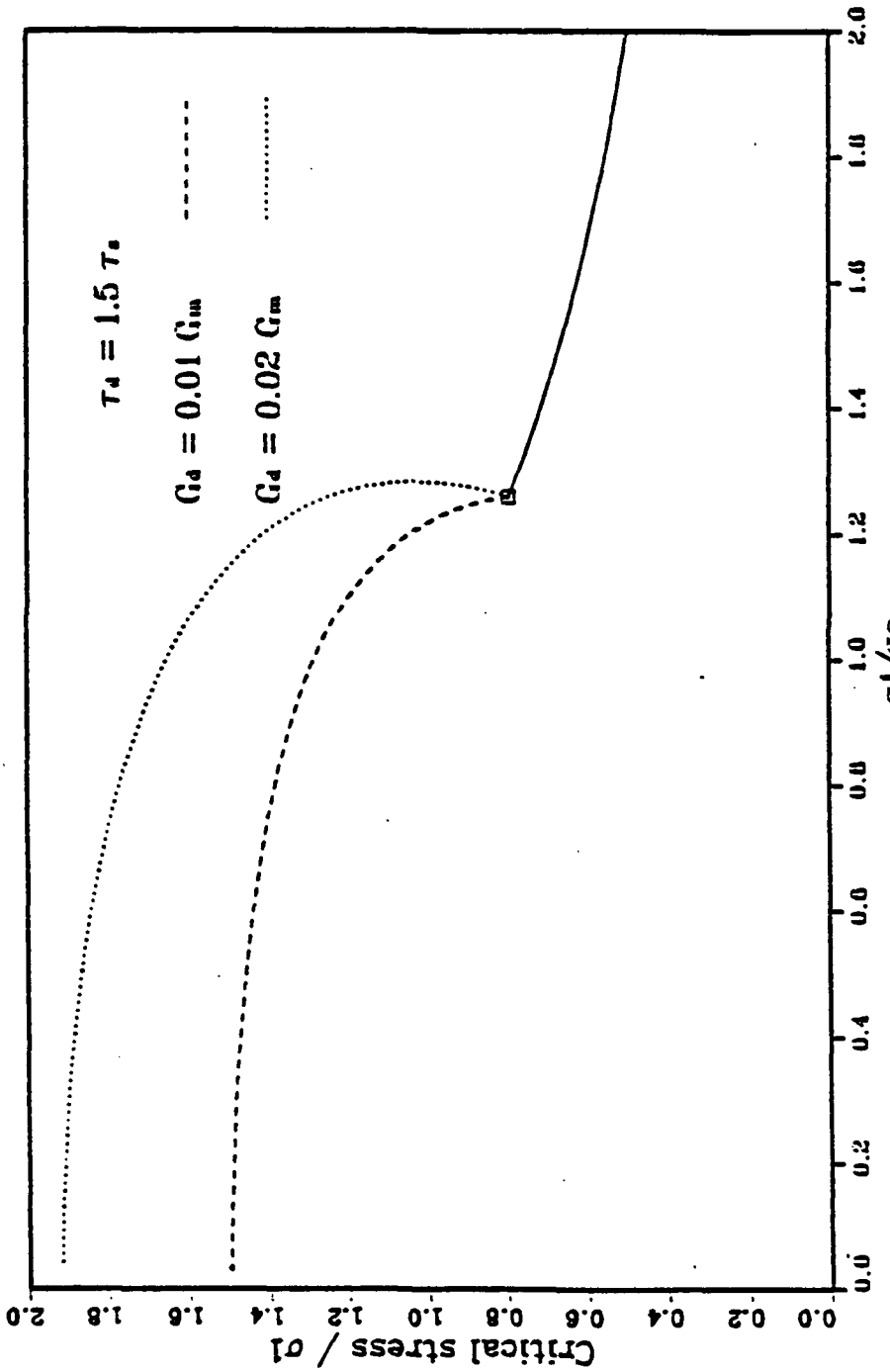

Fig. 8 Matrix cracking stress: initially bonded, frictionally constrained fibers.

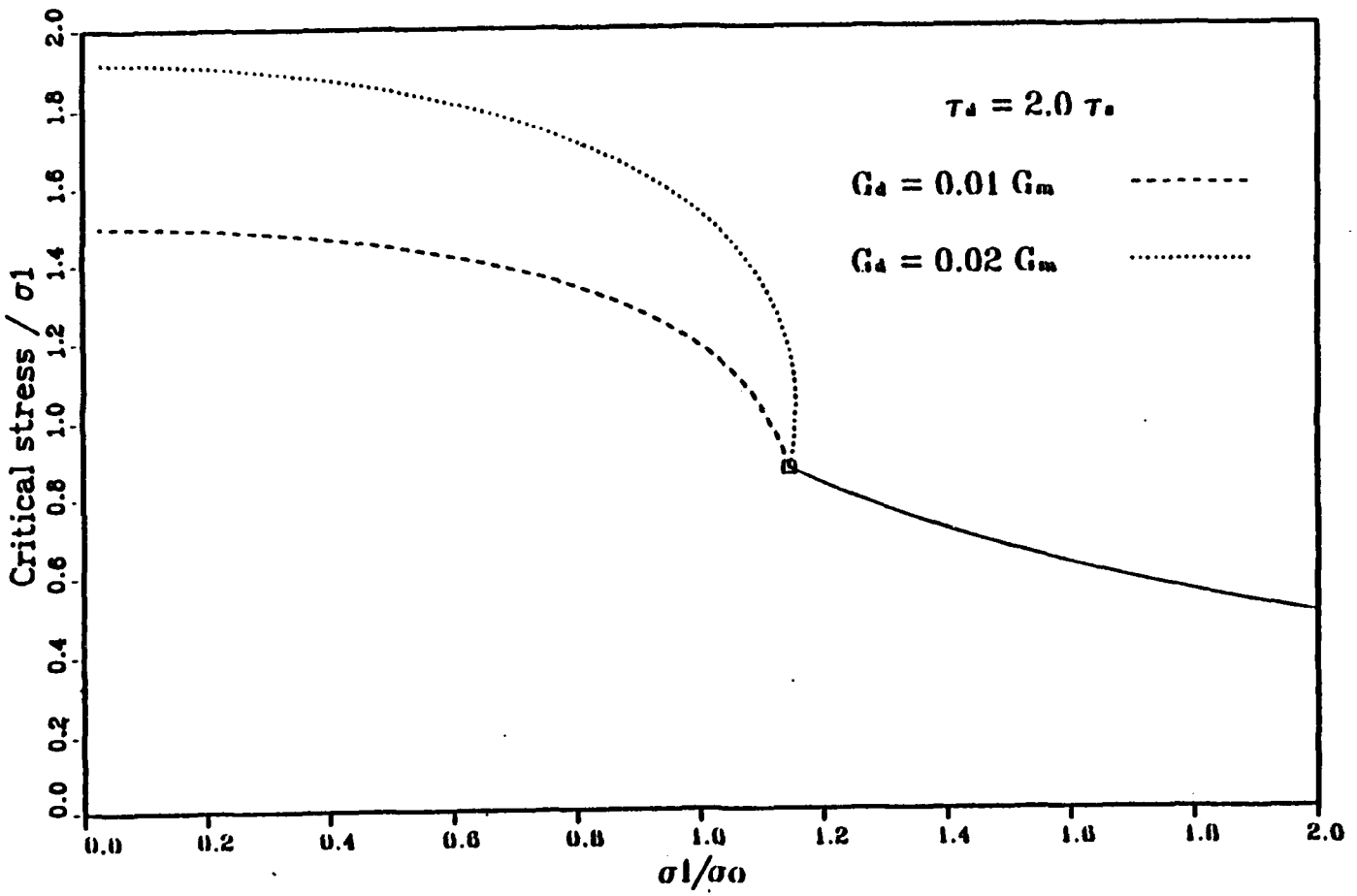

Fig. 9 Matrix cracking stress: initially bonded, frictionally constrained fibers.

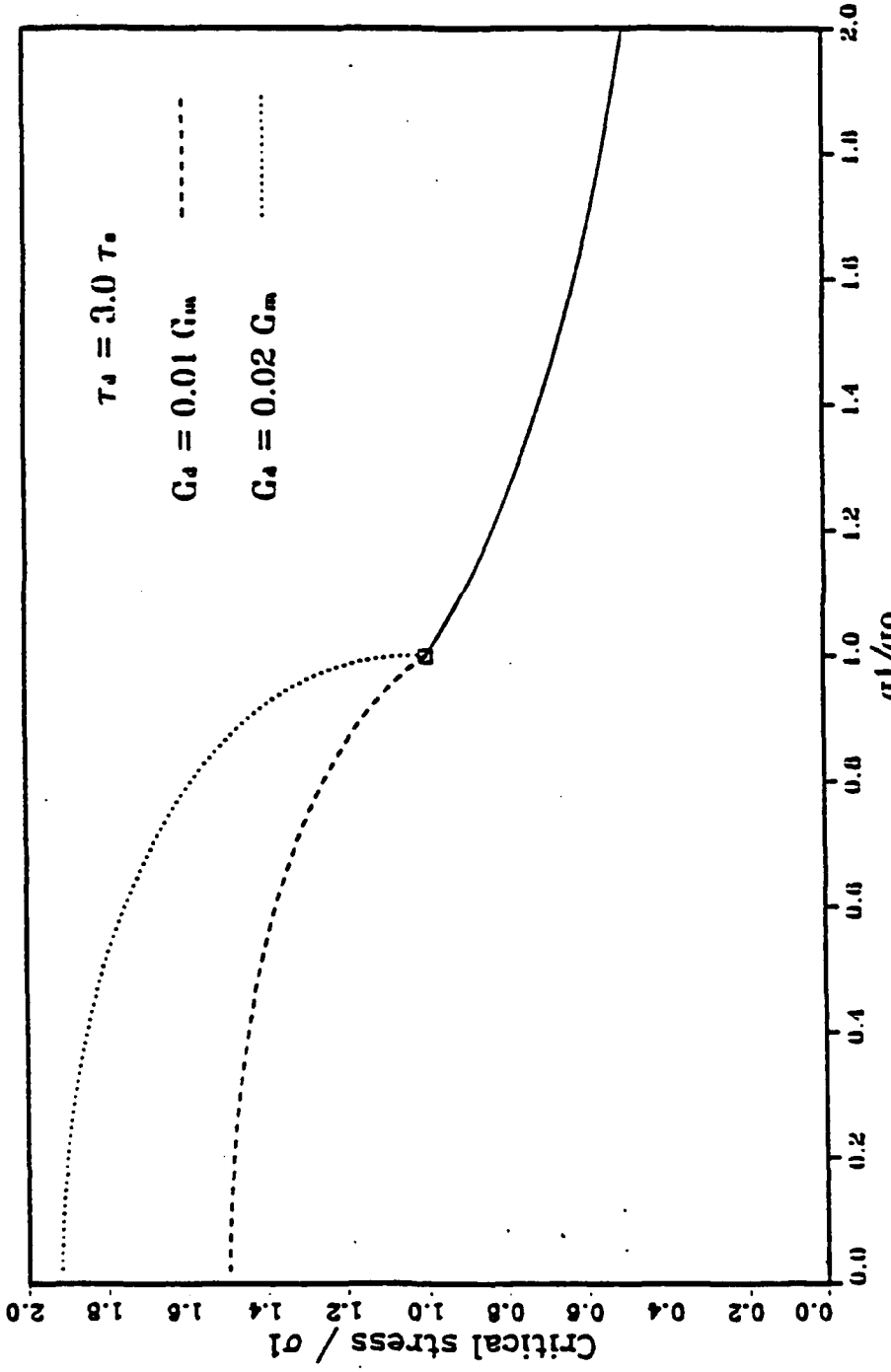

Fig. 10 Matrix cracking stress: initially bonded, frictionally constrained fibers.

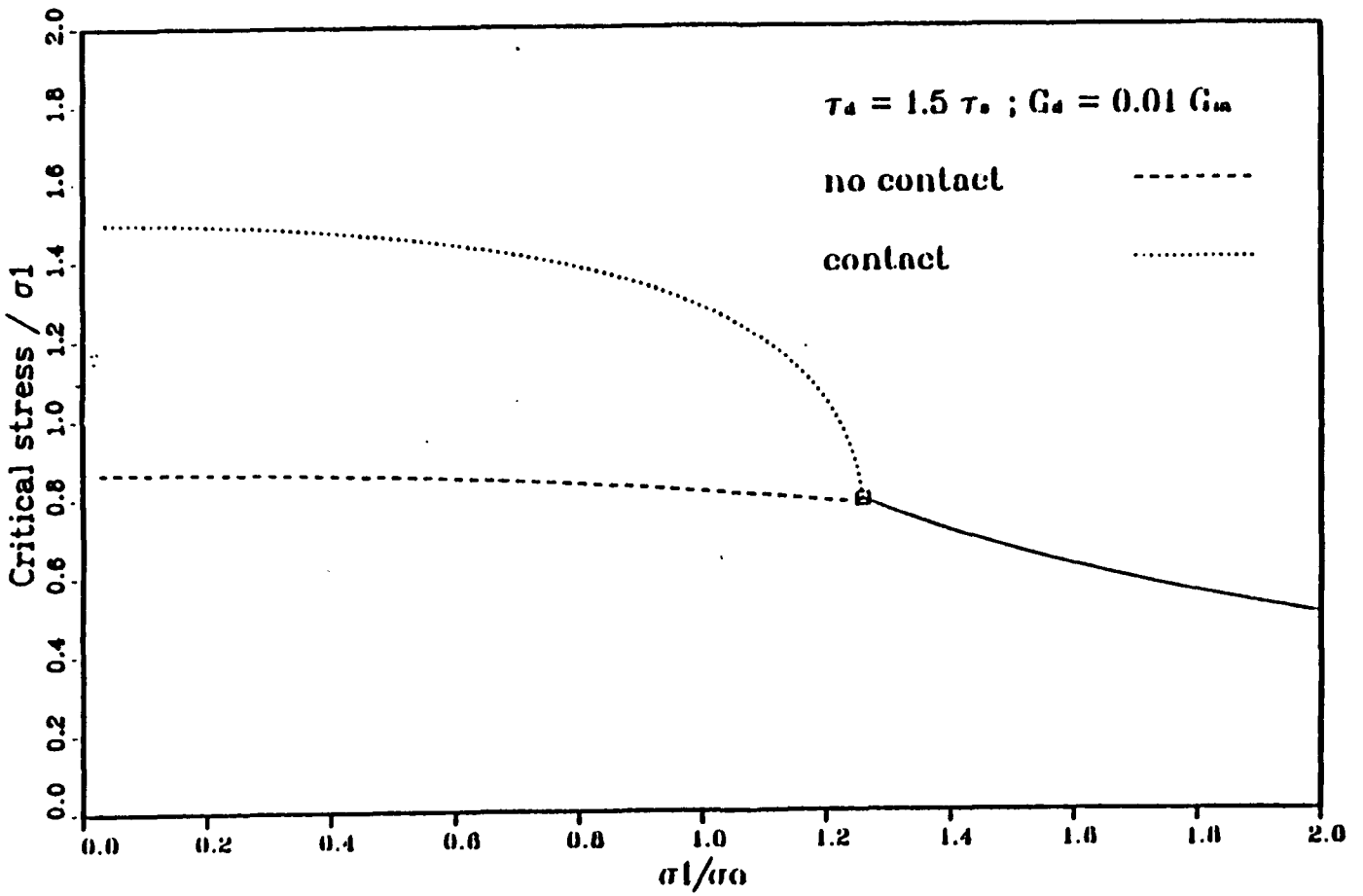

Fig. 11 Matrix cracking stress: initially bonded, debonding fibers: the effect of residual stress.

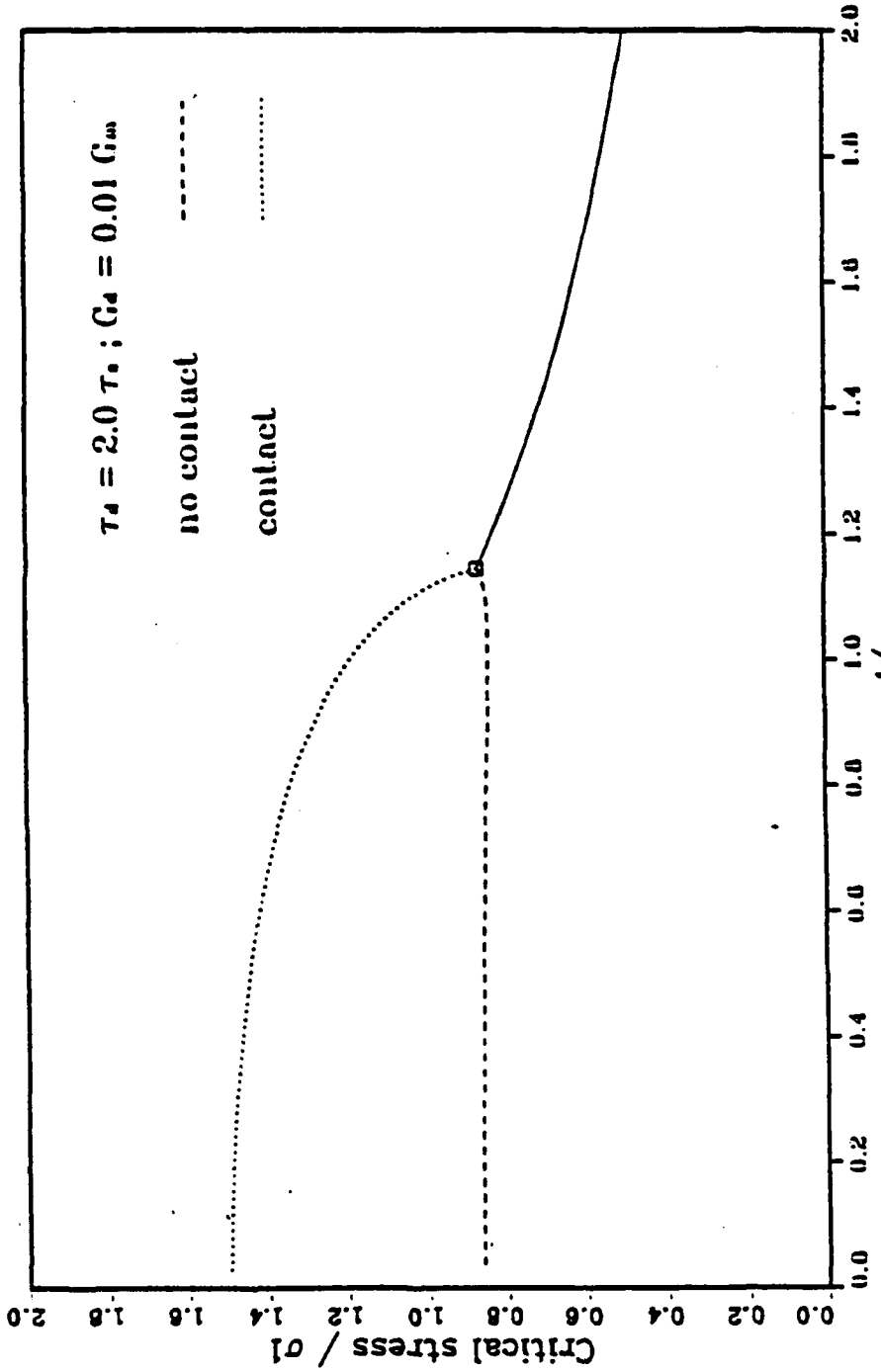

Fig. 12 Matrix cracking stress: initially bonded, debonding fibers: the effect of residual stress.

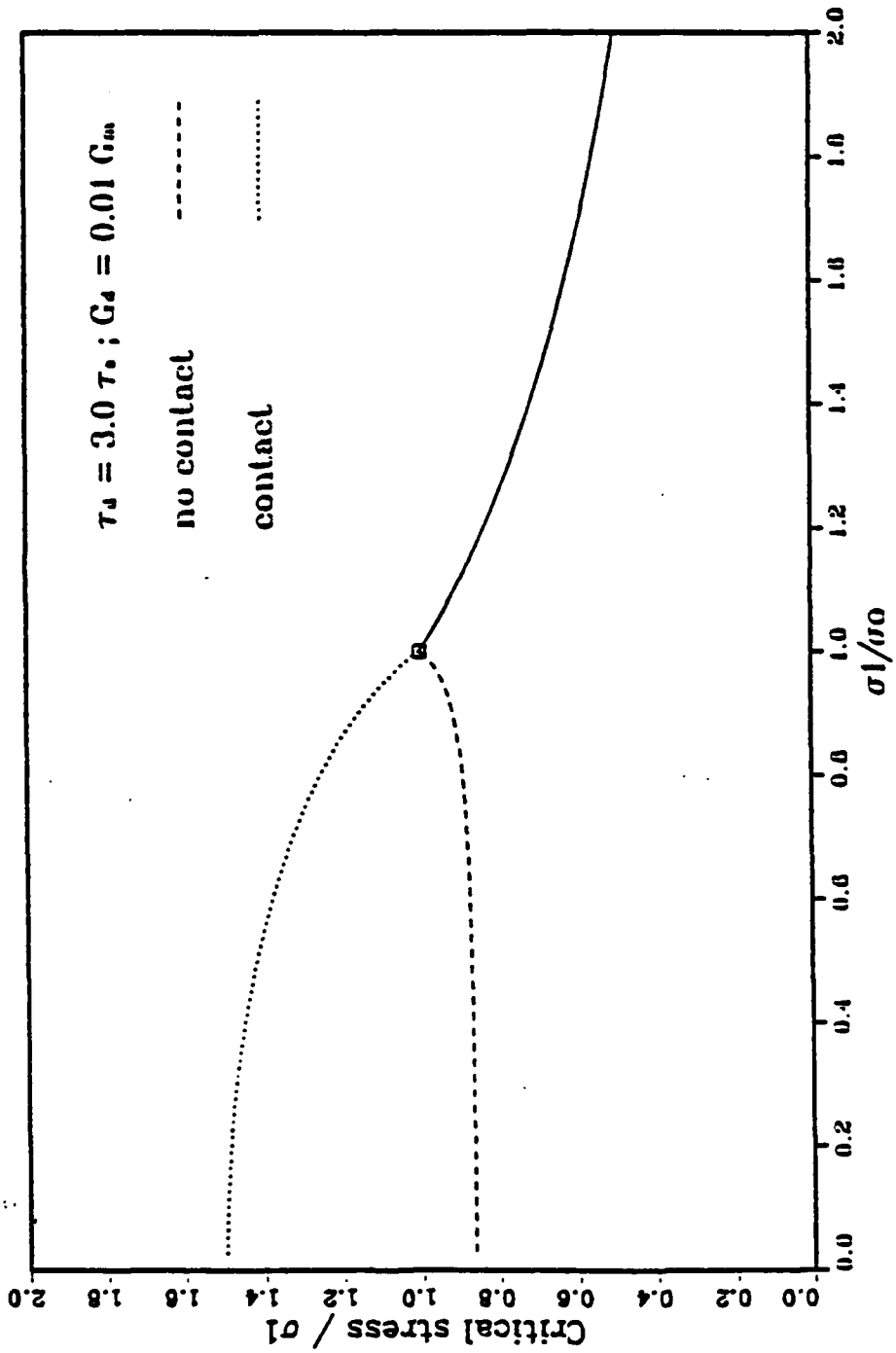

Fig. 13 Matrix cracking stress: initially bonded, debonding fibers: the effect of residual stress.

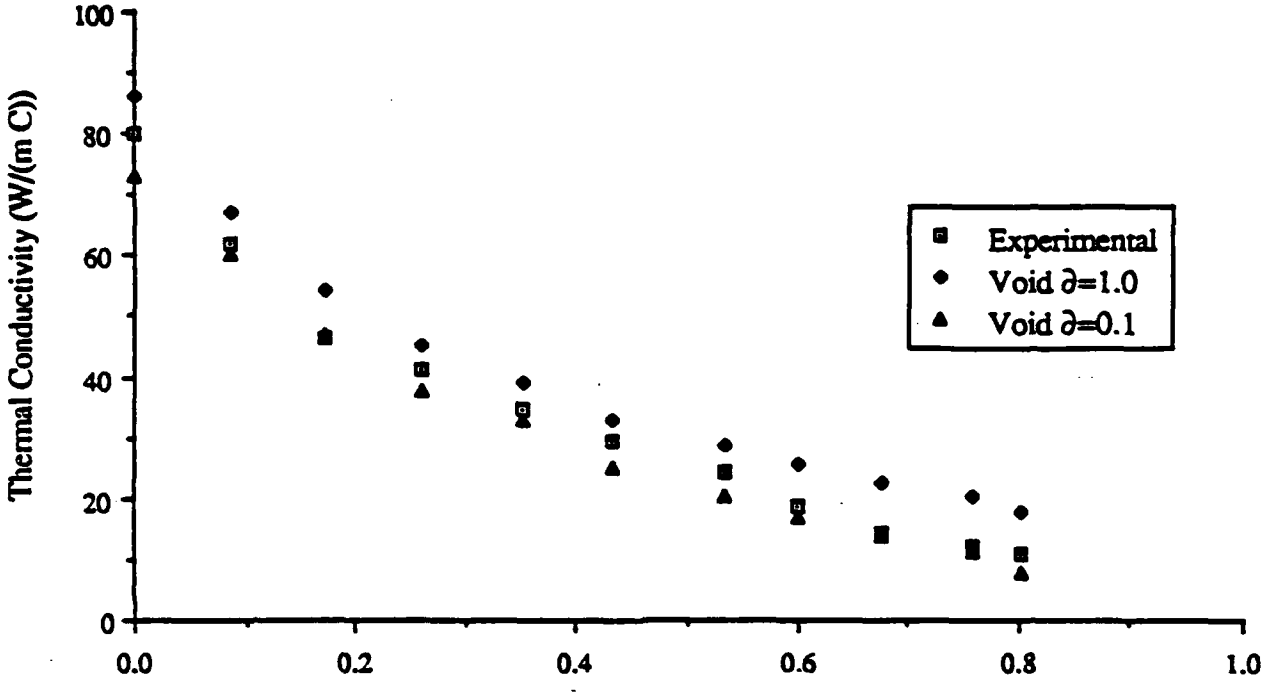

Fig. 14 Thermal conductivity of SiC/BN composites (containing voids of aspect ratio δ) parallel to the hot-pressing direction by the self consistent method.

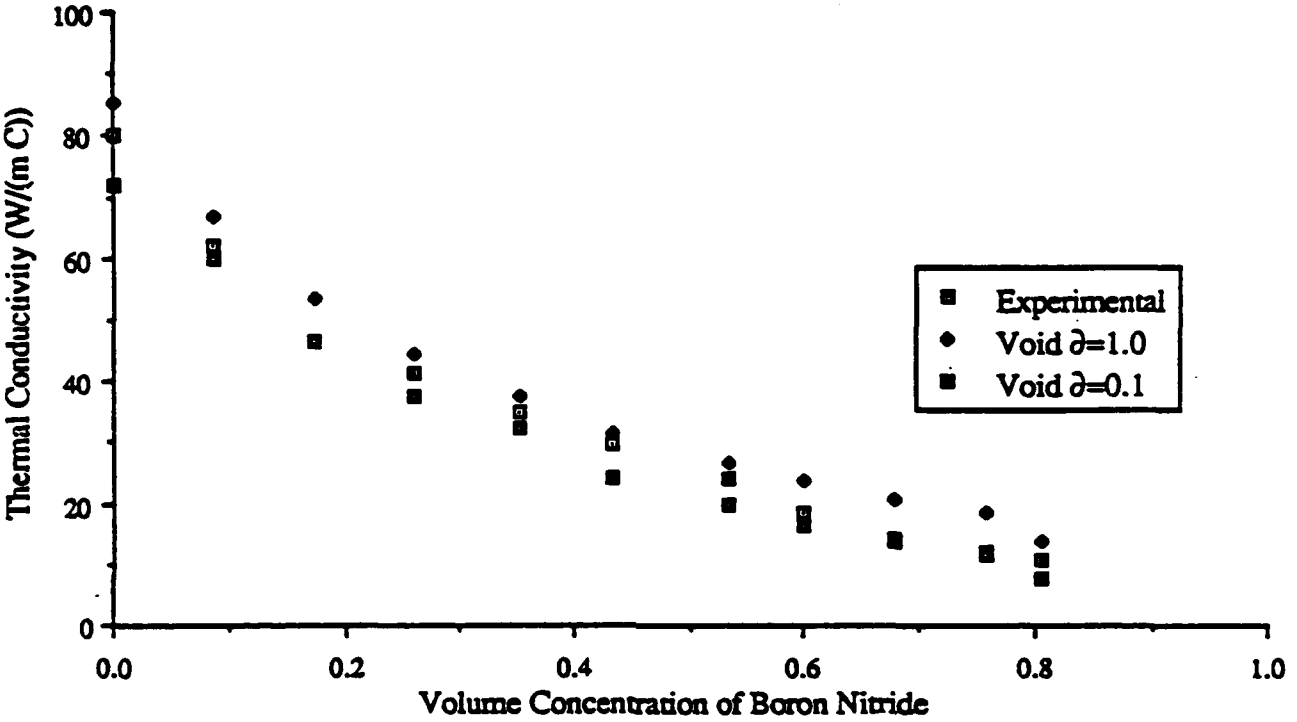

Fig. 15 Thermal conductivity of SiC/BN composites (containing voids of aspect ratio δ) parallel to the hot-pressing direction by the differential scheme.

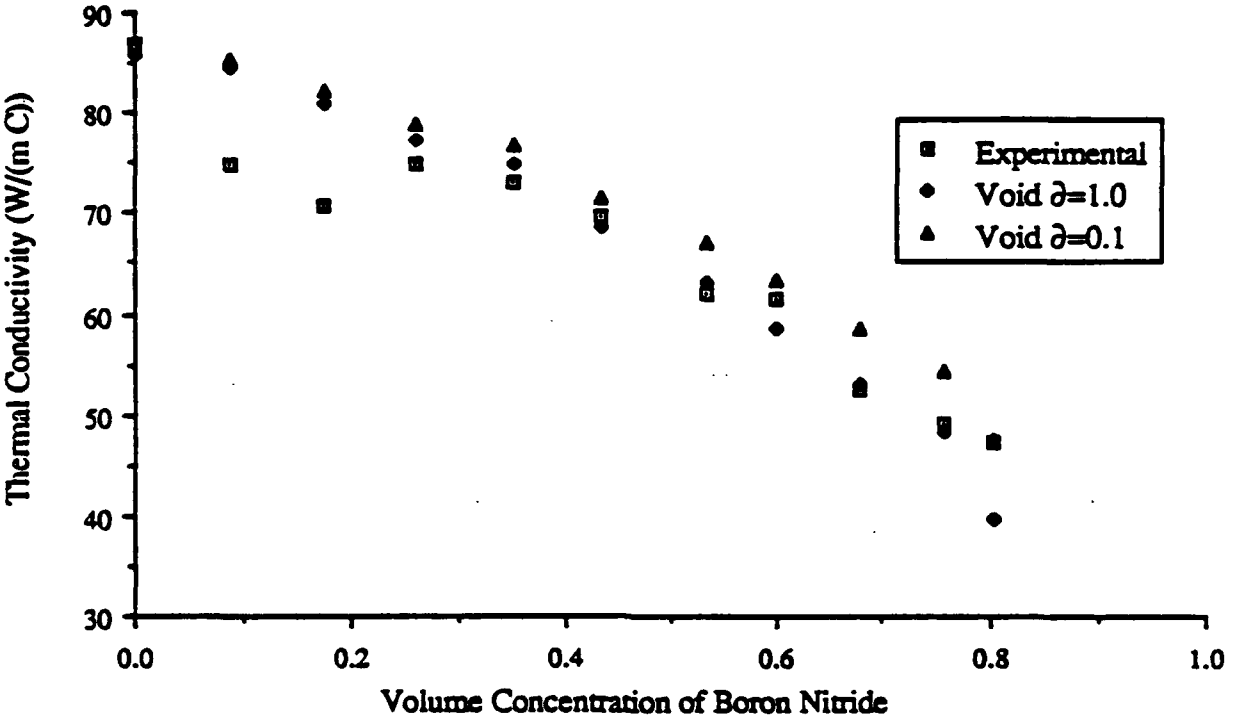

Fig. 16 Thermal conductivity of SiC/BN composites (containing voids of aspect ratio δ) parallel to the hot-pressing direction by the self consistent method.

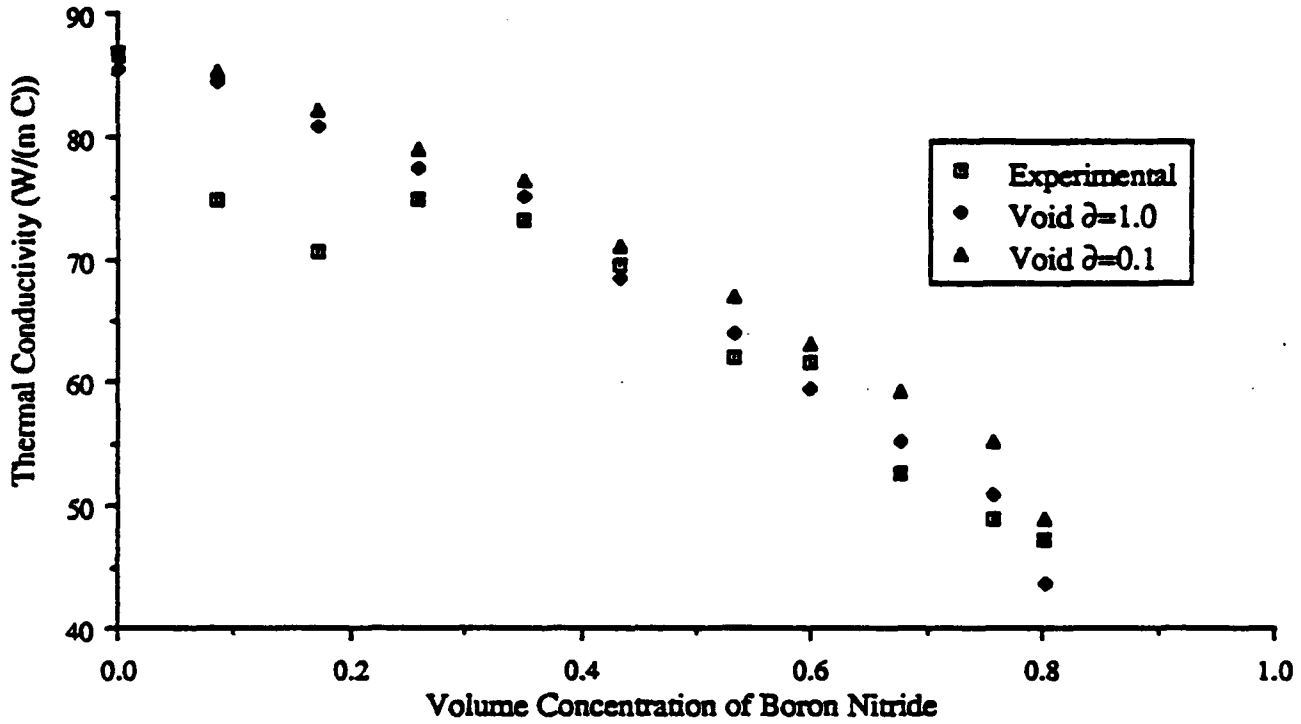

Fig. 17 Thermal conductivity of SiC/BN composites (containing voids of aspect ratio δ) parallel to the hot-pressing direction by the differential scheme.

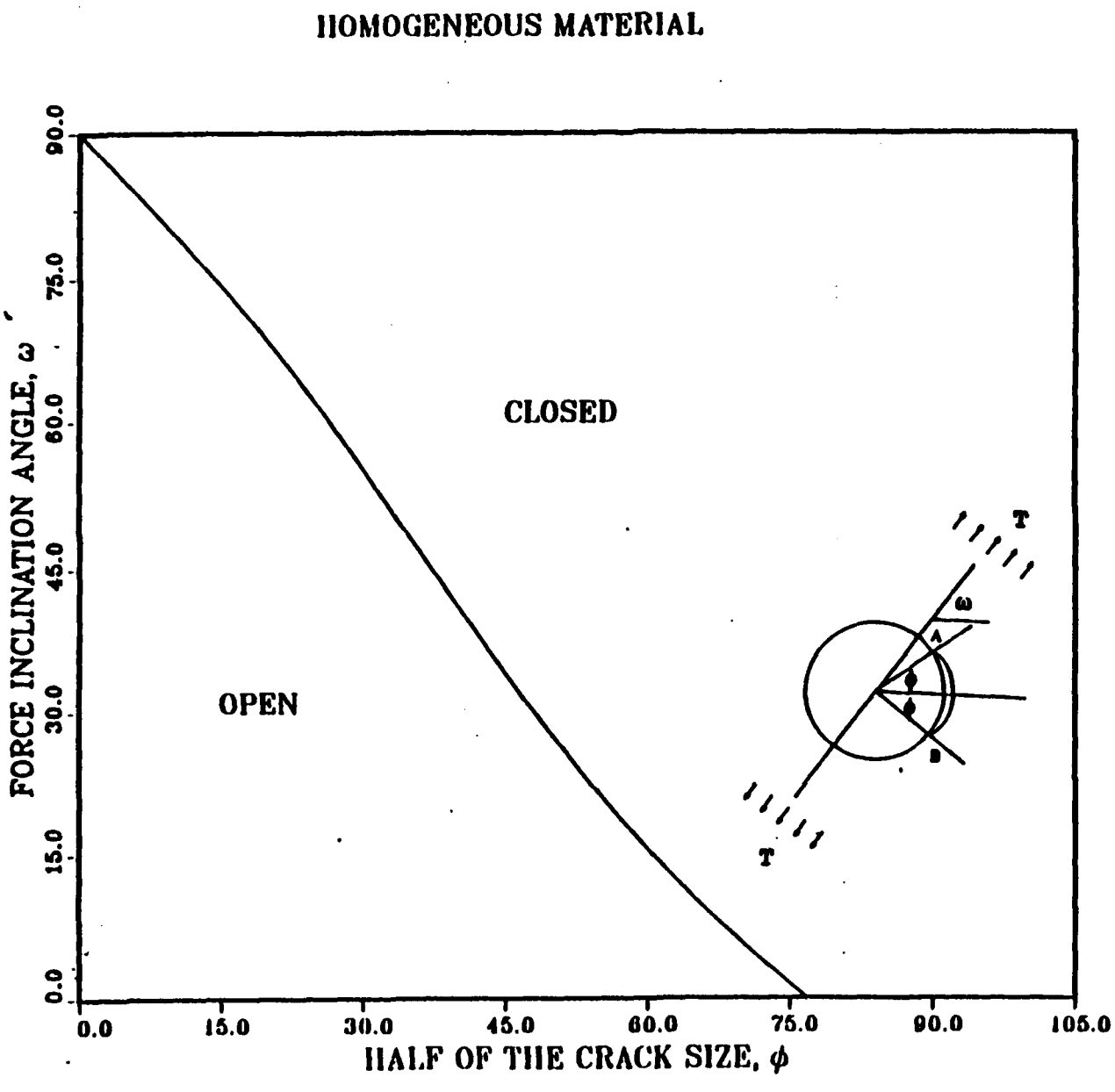

Fig. 18 Range of ω, ϕ for which arc crack remains open.

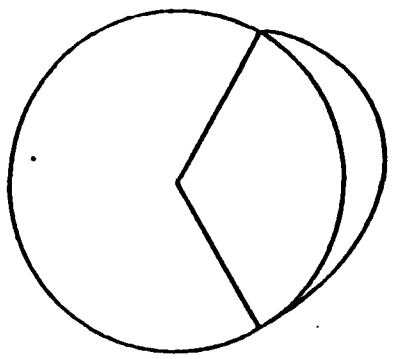

ω = 15.6 degrees

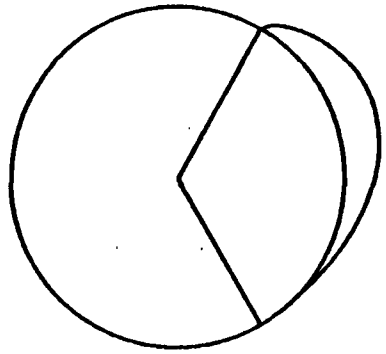

ω = 27.6 degrees

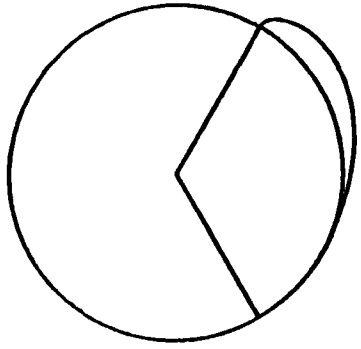

ω = 60.0 degrees

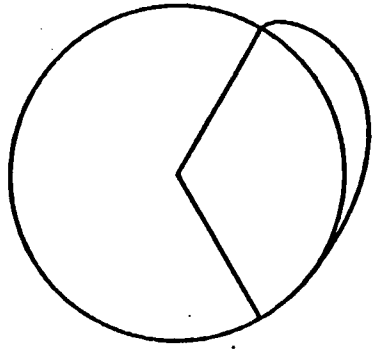

ω = 42.6 degrees

Fig. 19 Shape of partially closed crack for various load orientation with $\phi = 60°$ (not to scale).

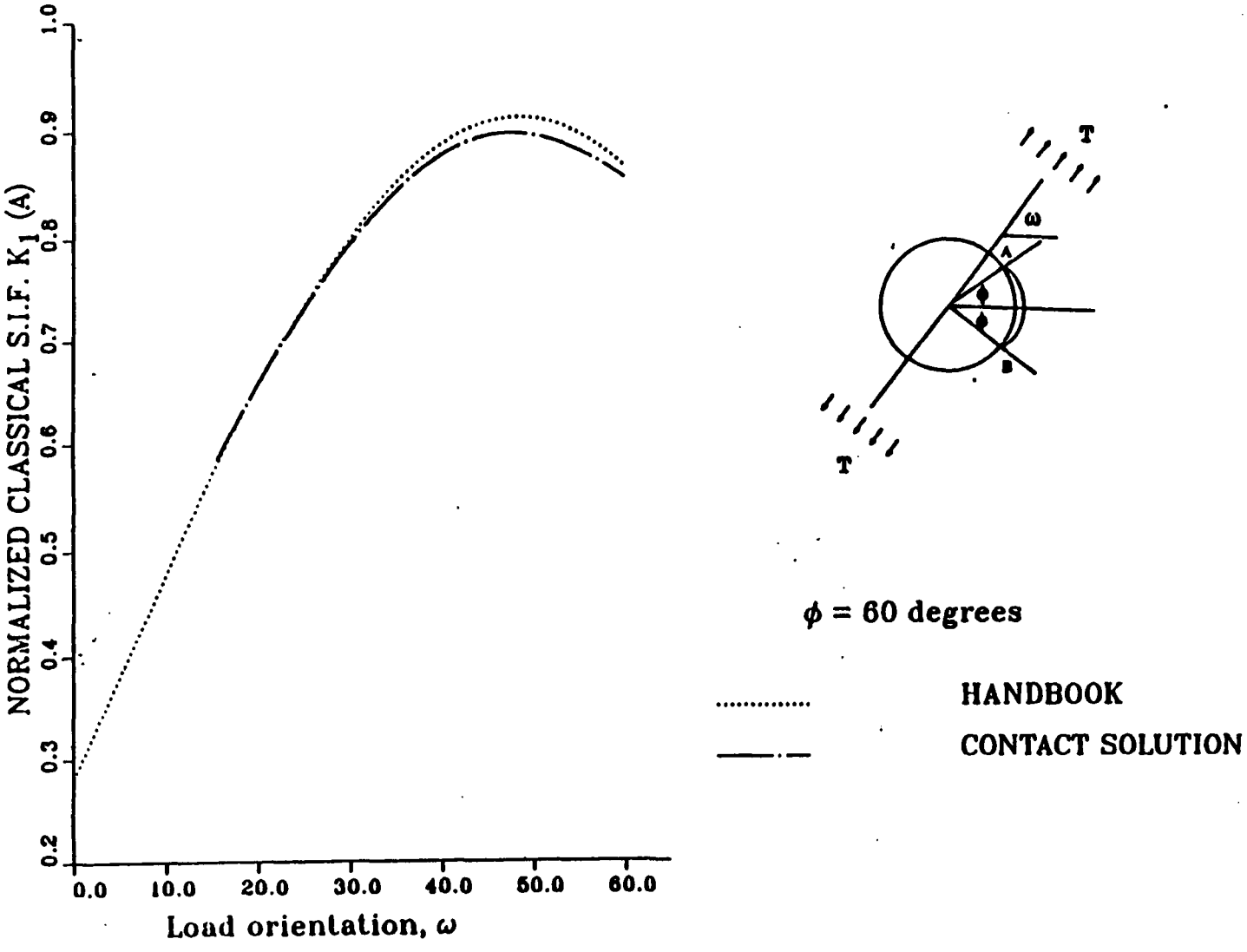

Fig. 20 Comparison of K_1 (A) for exact solution and handbook solution [34] when $\phi = 60°$..

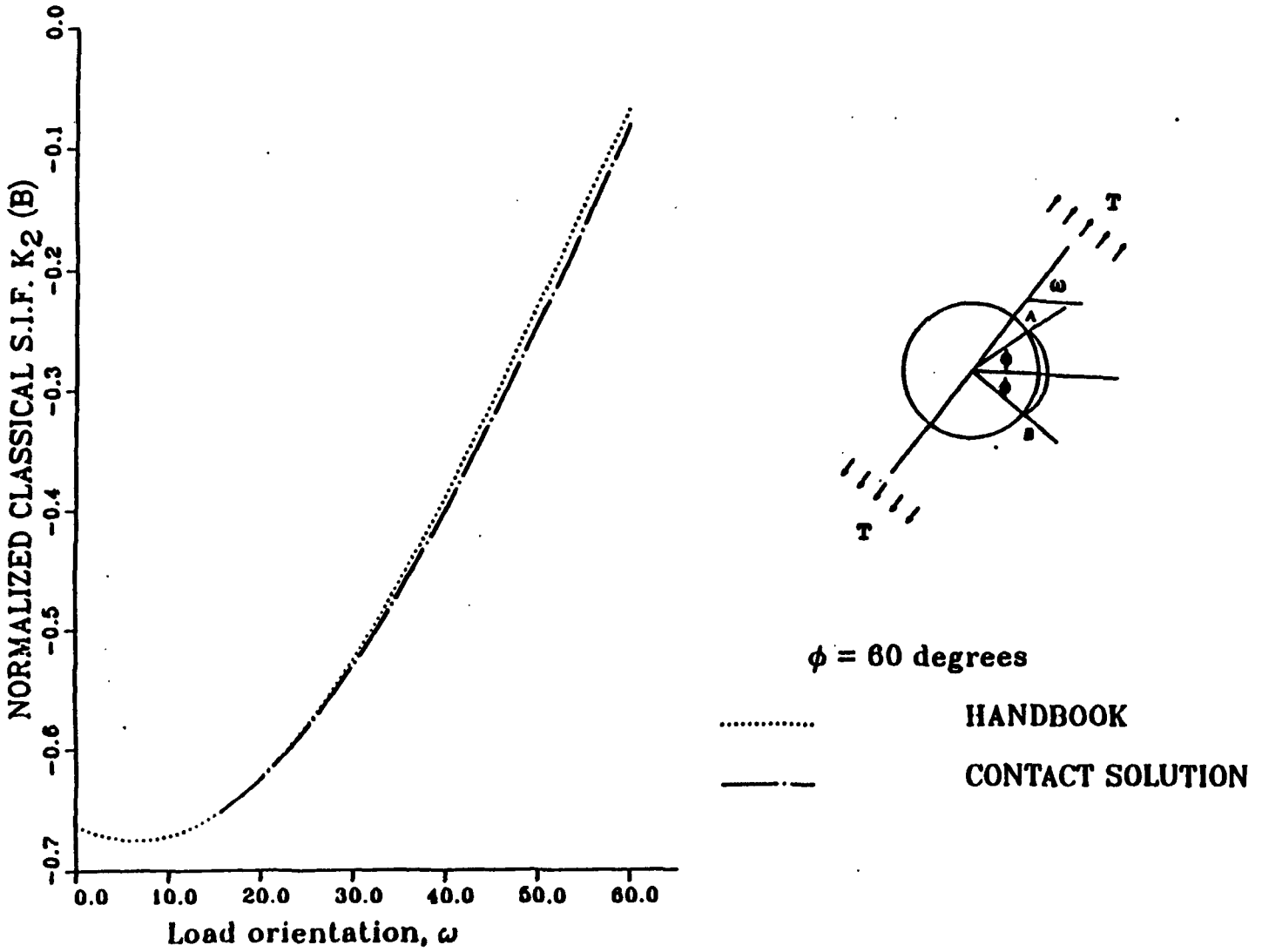

Fig. 21 Comparison of K_2 (B) for exact solution and handbook solution [34] when $\phi = 60°$..

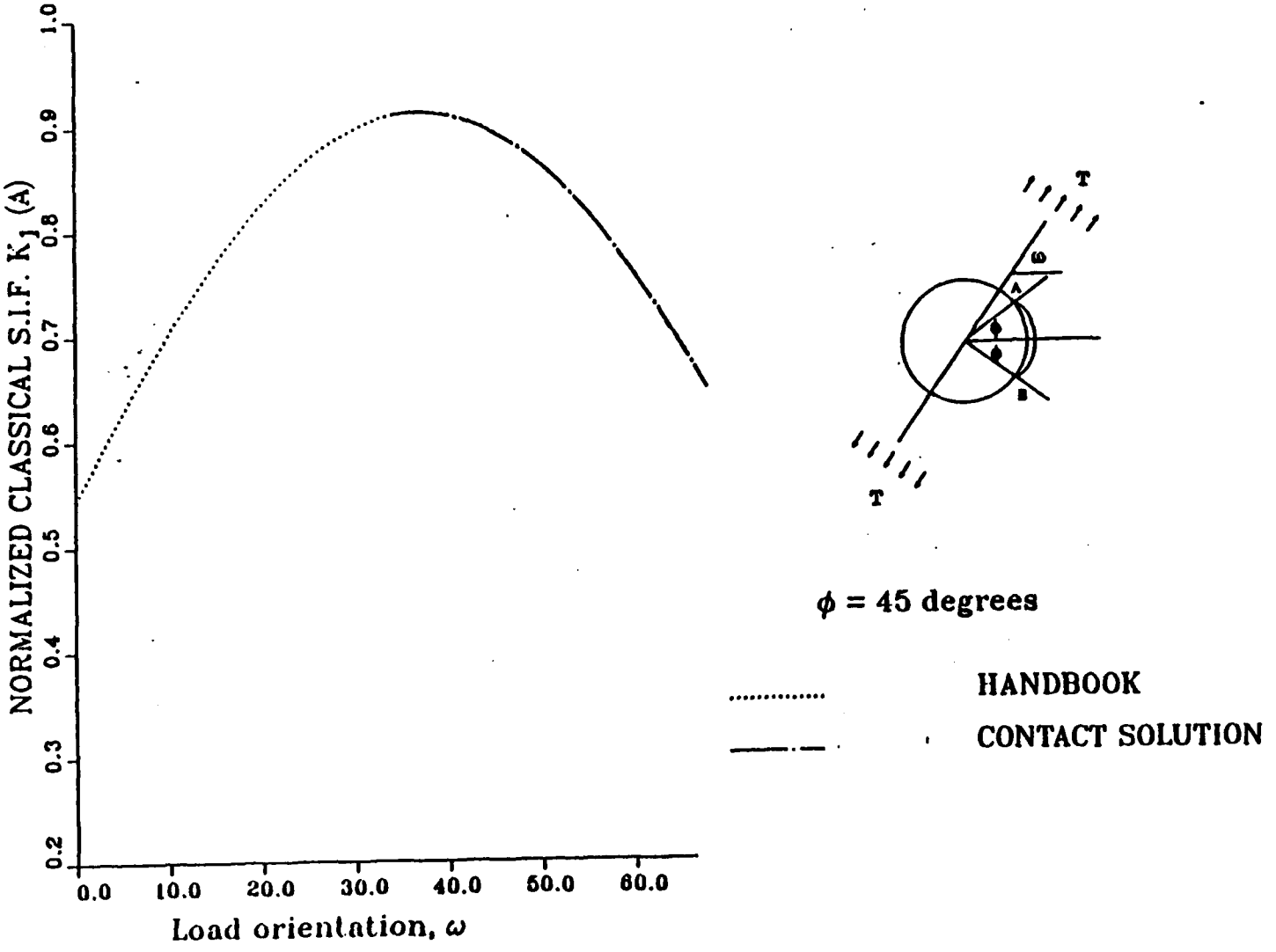

Fig. 22 Comparison of K_1 (A) for exact solution and handbook solution [34] when $\phi = 45°$.

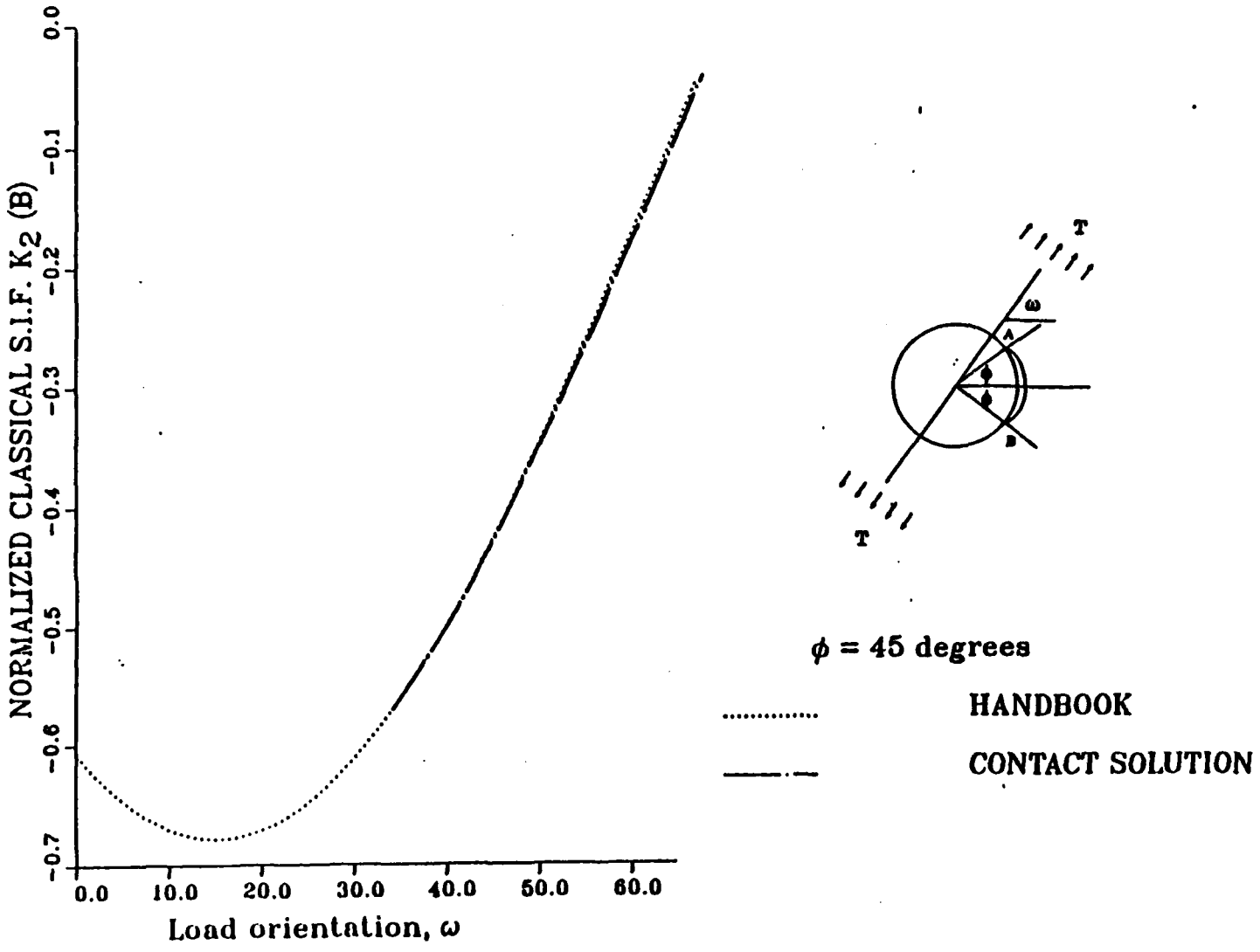

Fig. 23 Comparison of K_2 (B) for exact solution and handbook solution [34] when $\phi = 45°$.

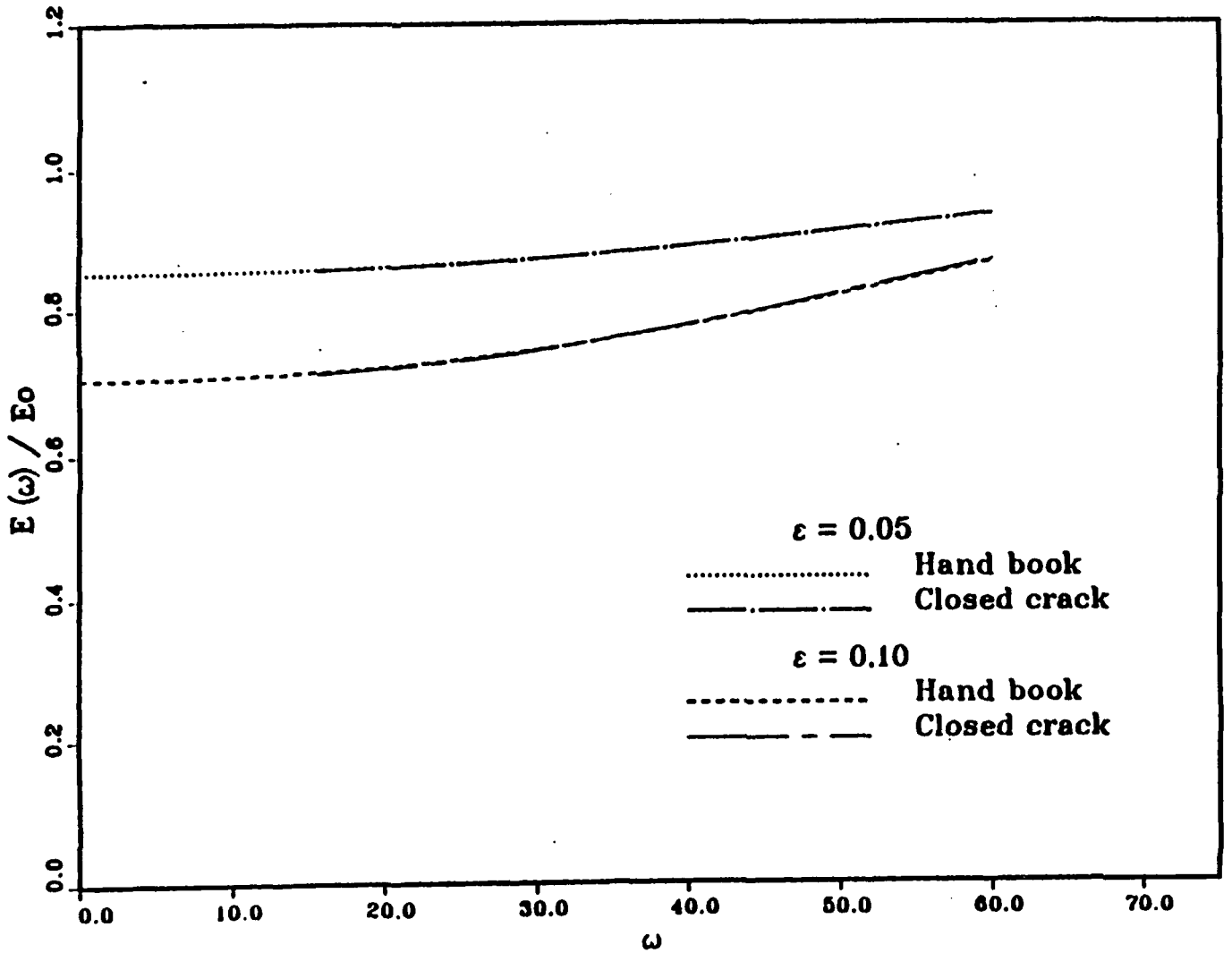

Fig. 24 Reduction in Young's modulus for given arc crack density (E), when $\phi = 60^{\circ}$ comparison of exact solution and handbook solution [34].

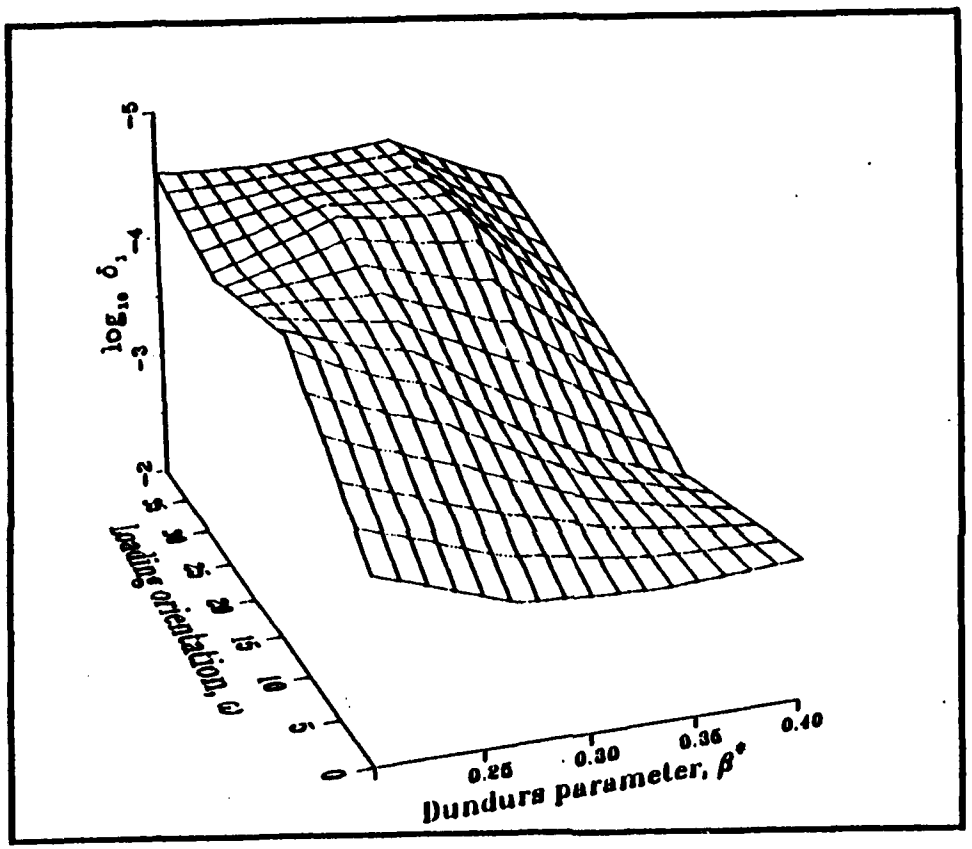

Fig. 25 Interfacial crack contact length (δ_1) at A for various values of the Dundurs parameter β^*, and load orientation, ω, when the first Dundurs parameter is $\alpha^* = 0.5$ and $\phi = 60°$.

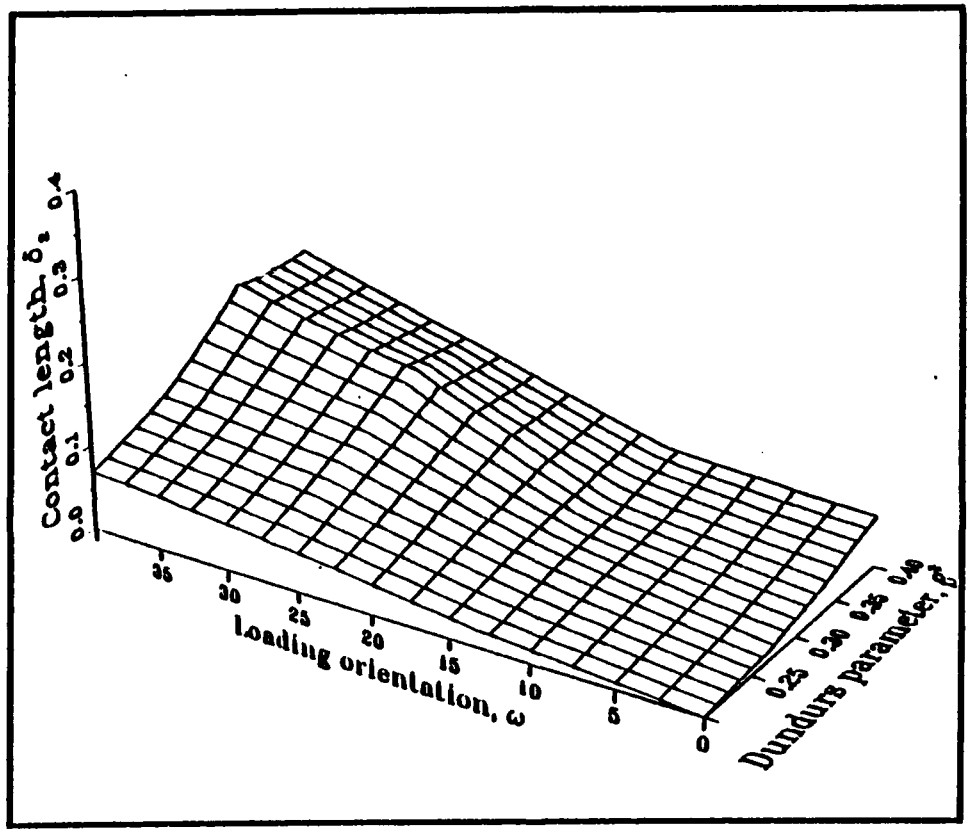

Fig. 26 Interfacial crack contact length (δ_2) at B for various values of the Dundurs parameter β^*, and load orientation, ω, when the first Dundurs parameter is $\alpha^* = 0.5$ and $\phi = 60°$.

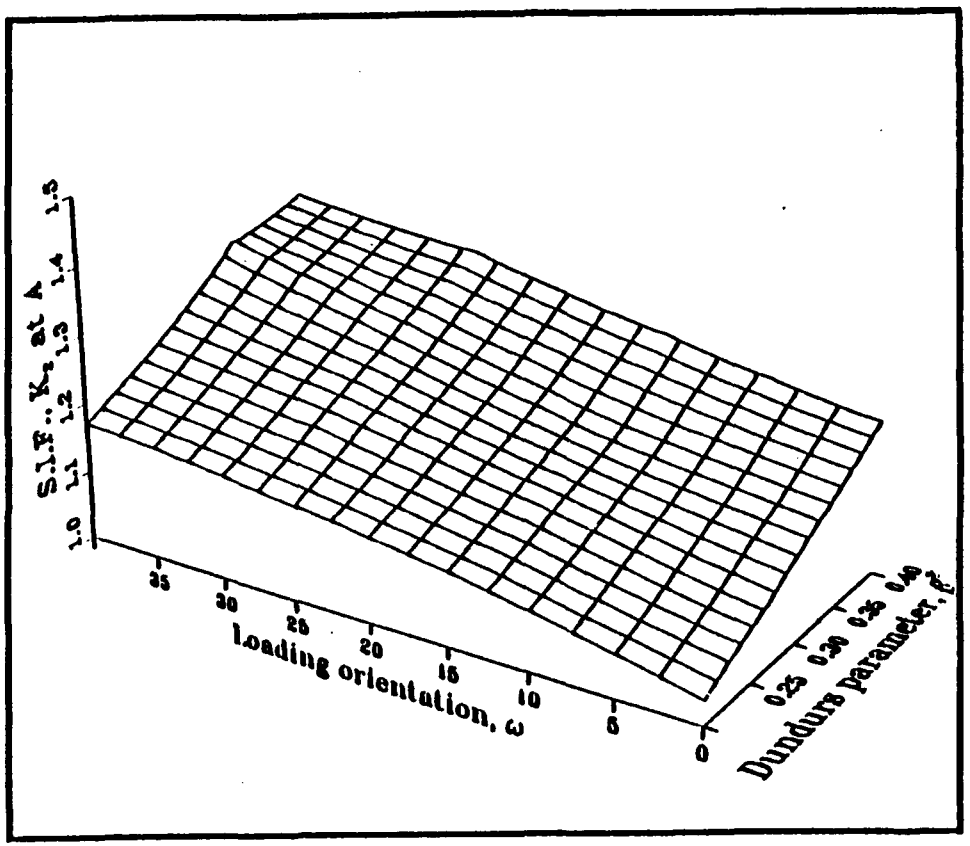

Fig. 27 Mode II S.I.F. at A for various values of the Dundurs parameter, β^*, and load orientation, ω, when the first Dundurs parameter $\alpha^* = 0.5$ and $\phi = 60°$.

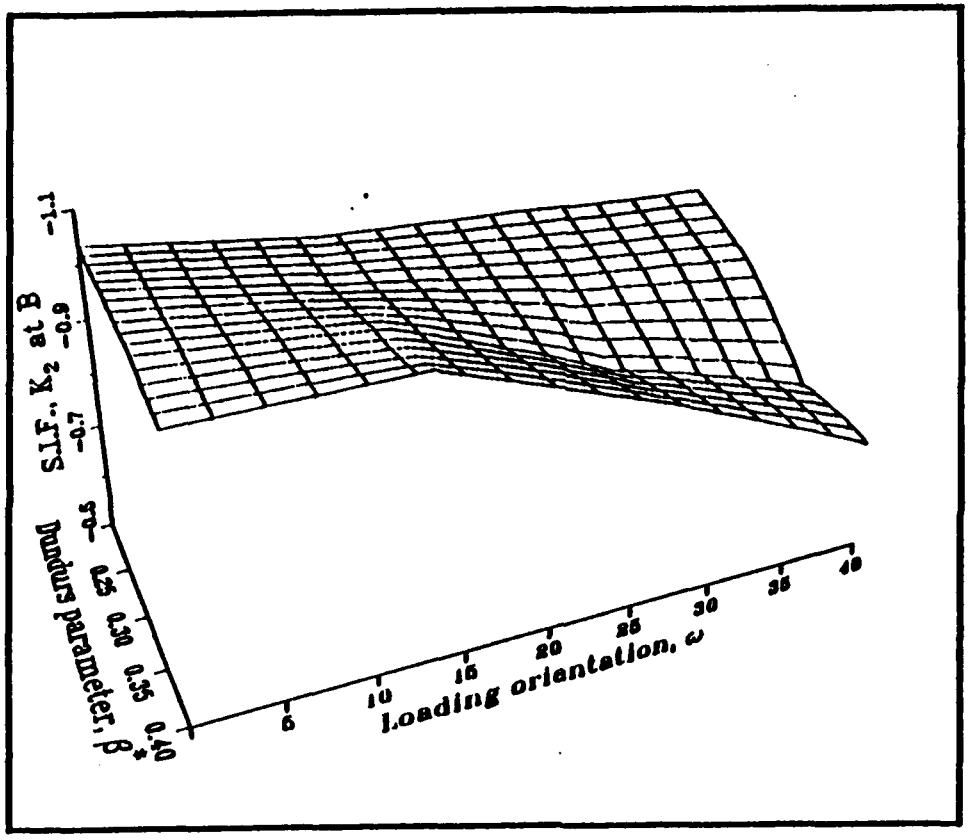

Fig. 28 Mode II S.I.F. at B for various values of the Dundurs parameter, β^*, and load orientation, ω, when the first Dundurs parameter $\alpha^* = 0.5$ and $\phi = 60°$.

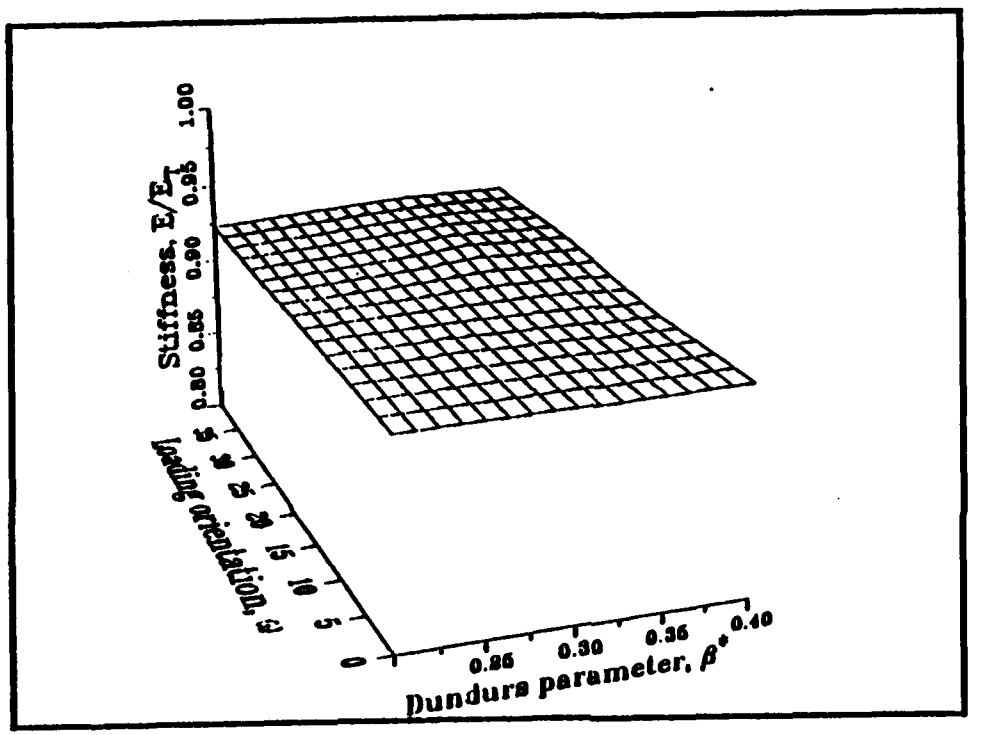

Fig. 29 Reduction in Young's modulus due to interfacial microcracking for various values of the Dundurs parameter, β^*, and load orientation, ω, when the first Dundurs parameter $\alpha^* = 0.75$, $\phi = 60°$ and the volume fraction of fibers = 0.05.

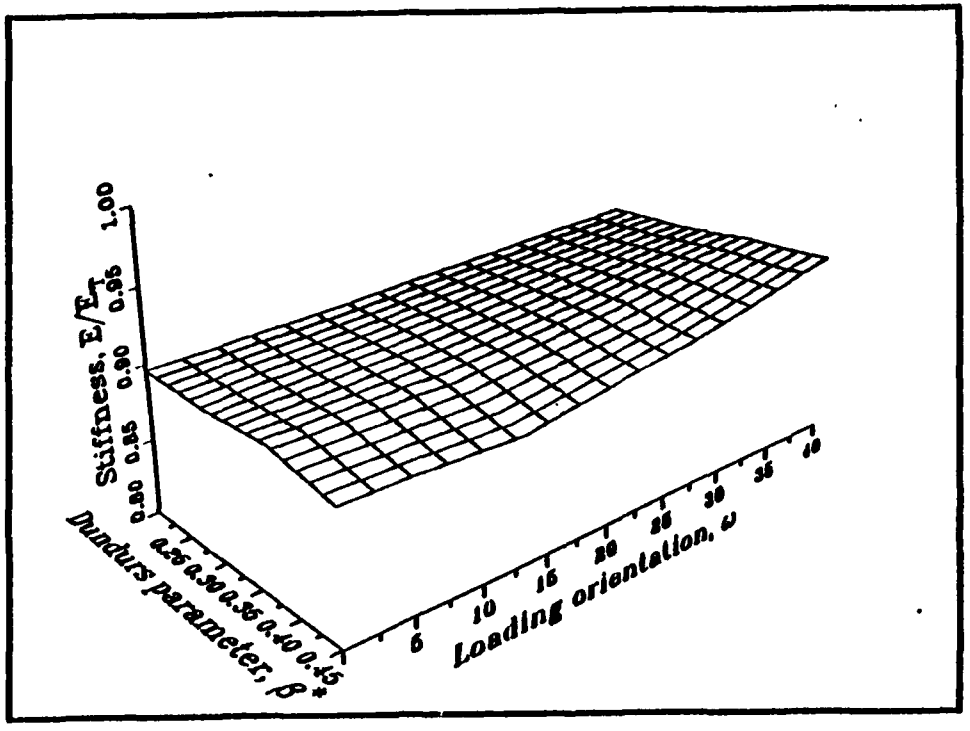

Fig. 30 Reduction in Young's modulus due to interfacial microcracking for various values of the Dundurs parameter, β^*, and load orientation, ω, when the first Dundurs parameter $\alpha^* = 0.5$, $\phi = 45°$ and the volume fraction of fibers = 0.1.

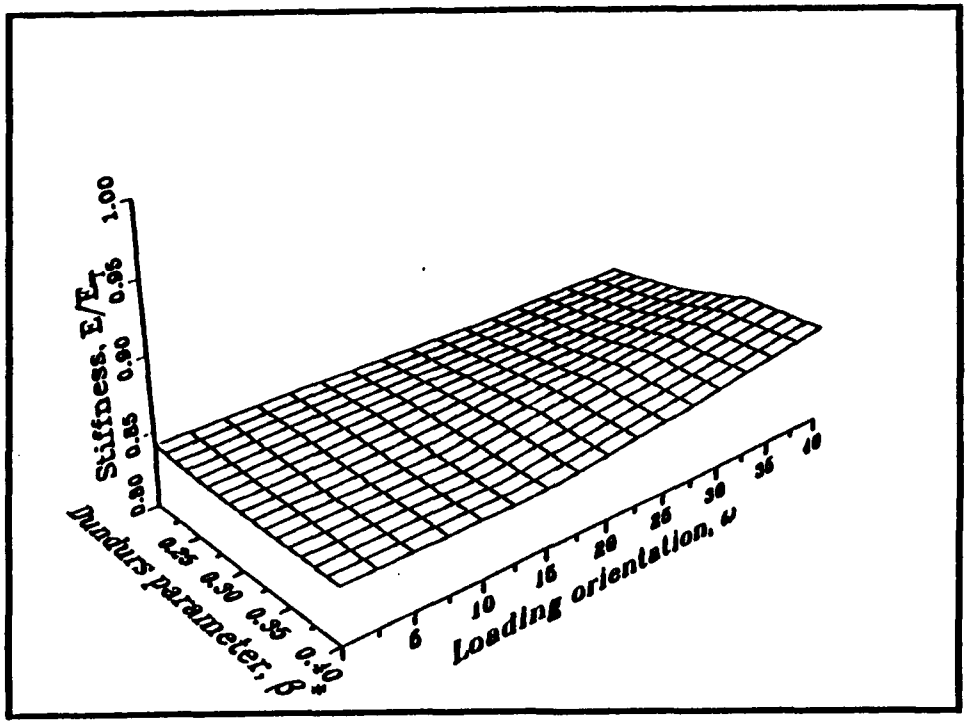

Fig. 31 Reduction in Young's modulus due to interfacial microcracking for various values of the Dundurs parameter, β^*, and load orientation, ω, when the first Dundurs parameter $\alpha^* = 0.5$ and $\phi = 60°$ and the volume fraction of fibers = 0.1.

6. LIST OF PUBLICATIONS

1. Laws, N., "Composite Materials: Theory v. Experiment," *J. Composite Materials*, *22*, 1988, 396.

2. Laws, N. and Dvorak, G. J., "Progressive Transverse Cracking in Composite Laminates," *J. Composite Materials*, *22*, 1988, 900.

3. Dvorak, G. J. and Laws, N., "Mechanics of Composite Materials - 1988," *ASME-AMD Vol. 92*, 1988.

4. Laws, N. and Dvorak, G. J., "Transverse Matrix Cracking in Composite Laminates," in Composite Materials Response (ed. by G. C. Sih, G. F. Smith, I. H. Marshall and J. J. Wu) Elsevier Applied Science, 1988, pp. 91-99.

5. Wang, J.B., Ph.D. dissertation "Stress Analysis of Cracked Cross-Ply Laminates, Theory and Applications," University of Pittsburgh, 1989.

6. Laws, N. and Lee J.C., "Microcracking in Polycrystalline Ceramics: Elastic Isotropy and Thermal Anisotropy," *J. Mech. Phys. Solids* *37*, 1989, 603.

7. Laws, N., "The Effect of Microcracks on Energy Density," International Symposium on the Mechanics and Physics of Energy Density, (ed. by E. E. Gdoutos and G. C. Sih) Elsevier Applied Science, 1990, pp. 189-195.

8 Chao, R. and Laws, N., "Loss of Stiffness Due to Microcracking in Unidirectional Ceramic Matrix Composites," *ASME-AMD Vol. 109*, 1990, pp. 57-62.

9. Chao, R., Ph.D. dissertation "Some Effects of Fiber-Matrix Interfacial Debonding on the Response of Uni-directional Ceramic Matrix Composite Materials," University of Pittsburgh, 1991.

10. Laws, N. and Wang, J.B., " A Complete Model for Transverse Cracking of Cross-Ply Composite Laminates," in preparation.

11. Engel, S. and Laws, N., "Thermal Conductivity of Some SiC/BN Composites," in preparation.

12 Chao, R. and Laws, N., "Closure of an Arc Crack Due to Uni-directional Loading," in preparation.

13. Chao, R. and Laws, N., "Loss of Stiffness of Uni-directional Ceramic Matrix Composites Due to Fiber-Matrix Interfacial Debonding," in preparation.

7. PRESENTATIONS

1. Georgia Institute of Technology, March 1988.
2. University of Windsor, Canada, April 1988.
3. ASME/SES Summer Meeting, University of California, June 1988.
4. Cranfield Institute of Technology, July 1988.
5. University of Nottingham, England, March 1989.
6. International Symposium on the Mechanics and Physics of Energy Density, Xanthi, Greece, August 1989.
7. Fourteenth Annual Mechanics of Composites Review, Dayton, OH, October 1989.
8. IUTAM Symposium on Inelastic Deformation of Composite Materials, RPI June 1990.
9. ASME Winter Annual Meeting, Dallas, November 1990.
10. University of Pittsburgh, February 1991.
11. Princeton University, April 1991.

ADDITIONAL ACTIVITIES

1. Chairman of Mechanics session at Symposium on Interfacial Phenomena in Composites; Processing, Characterization and Mechanical properties, Newport, RI, June 1988.
2. Joint organizer (with G. J. Dvorak) of Composite Materials Symposium at ASME/SES Summer Meeting, University of California, Berkeley. The proceedings were published as in 6.3.
3. Joint organizer (with T-W Chou) of Ceramic Matrix Composite Symposium at ASME Winter Annual Meeting, Chicago 1988.
4. Chairman of various sessions at many technical meetings.

8. PROFESSIONAL PERSONNEL

Dr. N. Laws	Principal Investigator
Dr. J. B. Wang	Graduate Student, Ph.D. awarded 1989
Mr. R. Chao	Graduate Student, Ph.D. awarded 1991
Mr. S. Engel	Graduate Student
Ms. V. Radel	Graduate Student

9. COPIES OF SELECTED PAPERS

(i) Progressive Transverse Cracking in Composite Laminates

(ii) Microcracking in polycrystalline ceramics: elastic isotropy and thermal anisotropy

(iii) The effect of microcracks on energy density

(iv) Loss of stiffness due to microcracking in unidirectional ceramic matrix composites.

Progressive Transverse Cracking In Composite Laminates

NORMAN LAWS
Department of Mechanical Engineering
University of Pittsburgh
Pittsburgh, PA 15261

GEORGE J. DVORAK
Department of Civil Engineering
Rensselaer Polytechnic Institute
Troy, NY 12180

(Received July 30, 1987)

1. INTRODUCTION

THE DEVELOPMENT OF a satisfactory theory for cross-ply laminates which have been damaged by transverse matrix cracking under monotonic loading has attracted a substantial number of investigators. The formulation of a shear lag model appears to have been first proposed in a series of papers by Bailey and his co-workers [1,2,3,4,5,6]. This work, in turn, relies on some studies of unidirectional composites by Aveston and Kelly [6]. Subsequent contributions to the theory have geen given by Wang [7], Highsmith and Reifsnider [8], Flaggs and Kural [9], Nuismer and Tan [10], Manders, Chou, Jones and Rock [11], Fukunaga, Chou, Peters and Schulte [12], Flaggs [13], Ohira [14] and Ogin, Smith and Beaumont [15,16]. Doubtless a diligent search of the literature would disclose other related work.

In an important series of papers Wang and Crossman [17,18] and Wang and his co-workers [19,20,21] have discussed transverse cracking from a different point of view. And, importantly for the present investigation, the work of these authors contains some comprehensive experimental data on the progressive transverse cracking of composite laminates.

Additional work on the loss of stiffness of cracked composite laminates which is based on three-dimensional stress analysis has been given by Laws and Dvorak [22,23,24,25] and Hashin [26].

It is not our aim here to give a critical survey of the existing literature. Nor do we attempt to point out the various similarities and differences between the published work and the work described below. Nevertheless, there are some major differences which should be emphasized here.

Reprinted from *Journal of* COMPOSITE MATERIALS, *Vol. 22—October 1988*

In the first place, the existence of residual stresses is fully accounted for throughout the whole of this analysis. Actually, we show that such stresses demand that there is a permanent strain when the applied load is large enough to cause transverse cracking. Physically this result is obvious. However, it turns out, both theoretically and experimentally, that this permanent strain is negligible. But perhaps the main difference between the model proposed here and existing models, lies in our treatment of the statistics of progressive cracking. In particular we note that Bailey et al. [1–5] assume that cracks always occur midway between existing cracks, whereas Manders et al. [11] and Fukunaga et al. [12] use a Weibull strength distribution of the transverse ply in their discussion of progressive cracking. On the other hand Wang and Crossman [17] introduce distributions of effective flaw sizes and locations in the transverse ply. By way of contrast, the approach adopted here supposes that a transverse crack will propagate when it is energetically favorable and that the location of this transverse crack is associated with a probability density function. Clearly, a crucial issue is the specification of this probability density function. Based on simple fracture mechanics we suggest a precise choice for the required probability density, namely that it is proportional to the stress in the transverse ply. Of course, normalization gives the factor of proportionality. This choice is explored and shown to give good agreement with experiment.

Given this choice of probability, the only parameter used here which is not determined by standard tests is the so-called shear lag parameter. However, we show that one can *infer* this parameter from standard data and knowledge of the first ply failure stress. We therefore, propose an explicit formula for the determination of the shear lag parameter ξ. We remark that the values thus obtained do not agree with those obtained from a formula, due to Garrett and Bailey [1].

Thus, the present analysis provides a well-defined model for transverse cracking in cross-ply composite laminates based on statistical fracture mechanics. This model is well-defined in the sense that no adjustable parameters are available to fit a particular set of experiments. Amongst other things, the model delivers explicit formulae for the loss of stiffness as a function of crack density, and for crack density as a function of applied load.

2. BASIC EQUATIONS

For simplicity, we are here concerned with a strictly one-dimensional theory of symmetric cross-ply composite laminates. In addition, we only consider monotonic simple tensile loading, see Figure 1. Generalization to angle-ply laminates and biaxial loading will be reported in a further paper.

It is well known that the strength of composite laminates depends upon the residual stresses due to cool-down. Thus let the initial stresses in the laminate be σ_t^R and σ_ℓ^R in the transverse and longitudinal plies respectively. Here, and subsequently, the subscripts t and ℓ are used to denote transverse and longitudinal respectively. Obviously

$$b\sigma_t^R + d\sigma_\ell^R = 0 \tag{1}$$

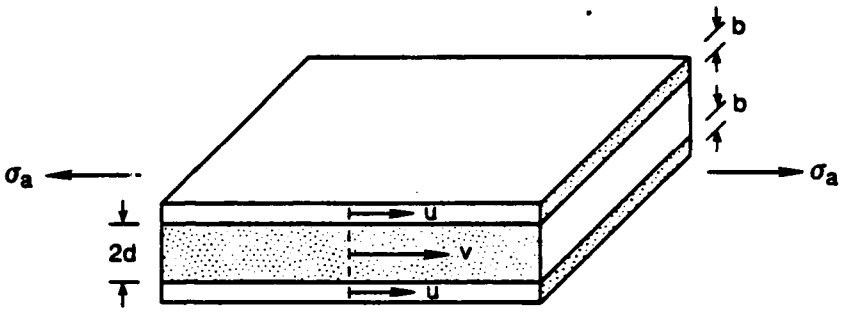

Figure 1. Symmetric cross-ply laminate under axial load.

where b is the thickness of the outer 0° plies and d is the half-thickness of the inner 90° plies, see Figure 1.

As usual, it is convenient to measure displacements from the state of initial stress with no mechanical loading. In shear lag theory, it is assumed that the displacement of a particular layer is uniform over the thickness of that layer: let $u(x)$ be the displacement of the 0° layer and $v(x)$ be the displacement of the 90° layer. The associated strains of the longitudinal and transverse plies are:

$$\epsilon_l = \frac{du}{dx}, \qquad \epsilon_t = \frac{dv}{dx} \tag{2}$$

Young's modulus for the uncracked laminate is, in this approximation,

$$E_0 = \frac{bE_l + dE_t}{b + d} \tag{3}$$

Let σ_l, σ_t be the *total* stress in the respective plies, then overall equilibrium of the laminate demands that

$$b\sigma_l + d\sigma_t = (b + d)\sigma_a \tag{4}$$

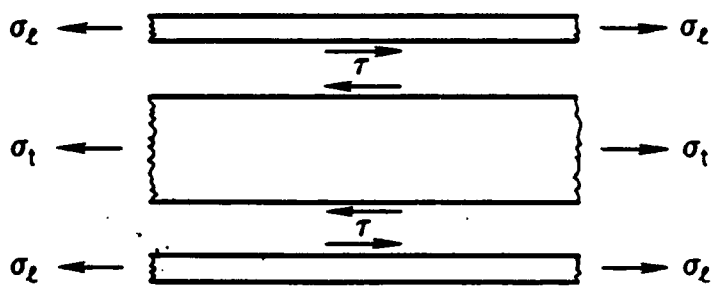

Figure 2. Stresses on individual layers in the laminate.

where σ_* is the applied stress. Also if τ is the shear stress in the shear layer, Figure 2, then equilibrium of the 0° and 90° plies separately implies that

$$\tau = -b\frac{d\sigma_t}{dx} = d\frac{d\sigma_t}{dx} \tag{5}$$

In this paper we examine cross ply laminates which are subject only to mechanical loading σ_*—as well as residual stress. There is no difficulty in extending the analysis to encompass thermal loading and this will be reported elsewhere. The stress-strain relations for the respective plies are, therefore,

$$\begin{aligned} \sigma_t &= \sigma_t^R + \tau_t, \qquad \tau_t = E_t\epsilon_t \\ \sigma_t &= \sigma_t^R + \tau_t, \qquad \tau_t = E_t\epsilon_t \end{aligned} \tag{6}$$

In other words, τ_t and τ_t are the stresses due to mechanical loading. Finally, the essential ingredient of shear lag theory is that the shear stress τ is assumed to be proportional to the relative displacement $(v - u)$:

$$\tau = K(v - u) \tag{7}$$

where K is a constant.

Analysis of the fracture mechanics of transverse plies requires knowledge of the strain energy of the laminate—or more precisely the total energy of the laminate. As a prelude to this calculation, we here evaluate the strain energy, per unit width of the laminate, between two sections PP and QQ, see Figure 3. Now the increase in strain energy, W, due to the application of mechanical loads τ_t and τ_t [see Equation (4)] is equal to the work done:

$$\begin{aligned} W &= b[(\tau_t + 2\sigma_t^R)u]\beta + d[(\tau_t + 2\sigma_t^R)v]\beta \\ &= b[(\sigma_t + \sigma_t^R)u]\beta + d[(\sigma_t + \sigma_t^R)v]\beta \end{aligned} \tag{8}$$

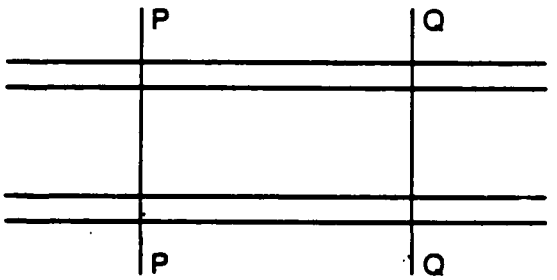

Figure 3. Section of uncracked laminate.

and we have used the notation

$$[u]_P^Q = u(Q) - u(P)$$

In order to obtain Equation (8) it is essential to remember that the applied loads on the respective plies increase from zero to τ_t and τ_t, whereas, the residual stresses are essentially dead loads—hence the factor 2. Clearly we can rewrite (8) in the form

$$W = b\int_P^Q \frac{d}{dx}\{(\sigma_t + \sigma_t^R)u\}dx + d\int_P^Q \frac{d}{dx}\{(\sigma_t + \sigma_t^R)v\}dx$$

With the help of (2), (5), (6), and (7) we may show that

$$W = \int_P^Q \left\{ b\frac{\sigma_t^2 - \sigma_t^{R2}}{E_t} + d\frac{\sigma_t^2 - \sigma_t^{R2}}{E_t} + \frac{\tau^2}{K} \right\} dx \tag{9}$$

It is now a trivial exercise to derive a complete set of differential equations for shear lag theory. In order to discuss transverse cracking, the most useful equation governs the stress in the transverse ply. One form of this equation is

$$\frac{d^2\sigma_t}{dx^2} - \frac{\xi^2}{d^2}\sigma_t = -\frac{\xi^2}{d^2}\left(\sigma_t^R + \frac{E_t}{E_0}\sigma_a\right) \tag{10}$$

where the *non-dimensional shear lag parameter* ξ is given by

$$\xi^2 = \frac{Kd(bE_t + dE_t)}{bE_tE_t} \tag{11}$$

Let us now consider the straightforward problem associated with two transverse cracks distant $2h$ apart, see Figure 4. We are particularly interested in the elastic field in that part of the laminate which is between the cracks. Thus, the appropriate boundary conditions for Equation (10) are

$$\sigma_t = 0 \quad \text{when} \quad x = \pm h \tag{12}$$

The required solution is

$$\sigma_t = (\sigma_t^R + \frac{E_t}{E_0}\sigma_a)\left(1 - \frac{\cosh\frac{\xi x}{d}}{\cosh\frac{\xi h}{d}}\right) \tag{13}$$

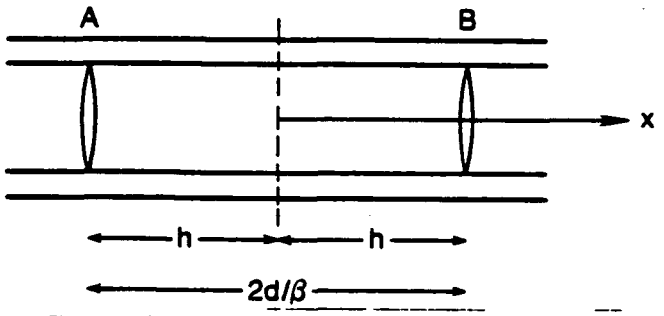

Figure 4. Two adjacent transverse cracks in the 90° plies.

The stress in the longitudinal plies is

$$\sigma_t = \frac{E_t}{E_0}\sigma_a\left(1 + \frac{dE_t}{bE_t}\frac{\cosh\frac{\xi x}{d}}{\cosh\frac{\xi h}{d}}\right) + \sigma_t^R\left(1 - \frac{\cosh\frac{\xi x}{d}}{\cosh\frac{\xi h}{d}}\right) \tag{14}$$

From (2), (6), (13) and (14) we find that the associated displacements are

$$u = \frac{\sigma_a}{E_0}x + \frac{d^2}{\xi bE_t}(\sigma_t^R + \frac{E_t}{E_0}\sigma_a)\frac{\sinh\frac{\xi x}{d}}{\cosh\frac{\xi h}{d}} + c_1 \tag{15}$$

$$v = \frac{\sigma_a}{E_0}x - \frac{d}{\xi E_t}(\sigma_t^R + \frac{E_t}{E_0}\sigma_a)\frac{\sinh\frac{\xi x}{d}}{\cosh\frac{\xi h}{d}} + c_2 \tag{16}$$

where c_1 and c_2 are constants.

3. LOSS OF STIFFNESS

With the help of the results of the preceding section we can now calculate the loss of stiffness of the cross-ply laminate due to transverse cracking. Thus, let the *average* distance between transverse cracks be $2h$, Figure 4. Then the average strain, ϵ_a, of the uncracked ligament AB, as measured at the surface of the laminate, is given by

$$\epsilon_a = \frac{u(B) - u(A)}{2h} = \frac{\sigma_a}{E_0}\left\{1 + \frac{d^2E_t}{\xi hbE_t}\tanh\frac{\xi h}{d}\right\} + \frac{d^2\sigma_t^R}{\xi bhE_t}\tanh\frac{\xi h}{d} \tag{17}$$

where we have used (15). We note that we would still recover (17) if we were to consider *any* two sections distant $2h$ apart. A trivial rearrangement of (17) together with use of the crack density parameter

$$\beta = d/h$$

now yields

$$\sigma_a = E_0\left\{\epsilon_a - \frac{\beta}{\xi}\frac{d\sigma_t^R}{bE_t}\tanh\frac{\xi}{\beta}\right\}\left\{1 + \frac{\beta}{\xi}\frac{dE_t}{bE_t}\tanh\frac{\xi}{\beta}\right\}^{-1} \tag{18}$$

which is the effective stress-strain relation for the cracked laminate. We observe that Equation (18) shows that, under cracking, the laminate acquires a permanent strain, ϵ_p, due to initial stress:

$$\epsilon_p = \frac{\beta}{\xi}\frac{d\sigma_t^R}{bE_t}\tanh\frac{\xi}{\beta} \tag{19}$$

It would be misleading to give the impression that the permanent strain (19) were important either experimentally or theoretically. In fact for all laminates considered here the shear lag parameter lies between 0.5 and 2.5—as is discussed later. Accordingly the value of ϵ_p is at most 5% of the value of ϵ_a in the worst possible situation, i.e. β large. Hence we can neglect ϵ_p in applications and arrive at the elegant formula for the Young's modulus $E(\beta)$ of a laminate containing transverse cracks of density β:

$$E(\beta) = E_0\left\{1 + \frac{\beta}{\xi}\frac{dE_t}{bE_t}\tanh\frac{\xi}{\beta}\right\}^{-1} \tag{20}$$

We note that as the crack density $\beta \to 0$, $E \to E_0$ as it should. In addition as $\beta \to \infty$ we see that

$$E \to E_0\left(1 + \frac{dE_t}{bE_t}\right)^{-1} = \frac{bE_t}{b + d}$$

which is the result given by ply discount theory.

An assessment of the validity of Equation (20) will be given in Section 5 when we have evaluated the shear lag parameter ξ.

4. PROGRESSIVE CRACKING

We now turn to the problem of determining the transverse crack density β as a function of the increasing applied load σ_a. Consider the uncracked ligament AB as in Figure 4. When the applied load σ_a reaches a critical value, this ligament will itself crack at some location C as in Figure 5. There is no reason to suppose that C lies at the mid-point of AB. Assuming that the additional cracking is pro-

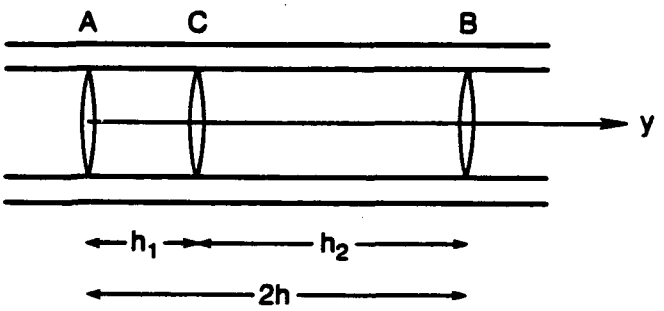

Figure 5. The ligament AB with an additional crack at C.

duced under *fixed loads*, we can use the analysis of Section 2 to calculate the required energy release rate.

Let us temporarily regard the configuration of Figure 4 as state 1 in which the displacements are u_1 and v_1, whilst the configuration of Figure 5 is state 2 with displacements u_2 and v_2. From (8) the strain energy, per unit width, of the ligament AB in state 1 is:

$$\begin{aligned} W_1 &= b[(\sigma_t + \sigma_t^R)u_1]_A^B + d[(\sigma_t + \sigma_t^R)v_1]_A^B \\ &= \{(b + d)\sigma_a + b\sigma_t^R\}\,[u_1]_A^B + d\sigma_t^R\,[v_1]_A^B \end{aligned} \tag{21}$$

since $\sigma_t(A) = \sigma_t(B) = 0$. Also the combined strain energy, per unit width, of the two ligaments AC and CB in state 2 is, from (21),

$$W_2 = \{(b + d)\sigma_a + b\sigma_t^R\}\{[u_2]_A^C + [u_2]_C^B\} + d\sigma_t^R\{[v_2]_A^C + [v_2]_C^B\} \tag{22}$$

But u_2 is continuous at C, hence

$$[u_2]_A^C + [u_2]_C^B = [u_2]_A^B \tag{23}$$

Under the assumption of cracking at fixed loads, the work done, per unit width, on the segment AB when the extra crack occurs at C is

$$2b[\sigma_t(u_2 - u_1)]_A^B = 2(b + d)\sigma_a[u_2 - u_1]_A^B \tag{24}$$

Thus the *total* energy, $\mathcal{E}$, per unit width, released by introduction of the crack at C is the work done by the applied loads minus the increase of strain energy. From (21) to (24) we have:

$$\begin{aligned} \mathcal{E} &= 2(b + d)\sigma_a[u_2 - u_1]_A^B - (W_2 - W_1) \\ &= \{(b + d)\sigma_a + d\sigma_t^R\}[u_2 - u_1]_A^B + d\sigma_t^R[v_1 - v_2]_A^C + d\sigma_t^R[v_1 - v_2]_C^B \end{aligned}$$

A series of routine, but tedious, calculations shows that

$$\mathcal{G} = \frac{2d^2(b + d)E_0}{\xi b E_t E_r} (\sigma_r^R + \frac{E_r}{E_0} \sigma_a)^2 \left\{ \tanh \frac{\xi h_1}{2d} + \tanh \frac{\xi h_2}{2d} - \tanh \frac{\xi h}{d} \right\}$$

But the energy release rate G, per unit length, for crack propagation across the ply is determined from $G = \mathcal{G}/2d$, see Dvorak and Laws [24]. Thus

$$G = \frac{d(b + d)E_0}{\xi b E_t E_r} (\sigma_r^R + \frac{E_r}{E_0} \sigma_a)^2 \left\{ \tanh \frac{\xi h_1}{2d} + \tanh \frac{\xi h_2}{2d} - \tanh \frac{\xi h}{d} \right\} \tag{25}$$

It is now easy to obtain a first ply failure criterion from (25) by taking h, h_1, h_2, to be large and setting $G = G_c$. The result is

$$\sigma_a^{fpf} = \left\{ \frac{\xi b E_t E_0 G_c}{d(b + d)E_r} \right\}^{1/2} - \frac{E_0}{E_r} \sigma_r^R \tag{26}$$

When we are given standard data, namely b, d, E_t, E_r, the coefficients of expansion and the temperature drop during cool-down, we easily calculate σ_r^R and E_0. Thus (26) provides a relationship between σ_a^{fpf}, G_c and ξ. However, σ_a^{fpf} and G_c are readily measured, and we therefore *regard Equation (26) as the rule which determines the shear lag parameter* ξ.

Once ξ has been so determined, Equation (20) provides an explicit formula for the loss of stiffness of the laminate.

As for subsequent cracking, a major complication arises because the location of the "next" crack cannot be obtained by deterministic methods. Indeed, this is precisely the situation indicated by experiment. Thus we must proceed on a statistical basis.

In order to analyze progressive cracking, suppose that the laminate contains transverse cracks with average separation $2h$ with associated crack density $\beta = d/h$ as in Figure 4. Then the next crack which appears in the ligament AB will be at some location C as in Figure 5. Let $\sigma_a(h_1)$ be the applied stress which is needed to produce the crack at C. We can determine $\sigma_a(h_1)$ directly from (25) by setting $G = G_c$. When use is also made of (26), it follows that

$$\sigma_a(h_1) = (\sigma_a^{fpf} + \frac{E_0}{E_r} \sigma_r^R) \left\{ \tanh \frac{\xi h_1}{2d} + \tanh \frac{\xi h_2}{2d} - \tanh \frac{\xi h}{d} \right\}^{-1/2} - \frac{E_0}{E_r} \sigma_r^R \tag{27}$$

Since the location of C is, in an appropriate sense, random, let p be the probability density function for the site of the next crack. Thus in a laminate which already contains cracks of density β, the expected value of the applied stress to

cause *additional* cracking is

$$E[\sigma_x(\beta)] = \int_0^{2h} p(y)\, \sigma_x(y)dy \tag{28}$$

where $\sigma_x(y)$ is given by (27). The choice of probability density function is crucial. Three candidates immediately present themselves.

Case 1

An extreme situation would arise if the next crack were *guaranteed* to occur at the mid-point of the unbroken ligament. This would imply the choice

$$p(y) = \delta(y - h) \tag{29}$$

where $\delta(y)$ is the Dirac delta function.

Case 2

Another extreme would be to assume that all locations in the ligament were equally likely, giving

$$p(y) = \frac{1}{2h} \tag{30}$$

Case 3

A more appealing hypothesis, based on simple fracture mechanics, would be to assume that $p(y)$ is proportional to the stress in the transverse ply:

$$p(y) \propto \sigma_t(y)$$

Thus from Equation (13) with $x = y - h$

$$p(y) = \frac{1}{2h}\left(1 - \frac{\cosh\dfrac{\xi(y-h)}{d}}{\cosh\dfrac{\xi h}{d}}\right)\left(1 - \frac{\tanh\dfrac{\xi h}{d}}{\dfrac{\xi h}{d}}\right)^{-1} \tag{31}$$

For Case 1, we can obtain the explicit solution

$$E[\sigma_x(\beta)] = (\sigma_x^{lp\prime} + \frac{E_0}{E_t}\sigma_t^R)\left\{2\tanh\frac{\xi}{2\beta} - \tanh\frac{\xi}{\beta}\right\}^{-1/2} - \frac{E_0}{E_t}\sigma_t^R \tag{32}$$

But for Cases 2 and 3, the integral must be evaluated numerically.

5. COMPARISON WITH EXPERIMENT

In the first place we compare the predictions of the foregoing theory with some experimental data of Highsmith and Reifsnider [8]. These authors reported data, and some theoretical results, for several E-glass-epoxy systems. Of particular concern here are the data for $(0, 90_3)_s$ specimens.

The data for the E-glass-epoxy systems studied in [8] are as follows

$$E_t = 41.7 \text{ GPa} \qquad E_r = 13.0 \text{ GPa}$$
$$\sigma_t^R = 8.4 \text{ MPa} \qquad \sigma_{ss}^{lpf} = 55 \text{ MPa}$$

ply thickness 0.20 mm.

Unfortunately Highsmith and Reifsnider [8] do not give a value for G_c. However, the data given above has been used by Laws and Dvorak [25] and by Hashin [26] to validate the loss of stiffness given by the self-consistent model and a lower bound prediction respectively. The Hashin [26] lower bound and the experimental data are displayed in Figure 6. We remark that the self-consistent prediction is *not* indicated in Figure 6 because it is only marginally greater than the Hashin [26] bound and thus the two curves are virtually indistinguishable.

But in order to obtain the shear lag prediction for loss of stiffness, lack of a definite value for G_c poses a problem. In this connection we note that in an earlier

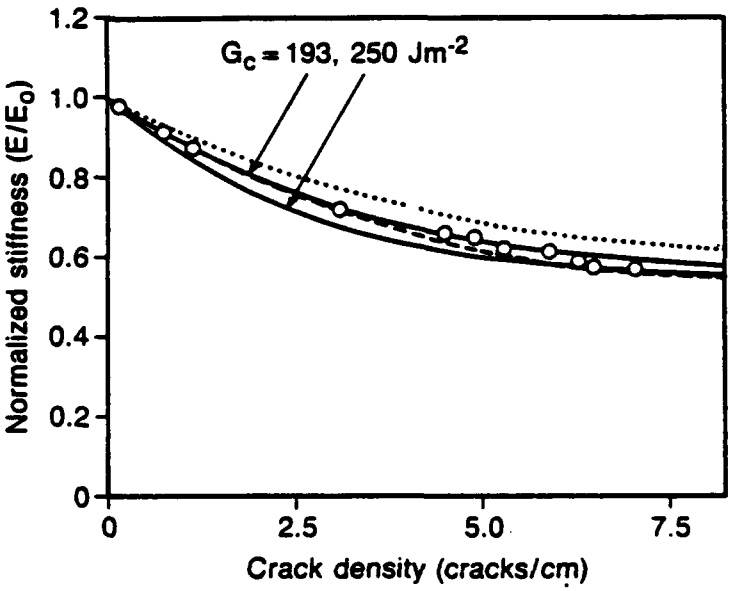

Figure 6. Experimental and theoretical values for stiffness loss of $(0,90_3)_s$ E-glass epoxy laminate: (1) Highsmith-Reifsnider prediction ·····, (2) shear lag————, (3) lower bound———. Experimental data from Reference [8].

paper Dvorak and Laws [24] studied some E-glass-epoxy systems and used the value $G_c = 250\ \mathrm{Jm^{-2}}$. If we were to use the same value here, then Equation (26) would imply the value $\xi = 0.7$. The loss of stiffness predicted by Equation (20) is indicated in Figure 10. We note that the resulting curve gives reasonable agreement with experiment but violates the Hashin lower bound for small crack densities. We might be prepared to accept this state of affairs as being an unfortunate but unavoidable consequence of the approximate shear lag theory. However, a more reasonable interpretation is that the *ad hoc* choice of $G_c = 250\ \mathrm{Jm^{-2}}$ is not correct. In order to develop this line of reasoning we note that the maximum value of G_c which implies that the predicted loss of stiffness is entirely consistent with the Hashin bound is $G_c = 193\ \mathrm{Jm^{-2}}$. This in turn implies that $\xi = 0.9$ and thus a predicted loss of stiffness which is shown in Figure 6.

For completeness Figure 6 also shows the comparison between the theoretical prediction of Highsmith and Reifsnider [8] with their experimental data. Although these authors also use a form of shear lag theory, it is not easy to compare their model with the theory given here.

We note that, for the graphite-epoxy systems discussed later, data is complete and there is no ambiguity in the value of G_c and hence of ξ.

Despite the incompleteness of the data for the E-glass systems, comparison of theory with experiment for the loss of stiffness of $(0, 90_3)_s$ laminates cannot be regarded as decisive. In the first place the loss of stiffness of typical graphite-epoxy systems due to transverse micro-cracking is minimal. In the second, the major advantage of the shear lag model lies in its ability to provide an explicit prediction of crack density as a function of applied load. In fact, if we agree to determine ξ from Equation (26), shear lag theory does not contain any adjustable parameters. Rather, we need to identify the correct probability density function. Once the choice of $p(y)$ has been made, the statistical theory presented here is well-defined.

Let us now turn to the Highsmith-Reifsnider [8] data for crack density as a function of applied load. In view of our earlier discussion we here take $G_c = 193\ \mathrm{Jm^{-2}}$ which implies that $\xi = 0.9$. Theoretical results for crack density as a function of applied load can be obtained from Equation (28) for the three choices of probability density function (29), (30) and (31). The various curves and the data are shown in Figure 7. We note in passing that the numerical evaluation of some of the integrals requires considerable attention to detail. Clearly the most promising choice of probability function is Case 3. Indeed one can make a strong *a priori* argument for Case 3 based on elementary fracture mechanics. We therefore propose the use of the probability density function (31) as appropriate for the prediction of progressive cracking.

It is of interest to show the sensitivity of the predicted crack density to the value of G_c. This is indicated in Figure 8 wherein it is clear that the theory makes the (necessary) prediction that the tougher the material the less the crack density for given load.

We now turn to some different work by Wang and Crossman [17–21]. The work of these authors is exclusively concerned with graphite-epoxy systems and is centered on the prediction of crack density as a function of the applied (mono-

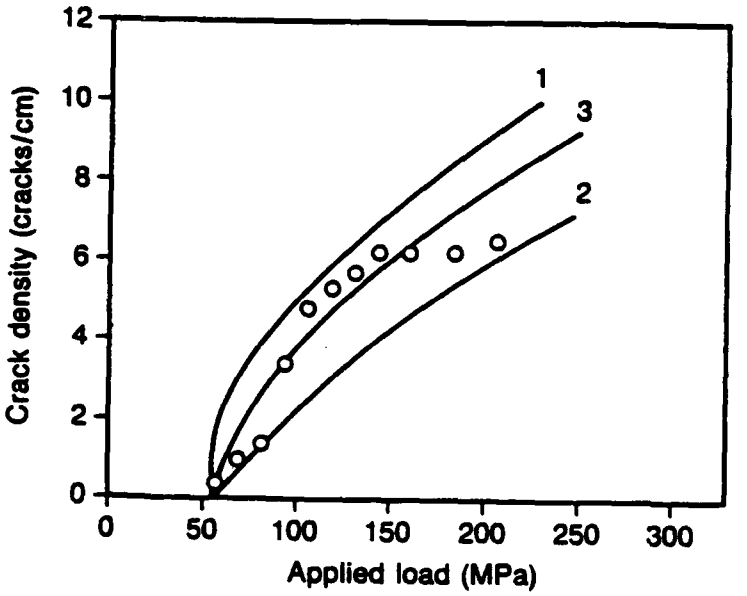

Figure 7. Crack density versus stress for E-glass epoxy $(0,90_3)_s$ laminates. Experimental data from Reference [8]. Theoretical curves for respectively numbered probability distributions in the text. G_c = 193 Jm^{-2}.

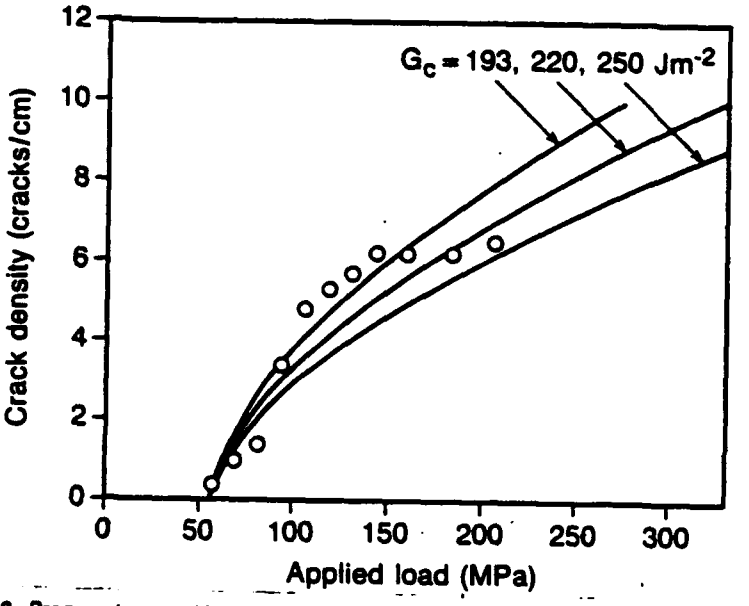

Figure 8. Progressive cracking in $(0,90_3)_s$ E-glass epoxy laminates. Data from Reference [8]. Predictions obtained from probability distribution 3 for indicated values of G_c.

tonic) load. Those parts of the work of these latter authors which are devoted to fatigue are not relevant to the present discussion.

For our present purpose the most convenient source for data is the survey article by Wang [20]. We first consider the AS-3501-06 graphite epoxy systems. Results for $(0_2, 90)_s$, $(0_2, 90_2)_s$ and $(0_2, 90_3)_s$ laminates are given in Figures 11, 12 and 13 of Wang's [20] article. When we make use of the data quoted by Wang [20], see also [21], we find the values of the shear lag parameters are as follows

$$(0_2, 90)_s \qquad \xi = 0.93$$

$$(0_2, 90_2)_s \qquad \xi = 1.38$$

$$(0_2, 90_3)_s \qquad \xi = 2.24$$

Comparison of the respective shear lag predictions with the experimental results are shown in Figure 9. The reader's attention is drawn to the fact that we have omitted Wang's [20] numerical results from Figure 9 because it is impossible to do justice by replicating the published graphs. The important observation is that both shear lag and the Wang-Crossman theory give very good predictions. This

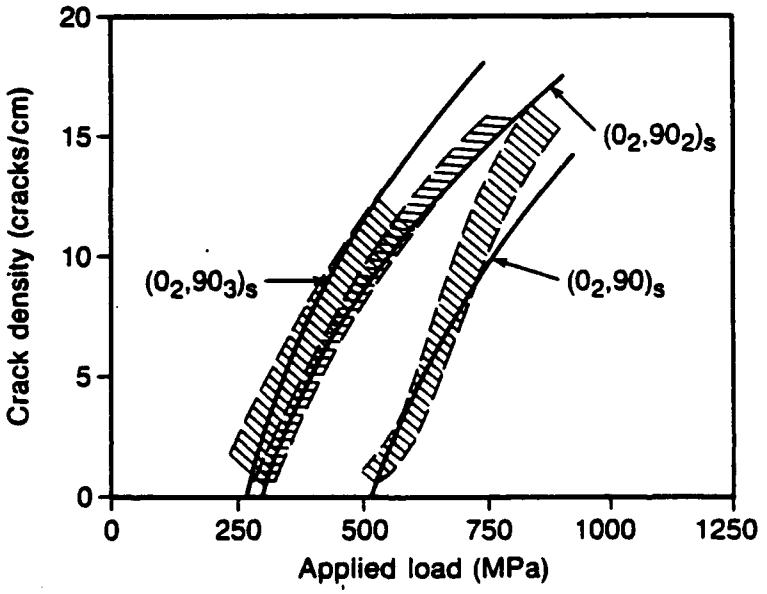

Figure 9. Theory versus experiment for progressive cracking of AS-3501-06 laminates. Data from Wang [20].

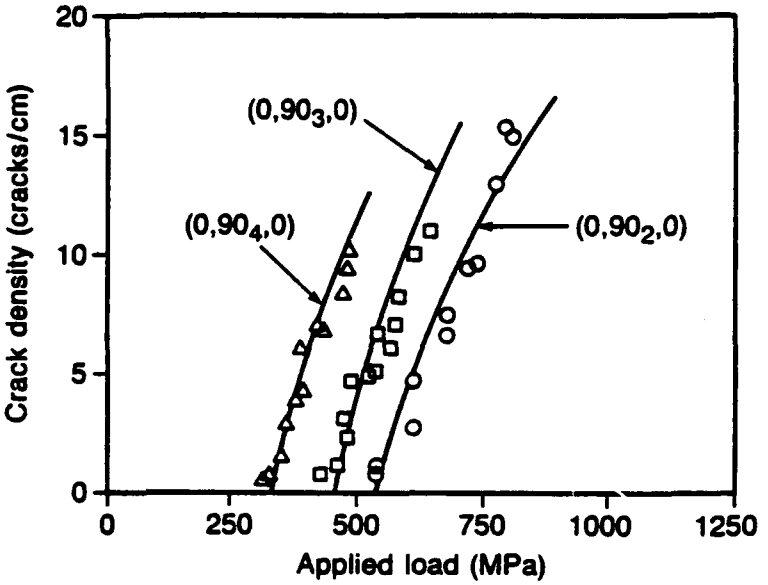

Figure 10. Theory versus experiment for progressive cracking of T300/934 laminates. Data from Wang [20].

is quite remarkable since the respective theories are based on entirely different premisses.

Finally, we turn to the data reported by Wang [20] for some T300/934 laminates. Again we use the data given by Wang [20,21] to obtain the following values for ξ for the indicated lay-ups:

$$(0, 90_2, 0) \qquad \xi = 1.08$$

$$(0, 90_3, 0) \qquad \xi = 1.70$$

$$(0, 90_4, 0) \qquad \xi = 1.79$$

The theoretical predictions are compared with the experimental data in Figure 10. Again it is encouraging to report excellent agreement.

ACKNOWLEDGEMENTS

This work was supported by a grant from the Air Force Office of Scientific Research. Mr. W. Li helped in the interpretation of the experimental data and computing.

REFERENCES

1. Garrett, K. W. and J. E. Bailey. "Multiple Transverse Fracture in 90° Cross-Ply Laminates of a Glass Fibre-Reinforced Polyester," *J. Mater. Sci.*, 12:157 (1977).
2. Parvizi, A., K. W. Garrett and J. E. Bailey. "Constrained Cracking in Glass Fibre-Reinforced Epoxy Cross-Ply Laminates," *J. Mater. Sci.*, 13:195 (1978).
3. Parvizi, A. and J. E. Bailey. "On Multiple Transverse Cracking in Glass Fibre Epoxy Cross-Ply Laminates," *J. Mater. Sci.*, 13:2131 (1978).
4. Bader, M. G., J. E. Bailey, P. T. Curtis and A. Parvizi. "The Mechanisms of Initiation and Development of Damage in Multi-Axial Fibre-Reinforced Plastic Laminates," *Proc. 3rd. Internat. Conf. on Mechanical Behavior of Materials*, Cambridge, p. 227 (1979).
5. Bailey, J. E., P. T. Curtis and A. Parvizi. "On the Transverse Cracking and Longitudinal Splitting Behavior of Glass and Carbon Fibre Reinforced Epoxy Cross Ply Laminates and the Effect of Poisson and Thermally Generated Strain," *Proc. R. Soc. Lond. A.*, 366:599 (1979).
6. Aveston, J. and A. Kelly. "Theory of Multiple Fracture of Fibrous Composites," *J. Mater. Sci.*, 8:352 (1973).
7. Wang, A. S. D. "Growth Mechanisms of Transverse Cracks and Ply Delamination in Composite Laminates," *Proc. ICCM-3*, Paris, 1:170 (1980).
8. Highsmith, A. L. and K. L. Reifsnider. "Stiffness Reduction Mechanisms in Composite Laminates," *ASTM STP 775*, p. 103 (1982).
9. Flaggs, D. L. and M. H. Kural. "Experimental Determination of the In Situ Transverse Lamina Strength in Graphite-Epoxy Laminates," *J. Composite Materials*, 16:103 (1982).
10. Nuismer, R. J. and S. C. Tan. "The Role of Matrix Cracking in the Continuum Constitutive Behavior of a Damaged Composite Ply," *Proc. IUTAM Symposium on Mechanics of Composite Materials*, Pergamon Press, p. 437 (1982).
11. Manders, P. W., T. W. Chou, F. R. Jones and J. W. Rock. "Statistical Analysis of Multiple Fracture in 0°/90°/0° Glass Fibre-Epoxy Resin Laminates," *J. Mater. Sci.*, 18:2876 (1983).
12. Fukanaga, H., T. W. Chou, P. W. M. Peters and K. Schulte. "Probabilistic Failure Strength Analyses of Graphite-Epoxy Cross-Ply Laminates," *J. Composite Materials*, 18:339 (1984).
13. Flaggs, D. L. "Predictions of Tensile Matrix Failure in Composite Laminates," *J. Composite Materials*, 19:29 (1985).
14. Ohiro, H. "Analysis of the Stress Distributions in the Cross-Ply Composite, *Proc. ICCM-5*, San Diego, p. 1115 (1985).
15. Ogin, S. L., P. A. Smith and P. W. R. Beaumont. "Matrix Cracking and Stiffness Reduction During the Fatigue of a (0, 90)$_s$ GFRP Laminate," *Composites Sci. Technology*, 22:23 (1985).
16. Ogin, S. L., P. A. Smith and P. W. R. Beaumont. "A Stress Intensity Factor Approach to the Fatigue Growth of Transverse Ply Cracks," *Composite Sci. Technology*, 24:47 (1985).
17. Wang, A. S. D. and F. W. Crossman. "Initiation and Growth of Transverse Cracks and Edge Delamination in Composite Laminates, Part I: An Energy Method," *J. Composite Materials Suppl.*, 14:71 (1980).
18. Crossman, F. W., W. J. Warren, A. S. D. Wang and G. E. Law, Jr. "Initiation and Growth of Transverse Cracks and Edge Delamination in Composite Laminates, Part 2: Experimental Correlation," *J. Composite Materials Suppl.*, 14:88 (1980).
19. Wang, A. S. D., P. C. Chou and S. C. Lei. "A Stochastic Model for the Growth of Matrix Cracks in Composite Laminates," *J. Composite Materials*, 18:239 (1984).
20. Wang, A. S. D. "Fracture Mechanics of Sublaminate Cracks in Composite Materials," *Composites Tech. Review*, 6:45 (1984).
21. Wang, A. S. D. "Fracture Analysis of Matrix Cracking in Laminated Composites," Report No. NADC 85118-60, Drexel University (1985).
22. Laws, N., G. J. Dvorak and M. Hejazi. "Stiffness Changes in Unidirectional Composites Caused by Crack Systems," *Mechanics of Materials*, 2:123 (1983).

23. Dvorak, G. J., N. Laws and M. Hejazi. "Analysis of Progressive Matrix Cracking in Composite Laminates I: Thermoelastic Properties of a Ply with Cracks," *J. Composite Materials*, 19:216 (1985).
24. Dvorak, G. J. and N. Laws. "Analysis of Progressive Matrix Cracking in Composite Laminates II: First Ply Failure," *J. Composite Materials*, 21:309 (1987).
25. Laws, N. and G. J. Dvorak. "The Loss of Stiffness of Cracked Laminates," *Proc. IUTAM Eshelby Memorial Symposium*, Cambridge University Press, p. 119 (1985).
26. Hashin, Z. "Analysis of Cracked Laminates: A Variational Approach," *Mechanics of Materials*, 4:121 (1985).

J. Mech. Phys. Solids Vol. 37, No. 5, pp. 603–618, 1989.
Printed in Great Britain.

0022-5096/89 $3.00 + 0.00

MICROCRACKING IN POLYCRYSTALLINE CERAMICS: ELASTIC ISOTROPY AND THERMAL ANISOTROPY

N. LAWS† and J. C. LEE‡

†Department of Mechanical Engineering, University of Pittsburgh, Pittsburgh, PA 15261, U.S.A. and
‡Product Design and Mechanics Division, Alcoa Laboratories, Alcoa Center, PA 15069, U.S.A.

(*Received* 18 *April* 1988; *in revised form* 13 *October* 1988)

ABSTRACT

A HEXAGONAL grain array model is used to study grain boundary microcracking of a polycrystalline aggregate due to residual stress. Each grain is assumed to be elastically isotropic but thermally anisotropic. The axes of thermal anisotropy for each grain are arbitrary. An explicit analytic solution is obtained for the entire residual stress field. This solution is used to give a detailed description of the grain boundary stress fields. Further, explicit algebraic formulae are given for stress intensity factors associated with grain boundary microcracks. The results are used to predict the critical grain size for the occurrence of spontaneous microcracking. Agreement between theory and experiment is good.

1. INTRODUCTION

THIS PAPER is devoted to the study of grain boundary microcracking in single phase polycrystalline brittle solids due to cooldown. It has long been held (CLARKE, 1964; CLEVELAND and BRADT, 1978; DAVIDGE, 1981; EVANS, 1978; FU and EVANS, 1982, 1985; KUSZYK and BRADT, 1973; OHYA *et al.*, 1987) that residual stresses in polycrystalline aggregates are due to thermal expansion anisotropy—it being invariably assumed that each grain is elastically isotropic. There is complete agreement that there is a critical minimum grain size for microcracking to occur. Further, there is agreement that for given cooldown temperature change (ΔT), Young's modulus E, difference between the larger and the mean coefficient of thermal expansion ($\Delta\alpha$) and grain boundary toughness (G_{gb}), the formula for the critical facet length (l_c) is of the form

$$l_c = Q\frac{G_{gb}}{E(\Delta\alpha\Delta T)^2}, \tag{1}$$

where Q is a constant. It is not our intention to give a critical review of the various arguments which have been used to arrive at proposed values for Q. All that need be said is that some authors use approximate stress analysis whereas others choose Q to fit certain experimental data.

The aim of the first part of this paper is to present an explicit analytic solution of the residual stress problem. This analysis is then used in conjunction with conventional linear elastic fracture mechanics to predict the critical grain size.

It is important here to note a recent paper by TVERGAARD and HUTCHINSON (1988) which addresses the problem of residual stress microcracking within the framework of thermal expansion *and* elastic anisotropy. For obvious reasons, it is difficult to compare the predictions of the analysis presented here, which is based on isotropic elastic response, with the TVERGAARD and HUTCHINSON (1988) work. But some discussion of the respective predictions is given.

Finally, we wish to draw attention to the work of FREDRICH and WONG (1986) which addresses the related problem of thermally-induced microcracking of rocks. These authors assume elastic isotropy together with thermal anisotropy and provide a thorough analysis of the two-dimensional model consisting of a square inclusion embedded in an isotropic aggregate.

In this paper, we follow EVANS (1978) and FU and EVANS (1985), by considering a plane hexagonal grain array embedded in an infinite isotropic elastic matrix (the effective polycrystalline aggregate). The orientation of the axes of thermal anisotropy of the individual grains is allowed to vary. In Section 2, we give the general solution of the residual stress problem using complex variable methods. Amongst other things, the analysis confirms a result due to EVANS (1978) that the stress singularity at a triple point is logarithmic. We go on to discuss the stress intensity factors at putative cracks on grain boundary facets. It is especially noteworthy that we are able to evaluate all the integrals analytically and thus reduce the determination of stress intensity factors to the evaluation of an algebraic sum.

To determine the residual stress field in an array with *given* orientation distribution of the axes of thermal anisotropy, it is necessary to add the contributions due to each facet. The question therefore arises as to how many grains need be considered in order to get accurate results. It turns out that it is essential to consider at least 200 grains to get proper accuracy.

Since the orientation distribution of the axes of thermal isotropy is not known, it is argued that the appropriate model for spontaneous microcracking of *randomly* oriented arrays is to take the most extreme local orientation at the considered interface, together with the ensemble average over all other grains. This interpretation shows that one can interpret the 2-grain and 4-grain models of FU and EVANS (1985) in a new light.

In Section 4 we use the results of our exact stress analysis to predict the minimum facet size for microcracking during cooldown. We show that the factor Q in (1) is very sensitive to the assumed length of the inherent flaw in the solid. Finally, we compare the predictions of this analysis with those of other workers and with some experimental data.

2. ANALYSIS

A standard model of a polycrystalline solid consists of a regular hexagonal array, see Fig. 1. In the study of microcracking due to residual stresses, it is usual to assume

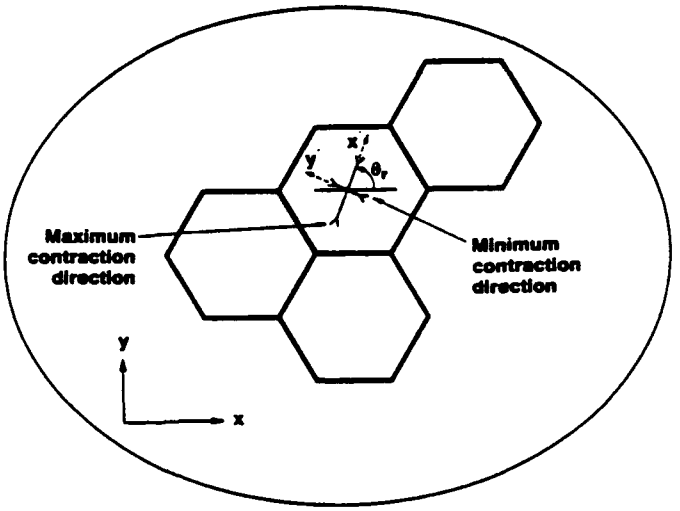

FIG. 1. Hexagonal grain array. Also shown are the global and local coordinates for the rth grain.

elastic isotropy and thermal anisotropy of the individual grains with the proviso that the coefficient of thermal expansion in the x_3 direction of Fig. 1 is the same for every grain. At the time of writing, little or no data is available concerning the orientation distribution of the axes of thermal anisotropy. Thus,we are led to the study of models with various orientation distributions. However, throughout this paper, we will focus on the micro-geometry shown in Fig. 1. We will show that the determination of residual stresses can be accomplished for arbitrary orientation distributions of the axes of thermal anisotropy. Accordingly, we defer the introduction of specific orientation models to Section 3.

The residual stress problem is, perhaps, most readily discussed with the help of the notation of LAWS (1973). Thus, for the rth grain, the constitutive equation is

$$\boldsymbol{\varepsilon}^r = M\boldsymbol{\sigma}^r + \theta\mathbf{m}^r, \tag{2}$$

where $\boldsymbol{\varepsilon}^r$ and $\boldsymbol{\sigma}^r$ are respectively the strain and stress in the rth grain, M is the common (isotropic) compliance tensor and θ the *increase* in temperature from the stress-free configuration. Also, $\mathbf{m}^r$ is the tensor of coefficients of thermal expansion.

When referred to the *local* axes of thermal symmetry, $Ox'_1x'_2x_3$, see Fig. 1, the tensor $\mathbf{m}^r$ is expressible in the form

$$\mathbf{m}^r = \begin{pmatrix} \alpha_1 & 0 & 0 \\ 0 & \alpha_2 & 0 \\ 0 & 0 & \alpha_3 \end{pmatrix}. \tag{3}$$

The components of $\mathbf{m}^r$ with respect to the global axes $Ox_1x_2x_3$ are then found by tensor transformation:

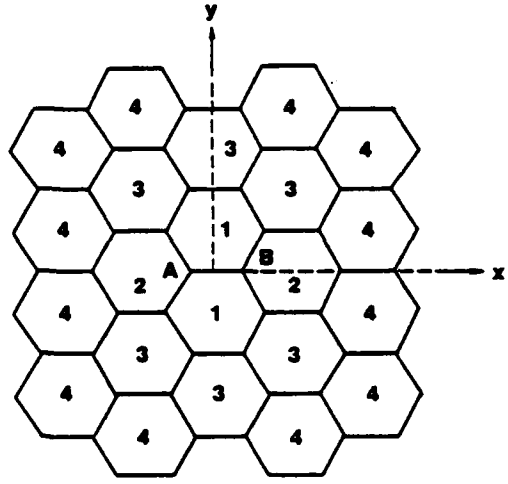

FIG. 2. Grain array showing those grains which are considered in the various N-grain models.

$$m'_{11} = \alpha_1 \cos^2\theta_r + \alpha_2 \sin^2\theta_r,$$
$$m'_{12} = (\alpha_2 - \alpha_1)\sin\theta_r \cos\theta_r,$$
$$m'_{22} = \alpha_1 \sin^2\theta_r + \alpha_2 \cos^2\theta_r,$$
$$m'_{13} = m'_{23} = 0, \quad m'_{33} = \alpha_3. \tag{4}$$

For the polycrystalline aggregate as a whole, it is obvious that the macroscopic compliance is M. Also, it is not difficult to show that the macroscopic tensor of coefficients of thermal expansion, $\mathbf{m}$, is just the orientation average of $\mathbf{m}'$ taken over all grains:

$$\mathbf{m} = \{\mathbf{m}'\}. \tag{5}$$

With the help of (4), it is easy to calculate the overall coefficient of thermal expansion for arbitrary orientation distributions of the axes of thermal anisotropy.

Throughout this paper, we will assume that the polycrystalline aggregate has macroscopic thermal isotropy so that

$$m_{11} = m_{22} = m_{33} = \alpha, \tag{6}$$
$$m_{23} = m_{31} = m_{12} = 0.$$

Nevertheless, we note in passing that it is easy to extend the analysis to textured aggregates.

The residual stresses in the *microcrack-free* solid maybe calculated using the ESHELBY (1961) technique. This calculation is performed by considering the configuration of Fig. 1 (see FU and EVANS, 1985) wherein the hexagonal array is surrounded by a material whose properties are those of the effective aggregate. The number of grains considered is at our disposal. Thus, for *given* orientation of the thermal axes of an array, we can have a hierarchy of models. To emphasize the point, let us suppose that we are interested in the interfacial stresses on a particular facet, AB, in Fig. 2. In the

first instance, we can consider the 2-grain model consisting of the two grains labelled 1 surrounded by the effective aggregate. Next, we can consider a 4-grain model consisting of the two grains labelled 1 plus the two grains labelled 2 surrounded by the effective aggregate. As shown in Fig. 4, we can then consider the $2+2+6=10$-grain model, followed by the $2+2+6+12=22$-grain model, etc. Clearly, other models for the given orientation are possible. However, as the considered number of grains increases, the predicted stresses on the facet AB will tend to a limit. An important part of this investigation is to determine the number of grains which must be considered in order to get accurate estimates of the stresses on the facet AB.

Returning now to the general problem, we recall that the Eshelby method requires that each grain and the surrounding matrix be considered as isolated and the temperature increased by θ. Thus, the rth grain is now subject to strain $\theta\mathbf{m}_r$. We next strain each grain so that it has the *same* strain as the surrounding matrix and all grains can then fit together into the matrix. The required extra strain of the rth grain is

$$\boldsymbol{\varepsilon}_e^r = \theta(\mathbf{m}-\mathbf{m}') \tag{7}$$

and this is accomplished by the application of surface stresses $\mathbf{s}_e^r$ where

$$\mathbf{s}_e^r = L\boldsymbol{\varepsilon}_e^r \quad (L = M^{-1}). \tag{8}$$

The final step in the procedure is to superpose a layer of body force over the surface of each grain to annihilate the surface tractions obtained from (8). Thus, on the interface between the rth grain and the qth grain, the resultant superposed body force is

$$\begin{aligned}\mathbf{t} &= -\mathbf{s}_e^r\mathbf{n}-\mathbf{s}_e^q(-\mathbf{n})\\ &= (\mathbf{s}_e^q-\mathbf{s}_e^r)\mathbf{n}\\ &= \theta L(\mathbf{m}_r-\mathbf{m}_q)\mathbf{n},\end{aligned} \tag{9}$$

where $\mathbf{n}$ is the unit normal from the rth grain to the qth grain. We note that the traction vector $\mathbf{t}$ is *constant* over the interface. It then follows that the entire residual stress distribution in the uncracked body is obtained by superposition of the stresses $\mathbf{s}_e^r$ and the stresses induced by the totality of interfacial body forces (9). It is important to remember the contribution to the stress field due to the interface between the outer grains and the surrounding matrix.

It is therefore clear that the residual stress problem for the microcrack-free aggregate is solved once we can evaluate the stress distribution in an infinite solid due to *constant* body force over a single line segment—superposition gives the final solution. This problem is readily solved using complex variable methods.

First, consider a point (or, more precisely, line) force with components P_1, P_2 at the point represented by the complex number $z_0 = x_0+iy_0$ in an infinite isotropic solid. For this problem, it is well known that the complex potentials are given by

$$\phi(z) = -\frac{P}{2\pi(\kappa+1)}\ln(z-z_0), \tag{10}$$

$$\psi(z) = \frac{\kappa\bar{P}}{2\pi(\kappa+1)}\ln(z-z_0)+\bar{z}_0\frac{P}{2\pi(\kappa+1)}\frac{1}{z-z_0}, \tag{11}$$

where $P = P_1 + iP_2$. Also, since we are interested in *plane strain*, $\kappa = 3\text{-}4\nu$, but the work described below also applies to generalized plane stress when $\kappa = (3-\nu)/(1+\nu)$. Next, consider the straight line segment joining two vertices (i.e. triple points) z_1 and z_2, and suppose that this segment (grain boundary facet) is subject to uniform distributed body force $t = t_1 + it_2$ per unit length. It may be shown that differentiation of (10) and (11) with respect to z, followed by integration along the segment z_1z_2, implies that

$$\Phi(z) = \phi'(z) = \frac{t|\omega|}{2\pi(\kappa+1)\omega}\ln\frac{z-z_2}{z-z_1}, \tag{12}$$

$$\Psi(z) = \psi'(z) = -\frac{(\kappa\bar{t}\omega + t\bar{\omega})|\omega|}{2\pi(\kappa+1)\omega^2}\ln\frac{z-z_2}{z-z_1} - \frac{t|\omega|}{2\pi(\kappa+1)\omega}\left[\frac{\bar{z}_2}{z-z_2} - \frac{\bar{z}_1}{z-z_1}\right], \tag{13}$$

where $\omega = z_2 - z_1$. It is now possible to obtain the complex potentials for the entire distribution of body forces over grain boundary facets and thus, the residual stress field in the *uncracked* solid. While the algebraic details are too cumbersome to be fully reported here, some particular considerations, related to the stress singularities at the triple points, are useful.

From (12) and (13) the total complex potentials are clearly of the form

$$\Phi(z) = \sum_{k=1}^{N} A_k \ln(z-z_k), \tag{14}$$

$$\Psi(z) = \sum_{k=1}^{N} B_k \ln(z-z_k) - \sum_{k=1}^{N} \frac{A_k\bar{z}_k}{z-z_k}, \tag{15}$$

where $z_k (k = 1, 2, \ldots N)$ is the set of triple points and where A_k, B_k are a set of known constants. With the help of the standard formulae

$$\sigma_{xx} + \sigma_{yy} = 2\{\Phi(z) + \overline{\Phi(z)}\},$$
$$\sigma_{yy} + i\sigma_{xy} = \Phi(z) + \overline{\Phi(z)} + z\Phi'(z) + \Psi(z),$$

we can compute the stresses in the form

$$\sigma_{xx} + \sigma_{yy} = 2\left\{\sum_{k=1}^{N}[A_k \ln(z-z_k) + \bar{A}_k \ln(\bar{z}-\bar{z}_k)]\right\}, \tag{16}$$

$$\sigma_{yy} + i\sigma_{xy} = \sum_{k=1}^{N}[A_k + B_k)\ln(z-z_k) + \bar{A}_k \ln(\bar{z}-\bar{z}_k)] + \sum_{k=1}^{N}\frac{A_k(\bar{z}-\bar{z}_k)}{z-z_k}. \tag{17}$$

Equation (17) immediately suggests the possibility of an r^{-1} type singularity at each triple point. However, if we write

$$z - z_k = r_k \exp(i\theta_k),$$

then it is clear that

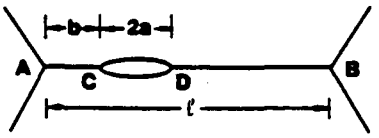

FIG. 3. Grain boundary crack of length $2a$ at the distance b from the triple point A.

$$\frac{z-\bar{z}_k}{z-z_k} = \exp(-2i\theta_k).$$

Hence there is no r^{-1} type singularity and the only stress singularity is logarithmic. Obviously, this singularity exists at every triple point, provided the axes of thermal anisotropy of the three associated grains do not coincide.

It is abundantly clear from (9), (16) and (17) that evaluation of the global residual stress field has been reduced to an algebraic problem. However, the complexity of the algebra should not be underestimated.

Let us now turn to the evaluation of stress intensity factors which are relevant in the study of grain boundary microcracking due to residual stress. It is commonly held that grain boundary microcracking is due to triple point defects. But there remains the possibility that defects occur elsewhere on the grain boundary. Since the stress intensity factors for arbitrarily located grain boundary cracks are readily inferred from our previous analysis, we consider the putative crack CD on the facet AB as shown in Fig. 3. For the required calculations it is convenient to orient the global x_1-axis along that facet. It then follows that the interfacial normal and shear stresses are given directly by (17).

A standard result in linear elastic fracture mechanics shows that the stress intensity factors at D are obtained from

$$K_I + iK_{II} = \frac{1}{\sqrt{\pi a}} \int_{-a}^{a} (\sigma_{yy} + i\sigma_{xy}) \sqrt{\frac{a+t}{a-t}}\, dt. \tag{18}$$

From (17) and (18) we observe that the calculation of K_I and K_{II} involves the evaluation of some elementary integrals together with integrals of two types:

$$J_1 = \int_{-1}^{1} \sqrt{\frac{1+t}{1-t}} \frac{1}{t+c}\, dt,$$

$$J_2 = \int_{-1}^{1} \sqrt{\frac{1+t}{1-t}} \ln(t+c)\, dt,$$

where c is complex and $|c| \leqslant 1$. The values of J_1 and J_2 may be obtained in closed form as

$$J_1 = \pi\left[1 - \left(\frac{c-1}{c+1}\right)^{1/2}\right],$$

$$J_2 = \pi[c - (c^2-1)^{1/2} + \ln\{c + (c^2-1)^{1/2}\} - \ln 2].$$

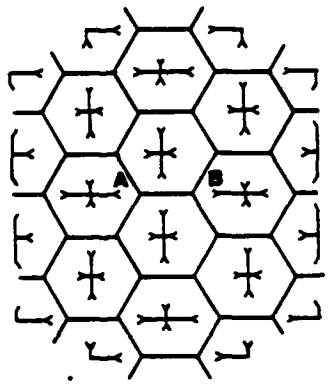

FIG. 4. Grain array with regular orientation distribution.

With the help of these explicit expressions for J_1 and J_2, it follows that the determination of stress intensity factors in the aggregate has been reduced to a simple algebraic sum. It is neither illuminating nor necessary to include details of the techniques which we use to handle the orientation distributions of the axes of thermal anisotropy and the summation over various grain arrays.

We emphasize that the preceding discussion also shows that we can readily compute residual stresses and the associated stress intensity factors for grain boundary microcracks for an *arbitrary* crystalline array, regular or otherwise.

3. THE RESIDUAL STRESS FIELD

The analysis presented in preceding sections provides an analytic solution for the entire residual stress field in the polycrystalline aggregate. From a practical point of view the usual thermoelastic moduli of an individual grain are taken as data, but the orientation distribution of the various grain arrays is not available at the time of writing. Thus, it will be essential to quantify the effect of grain orientation on the residual stress field and hence on microcracking during cooldown. However, from a computational standpoint, the first issue to be addressed must be the determination of the number of grains which is needed to get an accurate value for the interfacial stresses.

For illustration, we consider the regular orientation model shown in Fig. 4. First we remark that for this model, the overall coefficients of thermal expansion may be obtained from (5) as

$$m_{11} = m_{22} = (\alpha_1 + \alpha_2)/2, \quad m_{33} = \alpha_3.$$

At this stage, it is helpful to introduce some notation which is consistant with that of EVANS (1978). Thus, let the temperature drop during cooldown be ΔT, let the difference between the maximum thermal expansion coefficient and the average be denoted by $\Delta\alpha$, and let l be the facet length.

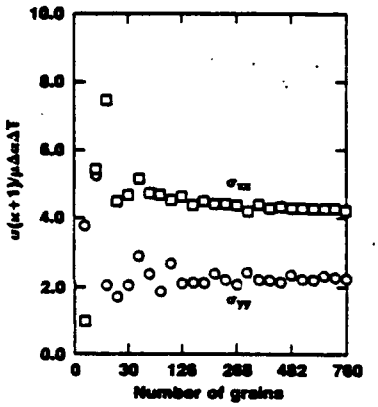

FIG. 5. Residual stress at the midpoint of AB vs number of grains. Note the variable scale on the x-axis.

We successively compute the normal and shear stresses, on AB, for the 2-grain model, the 4-grain model, etc. The predicted value of the normal stress at the midpoint of AB, for the various multi-grain models, is shown in Fig. 5. We note that it is essential to consider an array consisting of at least 200 grains to get an accurate estimate of the normal stress at the midpoint of the facet. We cannot emphasize too strongly that the preceding assertion also applies to other *fixed* orientation distributions. For example, we have investigated the grain orientation distribution studied by TVERGAARD and HUTCHINSON (1988), and we have found that the results obtained using our technique with 268 grains are entirely consistent with the finite element results of these authors. Thus, we repeat, that in order to get accurate predictions of the residual stresses on a particular facet in a *given* polycrystal, it is necessary to consider at least 200 grains surrounding that facet.

It is of interest to use Fig. 6 to calculate the residual normal stress on the facet AB for the particular alumina AD995. Here we can take

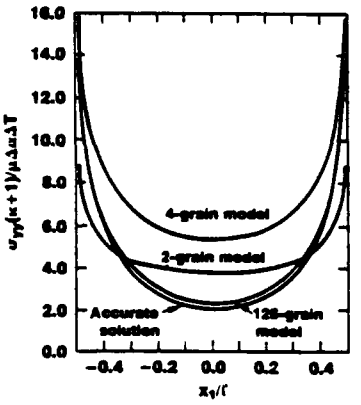

FIG. 6. Residual stress along the grain boundary AB for various grain arrays.

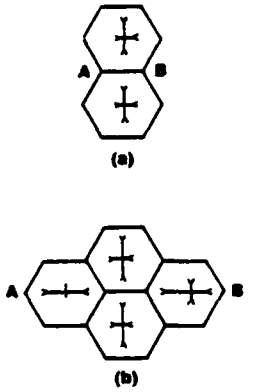

FIG. 7. Geometries and orientations for (a) 2-grain model and (b) 4-grain model.

$$E = 372\,\text{GPa}, \quad \nu = 0.25,$$

$$\Delta\alpha = 10^{-6}\text{C}^{-1}, \quad \Delta T = 1500°\text{C},$$

and it follows that the normal stress at the midpoint of AB is 150 MPa. This result may be contrasted with the tensile strength for AD995 which is 262 MPa.

An equally important issue pertains to sensitivity of the interfacial stresses to the assumed orientation distribution of the axes of thermal anisotropy. As has been emphasized, the orientation distribution function for a typical polycrystal is not known. Indeed, it is evident that the orientation distribution will vary from sample to sample. Therefore, when we examine models in which the orientation distribution is not fixed *a priori*, it is clear that we need to consider the appropriate *ensemble average*. In this sense we can arrive at an alternative interpretation of the various multi-grain models.

To explain, let us focus on the facet which will experience the greatest residual normal stress. We therefore consider two grains whose maximum contraction will be perpendicular to their interface, see Fig. 7(a). Now regard these grains as *fixed*. Since the orientation of the remaining grains is random, we can compute the ensemble average of the interfacial stresses by considering a large number of samples with randomly oriented axes of thermal anisotropy. But it is evident that the model obtained by taking two fixed grains together with the ensemble average over all orientations of the *surrounding* grains is equivalent to the model in which the two fixed grains are surrounded by the effective aggregate. We refer to this model as the 2-grain model for the randomly oriented aggregate. This model will give us the *average* stress on the interface AB. In similar fashion we can consider the model associated with the 4 fixed grains of Fig. 7(b). The model in which these 4 grains are surrounded by the effective aggregate, will give us the average stress on AB—the average referring to all orientations of the remaining grains. In this way we can arrive at the N-grain model for the randomly oriented aggregate.

It is obvious that the mathematics of the N-grain model for the aggregate with given *a priori* orientation distribution is the same as the mathematics of the N-grain

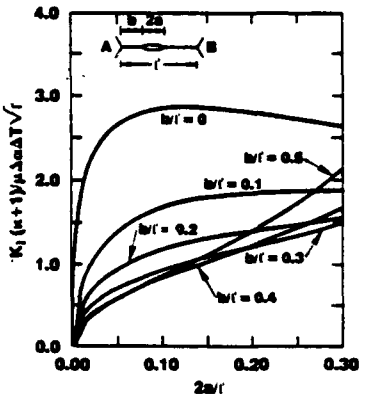

FIG. 8. Mode I stress intensity factors for cracks variously located in the facet AB: regular array orientation model.

model for the randomly oriented aggregate. However, the physical interpretation of the two models is completely different. To elaborate, we refer to Fig. 6, which amongst other things, shows the predicted normal stress for the 2-grain model of the given regular orientation distribution of Fig. 4. But we can also interpret the 2-grain model curve in Fig. 6 as giving the average normal stress on AB for a polycrystalline aggregate wherein two grains are held fixed and the remainder allowed to take all orientations.

While the magnitudes of the residual interfacial stresses are of interest and significance in their own right, it is perhaps more relevant to consider, in greater depth, the stress intensity factors which would exist at the tips of interfacial cracks. Indeed a careful analysis of the various stress intensity factors is an essential prerequisite to any understanding of microcracking due to cooldown or subsequent mechanical loading.

We first consider the regular array orientation of Fig. 4 and examine the stress intensity factors for variously located cracks on the interface AB, as shown in Fig. 3. We emphasize that for this configuration, the directions of maximum contraction of the grains on either side of AB are normal to the interface. The mode I stress intensity factor is shown in Fig. 8 as a function of initial defect length for various locations of the defect. We here restrict our attention to $2a/l \leqslant 0.3$. We see that for given initial defect length, the most critical crack emanates from the triple point. In addition, we emphasize that K_I is sensitive to the length of the initial defect.

Figures 9 and 10 show the variation in stress intensity factors at the right hand tip for triple point cracks on AB within the regular orientation array of Fig. 4, except that the orientation of one grain is allowed to vary. We note the sensitivity of the results to orientation of the single grain at the left of the critical triple point. In the same spirit, Figs 11 and 12 show the effect of changing the orientation of one grain to the right of B in the otherwise regular array of Fig. 4. In either case, K_{II} is much less than K_I. Finally, we investigate the effect of changing the orientation of the single grain above AB. The effect of orientation on K_I and K_{II} as a function of orientation is shown in Figs 13 and 14. We note that, even for small defects, the effect of orientation can be significant.

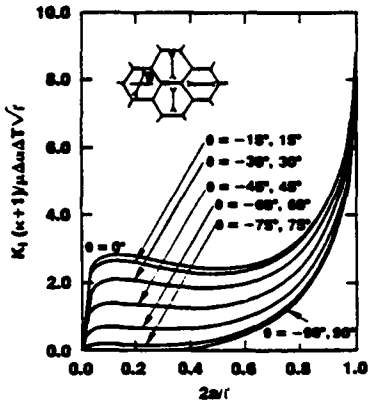

FIG. 9. Mode I stress intensity factors for various orientations of the grain to the left of the triple point crack—in the otherwise regular orientation array.

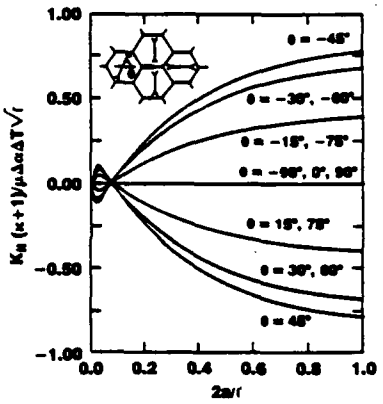

FIG. 10. Mode II stress intensity factors for various orientations of the grain to the left of the triple point crack—in the otherwise regular orientation array.

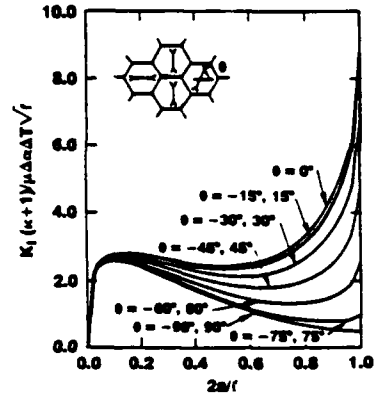

FIG. 11. Mode I stress intensity factors for various orientations of the grain to the right of the triple point crack—in the otherwise regular orientation array.

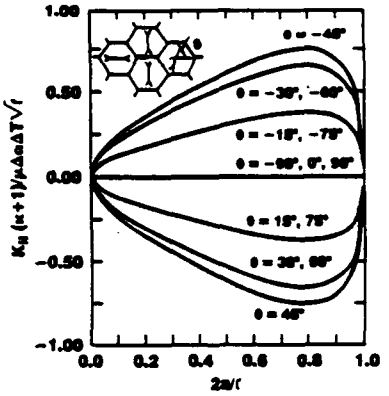

FIG. 12. Mode II stress intensity factors for various orientations of the grain to the right of the triple point crack—in the otherwise regular orientation array.

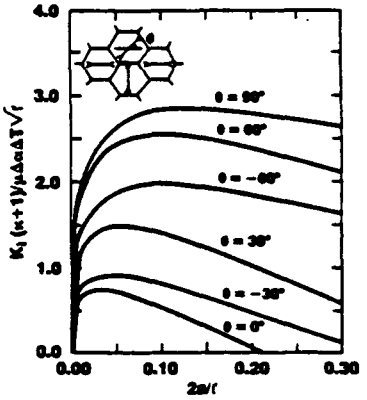

FIG. 13. Mode I stress intensity factors for various orientations of the grain above the triple point crack—in the otherwise regular orientation array.

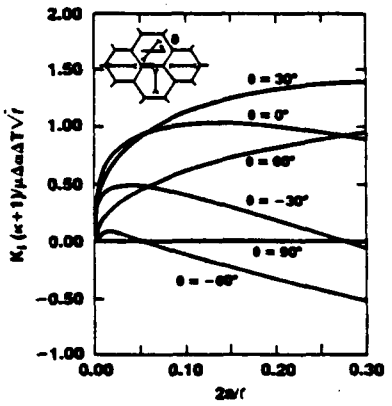

FIG. 14. Mode II stress intensity factors for various orientations of the grain above the triple point crack—in the otherwise regular orientation array.

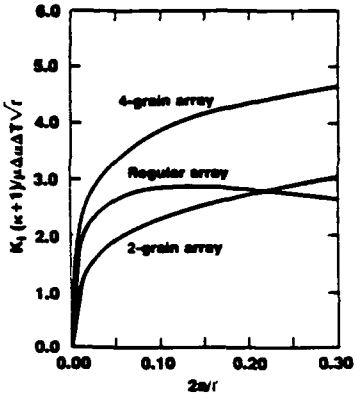

FIG. 15. Mode I stress intensity factors, for triple point cracks, for various grain arrays.

It is inappropriate to produce a multitude of figures to show the sensitivity of the stress intensity factors to orientation changes. Nevertheless, we can assert that, for the regular orientation array, microcracking is essentially a mode I phenomenon and that the orientation of contiguous grains is important.

Next, we consider some problems associated with the possibility of random orientation of the axes of thermal anisotropy. Here we focus on the 2-grain and 4-grain models in Fig. 7 which were discussed earlier. Hence, these models will give us *ensemble averages* for the stress intensity factor. Figure 15 shows the stress intensity factors which are predicted by the two models. For comparison, the regular orientation array result is also included in Fig. 15. Of course, for the regular array $K_{II} = 0$.

The obvious, and disconcerting, conclusion is that the various models give significantly different results. The status of the regular orientation array is clear. And it is likely that the 4-grain model of Fig. 7(b) gives the most extreme *local* orientations for potential cracking on the interface AB. Thus, when we consider grain boundary microcracking, we compare the regular orientation model with the 4-grain model. The reader is warned that other models give different results.

4. GRAIN BOUNDARY MICROCRACKING

The prediction of initial microcracking during cooldown is achieved by focusing on the worst possible scenario. Thus, we consider triple point cracks within the regular orientation array or the 4-grain model of Fig. 7(b). We recall that for practical purposes, K_{II} is negligible. From Fig. 15 we have

$$\frac{K_I(\kappa+1)}{\mu\Delta\alpha\Delta T\sqrt{l}} = f\left(\frac{2a}{l}\right), \tag{19}$$

where f depends upon the considered model. Next let G_{gb} be the grain boundary, mode I, plane strain toughness. It then follows from (19) that microcracking during cooldown first occurs at critical grain size, l_c, where

$$l_c = \frac{64(1-\nu^2)G_{gb}}{E(\Delta\alpha\Delta T)^2 f^2\left(\frac{2a}{l_c}\right)}. \tag{20}$$

where $2a$ is the length of the inherent triple point crack. An important parameter here is the ratio $(2a/l_c)$. As is obvious from Fig. 15, f changes rapidly for $0 < 2a/l < 0.1$. It is therefore clear that *any* prediction of critical grain size is highly sensitive to the flaw size in the material.

Let us now discuss some critical grain size predictions for specific polycrystalline ceramics. In the first instance we consider the magnesium titanate system studied by EVANS (1978). For this system EVANS (1978) suggests $2a/l = 0.1$. We can then read off the value of $f(0.1)$ from Fig. 15:

$$f(0.1) = 2.85 \text{ (regular orientation array)}$$
$$= 3.99 \text{ (4-grain model)}.$$

If we take the value $\nu = 0.25$, the above formulae in turn lead to

$$l_c = 7.39\frac{G_{gb}}{E(\Delta\alpha\Delta T)^2} \text{ (regular orientation array)},$$

$$= 4.02\frac{G_{gb}}{E(\Delta\alpha\Delta T)^2} \text{ (4-grain model)}.$$

The most recent formula proposed by FU and EVANS (1985) is

$$l_c = \frac{\beta(1+\nu)^2 G_{gb}}{E(\Delta\alpha\partial T)^2}. \tag{21}$$

The factor β is *chosen* to be approximately 3.5 in order to get an adequate correlation with experiment. If we interpret correctly, the proposed formula is independent of the ratio $(2a/l)$. For $\nu = 0.25$ the FU and EVANS (1985) formula becomes

$$l_c = 5.47\frac{G_{gb}}{E(\Delta\alpha\Delta T)^2}.$$

To calculate the critical grain size, we use the data given by EVANS (1978), namely

$$E = 240\,\text{GPa}, \quad \Delta\alpha = 5\times10^{-6}\text{C}^{-1}, \quad \Delta T = 1000^\circ\text{C}.$$

In addition, EVANS (1978) suggests that the value of G_{gb} lie between 2 Jm^{-2} and 10 Jm^{-2}. The various predictions of the three models are

$$l_c = 4.9\text{–}24.6\,\mu\text{m (regular orientation array)}$$
$$= 2.7\text{–}13.4\,\mu\text{m (4-grain model)}$$
$$= 3.6\text{–}18.3\,\mu\text{m (Fu and Evans)}.$$

The critical *average* grain size inferred from experiment [2] is about 3 μm, but as emphasized by EVANS (1978), the experimental value must be interpreted with care.

In the same spirit, we wish to emphasize the critical role played by the *assumption* that $(2a/l) = 0.1$.

Next we turn to the Al_2O_3 studied by RICE and POHANKA (1979) and by TVERGAARD and HUTCHINSON (1988). Following these authors we here take

$$E = 350\,\text{GPa}, \quad \nu = 0.2, \quad \Delta\alpha = 0.55 \times 10^{-6}\text{C}^{-1}, \quad \Delta T = 1000°\text{C},$$
$$2a/l = 0.02, \quad G_{gb} = 2\,\text{Jm}^{-2}.$$

From Fig. 14

$$f(0.02) = 2.21 \text{ (regular orientation array)}$$
$$= 2.63 \text{ (4-grain model)}.$$

It now follows that

$$l_c = 240\,\mu\text{m (regular orientation array)}$$
$$= 170\,\mu\text{m(4-grain model)}$$
$$= 103\,\mu\text{m (Fu and Evans)}.$$

TVERGAARD and HUTCHINSON (1988) also studied this Al_2O_3 system with the help of their periodic array and found $l_c = 216\,\mu$m. For the same array, the present model gives $l_c = 218\,\mu$m. The experimental value is $l_c = 200\,\mu$m.

ACKNOWLEDGEMENT

The work of N.L. was supported in part by the Aluminum Company of America and in part by a grant from the Air Force Office of Scientific Research.

REFERENCES

CLARKE, F. J. P.	1964	*Acta Metall.* **12**, 139.
CLEVELAND, J. J. and BRADT, R. C.	1978	*J. Am. Ceram. Soc.* **61**, 478.
DAVIDGE, R. W.	1981	*Acta Metall.* **29**, 1965.
ESHELBY, J. D.	1961	*Progress in Solid Mechanics*, Vol. 2, Ch. 3 (edited by I. N. SNEDDON and R. HILL), North-Holland, Amsterdam.
EVANS, A. G.	1978	*Acta Metall.* **26**, 1845.
FREDRICH, J. T. and WONG, T.-F.	1986	*J. geophys. Res.* **91**, 12,743.
FU, Y. and EVANS, A. G.	1982	*Acta Metall.* **30**, 1619.
FU, Y. and EVANS, A. G.	1985	*Acta Metall.* **33**, 1515.
KUSZYK, J. A. and BRADT, R. C.	1973	*J. Am. Ceram. Soc.* **56**, 420.
LAWS, N.	1973	*J. Mech. Phys Solids* **21**, 9.
OHYA, Y., NAKAGAWA, Z. and HAMANO, K.	1987	*J. Am. Ceram. Soc.* **70**, c-184.
RICE, R. W. and POHANKA, R. C.	1979	*J. Am. Ceram. Soc.* **62**, 559.
TVERGAARD, V. and HUTCHINSON, J. W.	1988	*J. Am. Ceram. Soc.* **71**, 157.

N. LAWS

13

The effect of microcracks on energy density

13.1 Introduction

In recent years, there has been considerable interest in the response of polycrystalline brittle solids which contain a homogeneously distributed family of microcracks. As far as the author is aware, the quantification of the effect of such a population of microcracks on the macroscopic response of the solid was initiated by Budiansky and O'Connell [1]. Other contributions have been given in a series of papers by Evans and coworkers [2–6], Hoagland and Embury [7], Clarke [8], Hoenig [9], Laws and Brockenbrough [10, 11] Hutchinson [12] and Charalambides and McMeeking [13].

The topics of major concern in this literature are the loss of stiffness due to a given family of microcracks and the nucleation of further microcracks. In addition, there is considerable interest in the extent to which microcracks in the process zone of a macroscopic crack can have a shielding effect on the macroscopic crack tip. These issues are further discussed in this paper. The development is presented in the same spirit as those of earlier studies [1–13].

All the foregoing contributions refer to *open* microcracks. And, for the most part, the respective authors focus on loss of macroscopic stiffness, rather than change of macroscopic energy density – since the latter (when relevant) is trivially obtained from the former.

At this stage of our discussion it is, perhaps, essential to emphasize a point which is developed by Hutchinson [12] and by Charalambides and McMeeking [13], namely that existence of the standard microscopic energy

G.C. Sih and E.E. Gdoutos (eds): Mechanics and Physics of Energy Density, 189–??

density does not imply existence of a macroscopic energy density in a microcracking solid. In fact, as will be shown later, severe restrictions must be placed on the microcrack nucleation function in order that the microcracking polycrystalline aggregate can be regarded as macroscopically hyperelastic. In addition we draw attention to the important paper of Horii and Nemat-Nasser [14] which pertains to the effects of microcrack closure and friction on the macroscopic response. These authors show that the macroscopic compliance tensor of such a solid depends on the load path and need not even be symmetric.

In this paper, a summary of results is given for loss of stiffness of a solid containing various families of microcracks. For simplicity, we restrict attention to dilute dispersions of microcracks (so that the microcracks do not interact). Further, we make the standard assumption that at least in a first approximation, each grain of the polycrystalline aggregate is isotropic and that residual stresses may be neglected. Next, we discuss some issues which arise from the choice of the microcrack nucleation function. In the absence of definitive experimental evidence, a simple nucleation function is proposed which leads to the microcracked solid being hyperelastic. This choice of nucleation function is not essential but leads easily to an assessment of the extent of microcrack shielding on a macroscopic crack tip. The results thus obtained are compared with some results of Hutchinson [12], Charalambides and McMeeking [13], and Ortiz [16].

13.2 Microcracked solid with given crack density

The approach adopted here closely follows that of Budiansky and O'Connell [1], Laws and Brockenbrough [10], and Hutchinson [12]. Consider an isotropic solid with compliance tensor M_0 which contains a family of variously oriented *open* microcracks. It is essential to assume that the microcracks are homogeneously dispersed. And it is convenient to assume that the microcracks are of similar elliptic planform and that crack orientation and size are not correlated. A convenient measure of microcrack density has been suggested by Budiansky and O'Connell [1]:

$$\beta = \frac{2N}{\pi}\left\{\frac{A^2}{P}\right\}, \tag{13.1}$$

where N is the number of cracks per unit volume. A is the area of a crack and P is perimeter. Also $\{\ \}$ denotes the orientation average of the bracketed quantity.

From [10], we can immediately read off the formula for the loss of stiffness of a solid containing a *dilute* distribution of similar microcracks:

$$M = M_0 + \beta \frac{8E(k)}{3}\{\Lambda\}, \tag{13.2}$$

where Λ is a tensor whose components are given in [10] for a variety of microcrack shapes, and where $E(k)$ is the complete elliptic integral of the second kind.

It is of interest to give some explicit deductions from equation (13.2) for particular microcrack distributions. For a three-dimensional randomly oriented family of penny-shaped cracks, we can recover the Budiansky and O'Connell [1] results

$$\frac{E}{E_0} = 1 - \beta \frac{16(1 - \nu_0^2)(10 - 3\nu_0)}{45(2 - \nu_0)}, \tag{13.3}$$

$$\frac{G}{G_0} = 1 - \beta \frac{32(1 - \nu_0)(5 - \nu_0)}{45(2 - \nu_0)}, \tag{13.4}$$

where G is the shear modulus and ν is Poisson's ratio. Also, for a family of aligned penny-shaped cracks

$$\frac{E}{E_0} = 1 - \frac{16}{3}\beta(1 - \nu_0^2) \tag{13.5}$$

$$\frac{G}{G_0} = 1 - \frac{16}{3}\beta\frac{1 - \nu_0}{2 - \nu_0} \tag{13.6}$$

where E is now Young's modulus normal to the microcrack faces and G is the transverse shear modulus.

When we have a family of aligned slit cracks, we find that the reduction in Young's modulus normal to the slits is given by

$$\frac{E}{E_0} = 1 - \frac{\pi^2}{2}\beta(1 - \nu_0^2), \tag{13.7}$$

whereas for a two-dimensionally randomly oriented family of slits [10]

$$\frac{E}{E_0} = 1 - \frac{\pi^2}{4}\beta(1 - \nu_0^2). \tag{13.8}$$

Other explicit results are obtainable but details are not given here.

13.3 Microcrack nucleation

Some potential nucleation functions have been discussed by Brockenbrough and Suresh [15], Hutchinson [12], Charalambides and McMeeking [13] and Ortiz [16]. It is particularly appropriate here to consider the nucleation function in [13] which is intimately associated with an isotropic distribution of three-dimensional randomly oriented penny-shaped cracks. According to Charalambides and McMeeking [13], a good approximation to the Budiansky and O'Connell [1] estimates for stiffness loss is given by

$$\frac{E}{E_0} = \frac{\nu}{\nu_0} = 1 - \beta\frac{16}{9}, \tag{13.9}$$

for all crack densities less than 9/16. The tensorial stress-strain relation corresponding to equations of (13.9) is given by Hutchinson [12] in the form

$$\varepsilon = \mathbf{M}_0\sigma - \frac{1}{E_0}\left[1 - \left(1 - \frac{16}{9}\beta\right)^{-1}\right]\sigma. \tag{13.10}$$

Further, the associated nucleation function is proposed for proportional loading to be

$$\beta = f(p), \tag{13.11}$$

where

$$p = (\sigma\cdot\sigma)^{1/2}. \tag{13.12}$$

Thus, under proportional loading, β is taken to increase monotonically until it reaches a saturation value β_s. It then follows from equations (13.10), (13.11) and (13.12) that a macroscopic energy density, U, exists. In fact, for the dilute case

$$U = \frac{1}{2}\sigma\cdot\mathbf{M}_0\sigma + \frac{16}{9}\frac{1}{E_0}F(p) \tag{13.13}$$

where

$$F'(p) = pf(p), \tag{13.14}$$

so that

$$\varepsilon = \frac{\partial U}{\partial\sigma}. \tag{13.15}$$

While it is true that equation (13.9) gives a good approximation to the Budiansky and O'Connell [1] results over a large range of crack densities, it is equally true that the approximations embodied in equation (13.9) are not necessarily good for small values of β – as is evident from equations (13.3) and (13.4). This observation has prompted the investigation of a different nucleation function which closely approximates the form in equation (13.11) but which also leads to the existence of a macroscopic energy density function.

The nucleation function proposed for investigation here is obtained by demanding that the macroscopic stress-strain relation in equation (13.2) be derivable from a macroscopic energy density $U(\sigma)$. Indeed, it is not difficult to show that this requirement implies that the nucleation function under proportional loading is

$$\beta = g(t), \tag{13.16}$$

where

$$t^2 = \sigma \cdot \{\Lambda\}\, \sigma. \tag{13.17}$$

Also the macroscopic energy density is here

$$U = \frac{1}{2}\sigma \cdot \mathbf{M}_0 \sigma + \frac{8E(k)}{3} G(t), \tag{13.18}$$

where

$$G(t) = tg(t). \tag{13.19}$$

Clearly the nucleation function in equation (13.16) is intimately bound up with the stress-strain relation in equation (13.2) and vice-versa. At this juncture, we are content to observe that the proposed function in equation (13.16) exhibits the same anisotropy as the stress-strain relation.

We note that other nucleation functions which do not lead to a macroscopic energy density function have been considered by Hutchinson [12].

A particularly useful consequence of the existence of an energy function is that we can easily determine the extent of shielding on a stationary macroscopic crack due to microcracking in the process zone. This is readily accomplished using the J integral. Following Hutchinson [12], we only consider Mode I small-scale microcracking. Repeating an argument of Evans and Faber [3], Laws and Brockenbrough [11], and Hutchinson [12], we assert that for a contour remote from a macroscopic crack in an isotropic solid

$$J = \frac{(1 - \nu_0^2) K^2}{E_0}, \tag{13.20}$$

where K is the "applied" stress intensity factor.

On the other hand, for contours in the saturation zone,

$$J_s = \frac{(1-\nu_0^2)K_{tip}^2}{E_0}. \tag{13.21}$$

Invariance of J gives a formula for K_{tip} for isotropic materials.

Thus for a randomly oriented distribution of penny-shaped cracks we find

$$\frac{K_{tip}}{K} = 1 - \frac{8\beta_s}{45(2-\nu_0)}(10 - 3\nu_0 + 8\nu_0^2 - 3\nu_0^3). \tag{13.22}$$

For anisotropic distributions of microcracks, the algebraic details are more tedious. Omitting details, we assert that for a distribution of aligned penny-shaped cracks in the process zone

$$\frac{K_{tip}}{K} = 1 - \frac{16 - 7\nu_0}{6(2-\nu_0)}\beta_s. \tag{13.23}$$

Also for aligned slit cracks

$$\frac{K_{tip}}{K} = 1 - \frac{3\pi^2}{16}\beta_s, \tag{13.24}$$

whereas for two-dimensionally randomly oriented slit cracks

$$\frac{K_{tip}}{K} = 1 - \frac{\pi^2}{8}\beta_s. \tag{13.25}$$

The preceding formula are readily compared and contrasted with the formulae obtained for different nucleation functions by Hutchinson [12], Charalambides and McMeeking [13] and Ortiz [16].

Acknowledgement

The work reported here was supported by the Air Force Office of Scientific Research under Grant Number AFOSR-88-0104.

References

[1] Budiansky B. and O'Connell R.J., "Elastic moduli of a cracked solid," Int. J. Solids Structures, 12, (1976), 81.

[2] Evans A.G., "Microfracture from thermal expansion anisotropy – I. Single phase systems," Acta. Metall., 26, (1978), 1845.

[3] Evans A.G. and Faber K.T., "Crack-growth resistance of microcracking brittle solids," J. Am. Ceram. Soc., 67, (1983), 255.

[4] Fu Y. and Evans A.G., "Microcrack zone formation in single phase polycrystals," Acta. Metall., 30, (1982), 1619.

[5] Fu Y. and Evans A.G., "Some effects of microcracks on the mechanical properties of brittle solids – I. Stress strain relations," Acta. Metall., 33, (1985), 1515.

[6] Fu Y. and Evans A.G., "Some effects of microcracks on the mechanical properties of brittle solids – 2. Microcrack toughening," Acta Metall., 33, (1985), 1525.

[7] Hoagland R.G. and Embury J.D., "A treatment of inelastic deformation around a crack tip due to microcracking," J. Am. Ceram. Soc., 63, (1980), 404.

[8] Clarke D.R, "A simple calculation of process-zone toughening by microcracking," Commun. Am. Ceram. Soc., (1984), C-15.

[9] Hoenig A., "Elastic moduli of a non-randomly cracked body," Int. J. Solids Structures, 15, (1979), 137.

[10] Laws N. and Brockenbrough J.R., "The effect of microcrack systems on the loss of stiffness of brittle solids," Int. J. Solids Structures, 23, (1987), 1247.

[11] Laws N. and Brockenbrough J.R., "Microcracking in polycrystalline solids," J. Engng. Materials Tech., 110, (1988), 101.

[12] Hutchinson J.W., "Crack tip shielding by microcracking in brittle solids," Acta. Metall., 35, (1987), 1605.

[13] Charalambides P.G. and McMeeking R.M., "Finite element method simulation of crack propagation in a brittle microcracking solid," Mech. of Materials, 6, (1987), 71.

[14] Horii M. and Nemat-Nasser S., "Overall moduli of solids with microcracks: Load-induced anisotropy," J. Mech. Phys. Solids, 31, (1983), 155.

[15] J.R. Brockenbrough and S. Suresh, "Constitutive behavior of a microcracking brittle solid in cyclic compression" J. Mech. Phys. Solids, 35, (1987), 721.

[16] Ortiz M., "A continuum theory of microcrack shielding," J. Appl. Mechanics, 54, (1987), 54.

The American Society of Mechanical Engineers

Reprinted From
AMD–Vol. 109, Damage Mechanics in Engineering Materials
Editors: J. W. Ju, D. Krajcinovic, and H. L. Schreyer
Book No. G00540 – 1990

LOSS OF STIFFNESS DUE TO MICROCRACKING IN UNIDIRECTIONAL CERAMIC MATRIX COMPOSITES

R. Chao and N. Laws
Department of Mechanical Engineering
University of Pittsburgh
Pittsburgh, Pennsylvania

ABSTRACT

In this paper we consider the problem of a debond crack on the interface of a circular fiber in an infinite matrix, when the matrix is loaded by uniaxial tension at infinity. We pay special attention to those orientations of applied load for which the crack remains open. Finally we use the analysis to calculate the loss of stiffness in an unidirectional ceramic matrix composite due to interfacial microcracking.

INTRODUCTION

This paper is concerned with fiber-matrix interfacial debonds in a unidirectional fiber reinforced composite. In the first place we discuss the problem of a single debond crack at the interface between a circular fiber and an infinite matrix. The crack is assumed to be open with zero tractions on the crack faces and the matrix is loaded by uniaxial tension at infinity. This problem has already been discussed by England (1966), Perlman and Sih (1967), Toya (1974) and Piva (1982). We draw explicit attention to the fact that the crack closes for a significant range of orientations of the applied load - as first noted by Toya (1974). We also draw attention to the fact that many standard tables of stress intensity factors for the homogeneous problem ignore this crucial limitation.

More precisely, we present a slight modification of the England (1966) solution. Of course, this solution involves overlapping of the crack faces near the tips. In view of recent work by Rice (1988), He and Hutchinson (1989) and Suo and Hutchinson (1989) we endeavor to give a proper interpretation of the solution of the stated problem. But we remark that the relationship between the present work and a properly formulated Comninou (1977) model, allowing for interfacial contact, will be reported at a later date.

The paper concludes with the application of the results to the determination of the reduction in transverse stiffness of a dilute unidirectional ceramic matrix composite.

Finally we remark that extensions of the present work to multiple debond cracks anisotropic fibers and matrix and large fiber concentrations are possible - but omitted here.

ANALYSIS

We consider the plane strain problem of an infinite isotropic matrix with moduli κ_1,μ_1 which contains a circular fiber, of radius a, with moduli κ_2,μ_2. The fiber is perfectly bonded to the matrix except over the region $r = a, |\theta| \le \phi$. The system is loaded by uniaxial tension T at infinity at angle ω to the x-axis. the faces of the crack are tractionfree.

A solution of the problem may be obtained in terms of the Muskhelishvil potentials $\phi(z)$ and $\psi(z)$. Perhaps the simplest form is obtained if we work with the potentials $\phi(z)$ and $\chi(z)$

where

$$\chi(z) = z\bar{\phi}'\left(\frac{a^2}{z}\right) + \bar{\psi}\left(\frac{a^2}{z}\right) . \tag{1}$$

Let ϕ_1, χ_1, ϕ_2, χ_2 denote the solutions in the two regions. Then continuity conditions over the interface imply the existence of two functions F(z), G(z) which are analytic except possibly at the origin, infinity and over the crack:

$$F(z) = \phi_1'(z) - \chi_2'(z) , \quad |z| > a , \tag{2}$$

$$F(z) = \phi_2'(z) - \chi_1'(z) , \quad |z| < a , \tag{3}$$

and

$$G(z) = \frac{\kappa_1}{\mu_1}\phi_1'(z) + \frac{1}{\mu_2}\chi_2'(z) , \quad |z| > a , \tag{4}$$

$$G(z) = \frac{\kappa_2}{\mu_2}\phi_2'(z) + \frac{1}{\mu_1}\chi_1'(z) , \quad |z| < a . \tag{5}$$

Moreover, in the present problem, the fact that the crack surface is traction free implies that

$$F(z) = A + B/z^2 . \tag{6}$$

With the help of the preceding definitions, the stated problem reduces to a standard Hilbert problem for G(z), see England (1966), who also gives the solution in closed form.

In the present study, quantities of particular interest are the asymptotic near-tip stresses and crack opening displacements. It is not difficult to show that near the tip A (see Fig. 2.)

$$\sigma_{rr} + i\sigma_{r\theta} \sim \frac{F(\phi, \omega, \beta)\sqrt{\pi a \sin\phi}}{\sqrt{2\pi r}}(1 + 2i\beta)\left(\frac{r}{2a\sin\phi}\right)^{i\beta} , \tag{7}$$

$$[u_r + iu_\theta]^+_- \sim \frac{\mu_1 + \kappa_1\mu_2}{\mu_1\mu_2\sqrt{\alpha}} F(\phi, \omega, \beta)\sqrt{\pi a \sin\phi}\sqrt{\frac{r}{2\pi}}\left(\frac{r}{2a\sin\phi}\right)^{i\beta} , \tag{8}$$

where

$$\alpha = \frac{\mu_1 + \kappa_1\mu_2}{\mu_2 + \kappa_2\mu_1} \tag{9}$$

and

$$\beta = \frac{1}{2\pi} ln\ \alpha , \tag{10}$$

and where $F(\phi, \omega, \beta)$ is a complicated, but known, function. Of course the above solution implies overlapping of the crack faces, and thus gives an estimate of that part of the crack length (r_c) over which contact take place. this situation has been carefully and extensively discussed by Rice (1988) in the case of an interface crack between two half spaces. Guided by the work of Rice (1988) we introduce the parameter

$$f = \frac{r_c}{2a\phi} \tag{11}$$

and assert that small scale contact at a particular tip will occur when $f << 1$. In such circumstances Rice (1988) defines a classical stress intensity factor which is essentially obtained from (7) by deleting the term $(r/2a \sin\phi)^{i\beta}$. For similar problems He and Hutchinson (1989) and Suo and

Hutchinson (1989) have argued the desirability of setting $\beta = 0$ in equations (7) and (8) - at least in the case of two half spaces. In the sequel we investigate the consequences of both hypotheses.

We first examine the range of parameters for which the interfacial arc crack remains open. Typical results are shown in Fig. 1. We first note the range of open cracks for various crack sizes and load orientations in the homogeneous case. For a given crack size there is always a limitation on the orientation of the applied load for the crack to remain open. In the inhomogeneous problem, we find that taking $\beta = 0$ implies a larger range of open cracks than we obtain for small scale contact. Further, the smaller the allowed scale of contact the smaller the range of open cracks.

We also present results for the classical stress intensity factors for a debond crack at the interface of an SCS6 fiber in an LAS matrix in Figs. 2 and 3. We note that these curves apply only when the cracks are open. And since the assumption of small scale contact leads to a smaller range of open cracks than taking $\beta = 0$, the indicated curves in Figs. 2 and 3 have different ranges of validity. However, in that range when both curves are valid, there is little between the S.I.F. in Figs. 2 and 3. An extensive discussion of this issue will be given elsewhere.

Next we use the preceding results to calculate the loss of transverse stiffness in a dilute unidirectional SCS6/LAS composite due to interfacial debonds. For simplicity we assume that the same debond crack occurs at every fiber - this merely has the effect of reducing the number of geometrical parameters. In addition we use the Budiansky and O'Connell (1976) definition of crack density:

$$\epsilon = \frac{4Nl^2}{\pi}$$

where N is the number of cracks per unit area and l is the half length of the crack.

It must be emphasized that the present discussion only applies to open cracks. In the first instance we give in Fig. 4 the results for a homogeneous material - so that the overlapping problem is absent. Similar results are presented in Figs. 5 and 6 for the composite material. Again the difference between Figs. 5 and 6 merely lies in the range of validity of the curves for which the cracks are open.

Finally we remark that an extensive discussion of the issues raised herein will be presented elsewhere.

ACKNOWLEDGEMENTS

This work was supported by the U.S. Air Force Office of Scientific Research. The authors gratefully acknowledge useful discussions with Lieutenant-Colonel G.K. Haritos, Dr. T. Nicholas and Dr. N.J. Pagano.

REFERENCES

Budiansky, B., and O'Connell, R.J., 1976, "Elastic Moduli of a Cracked Solid," Int. J. Solids Structures, Vol. 12, pp. 81-97.

Comninou, M., 1977, "The Interface crack," J. Appl. Mech., Vol. 44, pp. 631-636.

England, A.H., 1966, "An Arc Crack Around a Circular Elastic Inclusion," J. Appl. Mech., Vol. 33, pp. 637-640.

He, M.-Y., and Hutchinson, J.W., 1989, "Kinking of a Crack Out of an Interface," J. Appl. Mech., Vol. 56, pp. 270-278.

Perlman, A.B., and Sih, G.C., 1967, "Elastostatic Problems of Curvilinear Cracks in Bonded Dissimilar Materials," Int. J. Engrg. Sci., Vol. 5, pp. 845-867.

Piva, A., 1982, "A Crack Along a Circular Interface Between Dissimilar Media," Meccanica, vol. 17, pp. 85-90.

Rice, J.R., 1988, "Elastic Fracture Mechanics Concepts for Interfacial Cracks," J. Appl. Mech., Vol. 55, pp. 98-103.

Suo, Z., and Hutchinson, J.W., 1989, "Sandwich Test Specimens for Measuring Interfacial Crack Toughness," Matls. Sc. and Engrg., Vol. A107, pp. 135-143.

Toya, M., 1974, "A Crack Along the Interface of a Circular Inclusion Embedded in an Infinite Solid," J. Mech. Phys. Solids, Vol. 22, pp. 325-348.

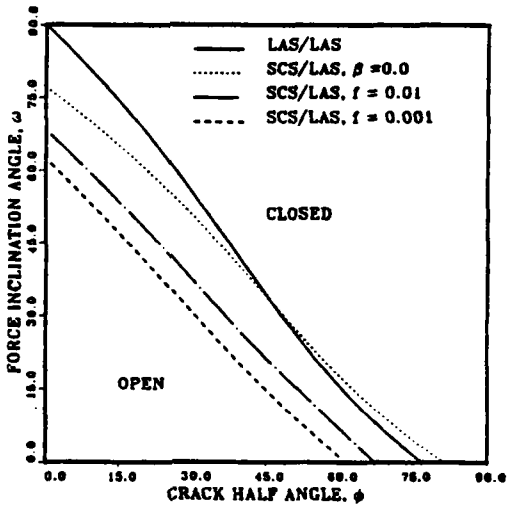

Fig. 1. Range of load orientation for which crack remains open.

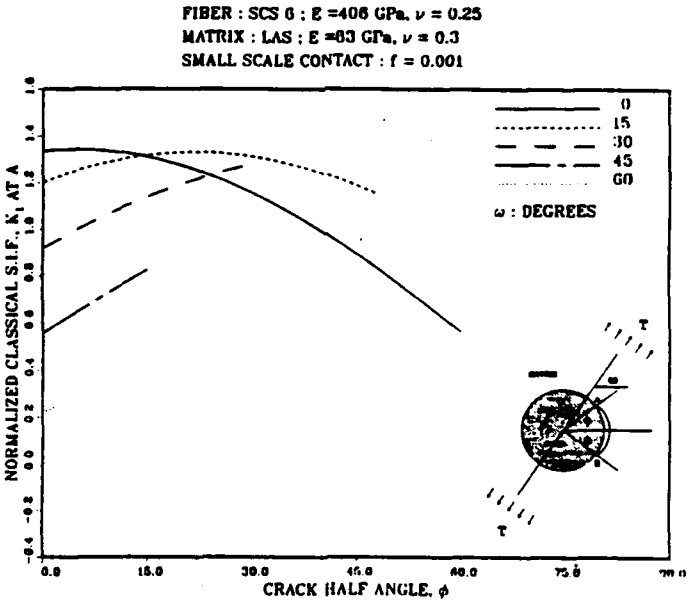

Fig. 2. Classical stress intensity factor for open cracks and small scale contact.

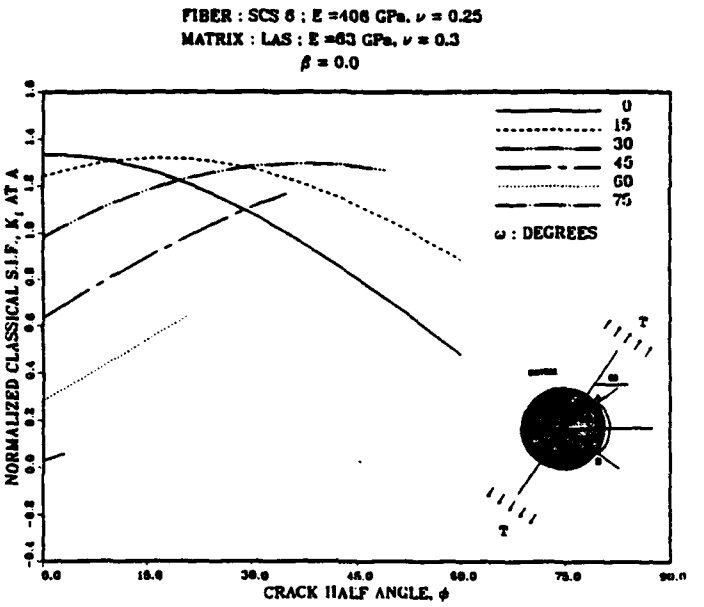

Fig. 3. Classical stress intensity factor for open cracks with $\beta = 0$.

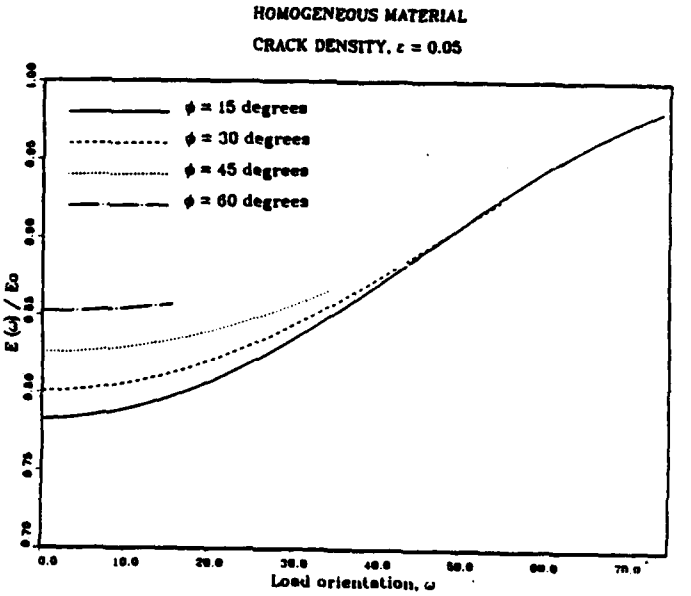

Fig. 4. Loss of transverse stiffness as a function of orientation of applied load for open cracks in homogeneous material.

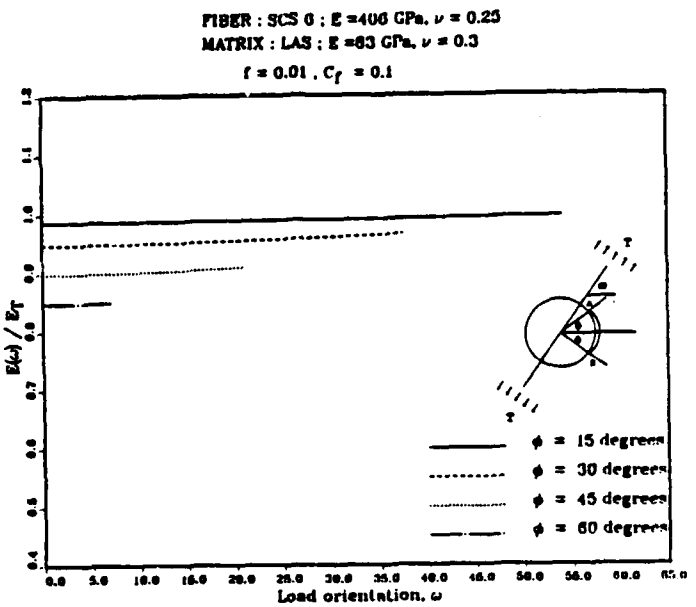

Fig. 5. Loss of transverse stiffness as a function of orientation of applied load for open cracks in SCS6/LAS and small scale contact.

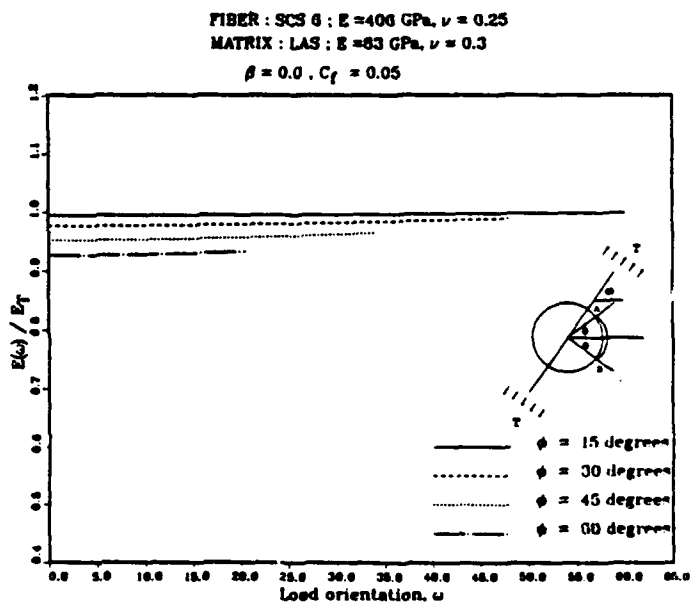

Fig. 6. Loss of transverse stiffness as a function of orientation of applied load for open cracks in SCS6/LAS with $\beta = 0$.

Unclassified
SECURITY CLASSIFICATION OF THIS PAGE

REPORT DOCUMENTATION PAGE

1a. REPORT SECURITY CLASSIFICATION Unclassified	1b. RESTRICTIVE MARKINGS
2a. SECURITY CLASSIFICATION AUTHORITY	3. DISTRIBUTION / AVAILABILITY OF REPORT Approved for public release; distribution unlimited
2b. DECLASSIFICATION / DOWNGRADING SCHEDULE	
4. PERFORMING ORGANIZATION REPORT NUMBER(S)	5. MONITORING ORGANIZATION REPORT NUMBER(S)
6a. NAME OF PERFORMING ORGANIZATION University of Pittsburgh 6b. OFFICE SYMBOL (If applicable)	7a. NAME OF MONITORING ORGANIZATION AFOSR
6c. ADDRESS (City, State, and ZIP Code) Department of Mechanical Engineering Benedum Hall Pittsburgh, PA 15261	7b. ADDRESS (City, State, and ZIP Code) AFOSR/NA Bldg 410 Bolling AFB DC 20332-6448
8a. NAME OF FUNDING / SPONSORING ORGANIZATION AFOSR 8b. OFFICE SYMBOL (If applicable) NA	9. PROCUREMENT INSTRUMENT IDENTIFICATION NUMBER AFOSR-88-0104
8c. ADDRESS (City, State, and ZIP Code) Bolling AFB DC 20332	10. SOURCE OF FUNDING NUMBERS PROGRAM ELEMENT NO. 61102F; PROJECT NO. 2302; TASK NO. BS; WORK UNIT ACCESSION NO.

11. TITLE (Include Security Classification)
The Mechanics of Progressive Cracking in Ceramic Matrix Composites and Laminates (U)

12. PERSONAL AUTHOR(S)
Norman Laws

13a. TYPE OF REPORT	13b. TIME COVERED	14. DATE OF REPORT (Year, Month, Day)	15. PAGE COUNT
Technical	FROM 2/89 TO 9/91	September 30, 1991	

16. SUPPLEMENTARY NOTATION

17. COSATI CODES			18. SUBJECT TERMS (Continue on reverse if necessary and identify by block number)
FIELD	GROUP	SUB-GROUP	Composite materials, ceramics, laminates, cracks, damage.

19. ABSTRACT (Continue on reverse if necessary and identify by block number)

This report provides a brief summary of the principal results obtained in a research program on the mechanics of progressive cracking in ceramic matrix composites and laminates. The report concentrates on (i) progressive transverse matrix cracking in cross-ply laminates, (ii) the effect of transverse matrix cracks on the axial response of unidirectional ceramic matrix composites, (iii) thermal conductivities of hot pressed SiC/BN composites, (iv) microcracking in polycrystalline ceramics, and (v) the effect of matrix cracking and fiber-matrix interfacial debonding on the response of unidirectional ceramic matrix composites.

20. DISTRIBUTION / AVAILABILITY OF ABSTRACT ☐ UNCLASSIFIED/UNLIMITED ☐ SAME AS RPT. ☑ DTIC USERS	21. ABSTRACT SECURITY CLASSIFICATION (U)
22a. NAME OF RESPONSIBLE INDIVIDUAL Walter Jones	22b. TELEPHONE (Include Area Code) (202) 767-0420 22c. OFFICE SYMBOL NA

DD FORM 1473, 84 MAR 83 APR edition may be used until exhausted. All other editions are obsolete.

SECURITY CLASSIFICATION OF THIS PAGE